UNIVERSITAT POLITÈCNICA DE VALÈNCIA

ESCUELA TÉCNICA SUPERIOR INGENIEROS INDUSTRIALES VALENCIA

TRABAJO FIN DE MASTER EN INGENIERÍA BIOMEDICA

REGULARIZATION TECHNIQUES FOR ELECTROCARDIOGRAPHIC IMAGING DURING ATRIAL FIBRILLATION

AUTOR: MACARENA CASTILLO FABREGAT

TUTOR: DRA. MARÍA DE LA SALUD GUILLEM SÁNCHEZ
DR. BATISTE ANDREU MARTÍNEZ CLIMENT
DR. MIGUEL RODRIGO BORT

Curso Académico: 2016-17

Agradecimientos

A María y Andreu, por haber confiado en mí al darme la oportunidad de realizar este trabajo con ellos. Por su profesionalidad y por todo lo que me han enseñado y ayudado estos últimos meses. A Ismael, por su colaboración desde el otro lado del charco.

A mi madre, por su apoyo y ánimo incondicional. Por levantarme cada vez que he caído y celebrar mis logros como si fueran suyos. Por estar siempre conmigo a pesar de la distancia. A mi padre, por confiar siempre en mí. Por haber hecho posible toda experiencia en mi vida y haberme guiado hasta aquí. A mi hermano, por enseñarme las lecciones más importantes de la vida.

A mis padrinos, por haberse preocupado siempre como mis propios padres. Y a mis primas, que más que primas, hermanas. Gracias por darme tanto y hacerme sentir siempre en casa.

A mis amigas, por demostrar que no importa el tiempo ni la distancia. Por esos momentos de desconexión tan necesarios.

A mis amigos del Máster, por haber hecho que este año pasara volando. Por todas las mañanas, tardes y noches, ya fuera estudiando o sin estudiar. Gracias por hacer que fuera inolvidable.

Resumen

El trabajo final de máster propuesto es un estudio centrado en la evaluación de la eficacia del método Bayesiano para reconstruir el problema inverso que plantea la cartografía eléctrica no invasiva (ECGI), así como el número y posición de señales intracavitarias que serían necesarias para su correcto funcionamiento.

El ECGI permite identificar las regiones auriculares que causan la fibrilación auricular y que, por tanto, son susceptibles de ser ablacionadas. Sin embargo, los métodos que se utilizan para calcular los potenciales epicárdicos a partir de señales en el torso requieren de un proceso de regularización muy sensible al ruido. Recientemente, se ha demostrado que el uso de registros superficiales en combinación con registros intracardiacos en métodos Bayesianos es más preciso que los métodos clásicos de regularización. La aplicabilidad clínica de este nuevo método depende de cuál sea la cantidad de registros intracavitarios necesarios para alcanzar una resolución precisa.

En este trabajo se han implementado diversos métodos de interpolación para el software Matlab®, con el fin de recuperar en primer lugar la totalidad de señales intracavitarias para después proceder con la reconstrucción de potenciales epicárdicos. Con ello se pretende reconstruir el problema inverso mediante el método Bayesiano utilizando un número reducido de señales intracavitarias, y conseguir con este método de reconstrucción una mayor precisión que el método clásico de Tikhonov.

Para ello será necesaria la implementación de diversos algoritmos de interpolación que permitan recuperar el número inicial de señales intracavitarias. A continuación, se procederá con la reconstrucción del problema inverso siguiendo el método Bayesiano. Finalmente se comparará la eficacia en este proceso de reconstrucción con la proporcionada por el método de Tikhonov con el número total de nodos.

Se han empleado modelos geométricos de torso y aurícula humana, así como 3 modelos matemáticos de señales intracavitarias, cada uno representando una actividad epicárdica distinta: ritmo sinusal (SR), fibrilación auricular simple (SAF) y fibrilación auricular compleja (CAF). El número de nodos que proporcionan señales intracavitarias ha ido disminuyéndose progresivamente desde el número inicial (2039), hasta una octava parte (255). Para estos 3 modelos se han empleado y comparado 2 lugares y 2 métodos de interpolación, así como 2 alternativas de ventanas temporales para proceder con el método Bayesiano. Esto ha dado lugar a 8 algoritmos distintos: interpolación realizada sobre el electrograma (EG) o sobre una matriz intermediaria creada en el método Bayesiano (matriz de covarianza); método de interpolación basado en el vecino más cercano, o en la segunda derivada espacial(Laplaciano);y finalmente simultaneidad temporal entre todos los nodos del modelo, o en tandas de 120 nodos.

Los resultados dependen del modelo matemático empleado. Para SR y SAF, el algoritmo que permite una mayor disminución de la actividad intracavitaria manteniendo o superando la eficacia de Tikhonov es el de interpolación sobre el EGM utilizando el Laplaciano, mientras que el modelo CAF presenta los mejores resultados con interpolación sobre el EGM mediante el vecino más cercano.

Palabras clave: aurícula humana, cartografía eléctrica no invasiva, fibrilación auricular, interpolación, potenciales epicárdicos, problema inverso, reconstrucción, regularización, señal intracavitaria, simulación computacional.

Resum

El treball final de màster proposat és un estudi centrat en l'evaluació de l'eficàcia del mètode Bayesiano per a reconstruir el problema invers que planteja la cartografia elèctrica no invasiva (ECGI), així com el nombre i posició de senyals intracavitàries que serien necessàries per al seu correcte funcionament.

L'ECGI permet identificar les regions auriculars que causen la fibril·lació auricular i que, per tant, són susceptibles de ser ablacionades. No obstant això, els mètodes que s'utilitzen per a calcular els potencials epicàrdics a partir de senyals en el tors requerixen d'un procés de regularització molt sensible al soroll. Recentment, s'ha demostrat que l'ús de registres superficials en combinació amb registres intracardíacs en mètodes Bayesianos és més precís que els mètodes clàssics de regularització. L'aplicabilitat clínica d'este nou mètode depén de quina siga la quantitat de registres intracavitaris necessaris per a aconseguir una resolució precisa.

En aquest treball s'han implementat diversos mètodes d'interpolació per al programari Matlab®, a fi de recuperar en primer lloc la totalitat de senyals intracavitàries per a després procedir amb la reconstrucció de potencials epicàrdics. Amb això es pretén reconstruir el problema invers per mitjà del mètode Bayesiano utilitzant un nombre reduït de senyals intracavitàries, i aconseguir amb aquest mètode de reconstrucció una major precisió que el mètode clàssic de Tikhonov.

Per a això será necessària la implementació de diversos algoritmes d'interpolació que permeten recuperar el nombre inicial de senyals intracavitàries. A continuació, es procedirà amb la reconstrucció del problema invers seguint el mètode Bayesiano. Finalment es comparará l'eficàcia d'aquest procés de reconstrucció amb la proporcionada pel mètode de Tikhonov amb el nombre total de nodes.

S'han empleat models geomètrics de tors i aurícula humana, així com 3 models matemàtics de senyals intracavitàries, cada un representant una activitat epicàrdica distinta: ritme sinusal (SR), fibril·lació auricular simple (SAF) i fibril·lació auricular complexa (CAF). El nombre de nodes que proporcionen senyals intracavitàries ha anat disminuint-se progressivament des del nombre inicial (2039), fins una octava part (255). Per a aquestos 3 models s'han empleat i comparat 2 llocs i 2 mètodes d'interpolació, així com 2 alternatives de finestres temporals per a procedir amb el mètode Bayesiano. Açò ha donat lloc a 8 algoritmes distints: interpolació realitzada sobre l'electrograma (EG) o sobre una matriu intermediària creada en el mètode Bayesiano (matriu de covariança); mètode d'interpolació basat en el veí més pròxim, o en la segona derivada espacial (Laplaciano); i finalment simultaneïtat temporal entre tots elsnodes del model, o en tandes de 120 nodes.

Els resultats depenen del model matemàtic empleat. Per a SR i SAF, l'algoritme que permet una major disminució de l'activitat intracavitària mantenint o superant l'eficàcia de Tikhonov és el d'interpolació sobre l'EGM utilitzant el Laplaciano, mentres que el model CAF presenta els millors resultats amb interpolació sobre l'EGM per mitjà del veí més pròxim.

Paraules clau: Aurícula humana, cartografia elèctrica no invasiva, fibril·lació auricular, interpolació, potencials epicárdicos, problema invers, reconstrucció, regularització, señal intracavitària, simulació computacional.

Abstract

This Master's final project evaluates the efficiency of Bayes' regularization to reconstruct the inverse problem of electrocardiographic imaging (ECGI), as well as the number and position of intracavitary signals which are needed to achieve a successful performance in the reconstruction.

ECGI is a useful tool for identifying atrial regions which cause atrial fibrillation, and whose ablation terminates the fibrillation episode. However, the methods which are used to calculate epicardial potentials from torso signals require a regularization process which is very sensitive to noise. Recently, mathematical models of atrial fibrillation have been used to demonstrate that the combination of surface and intracardiac signals used in Bayes' regularization is more accurate than classical methods. The clinical application of this new method depends on the amount of intracavitary signals which are needed to achieve an adequate resolution in the reconstruction process.

This work implements several interpolation methods for Matlab®'s software, with the purpose of recovering the total intracavitary information to proceed with the reconstruction of epicardial potentials. The aim is to solve the inverse problem using Bayes' regularization with a reduced number of intracavitary signals, and to achieve with this reconstruction process a better precision than the classical Tikhonov regularization with the total number of nodes.

To do so, several interpolation algorithms have been implemented to recover the complete signal with the initial number of nodes. Then, the inverse problem was solved using Bayes' regularization. Finally, the accuracy of this reconstruction process was compared with that obtained by Tikhonov's regularization with the total number of nodes.

Geometrical models of human torso and atria have been used, as well as 3 mathematical models of intracavitary signals, each one representing a different epicardial activity: sinus rhythm (SR), simple atrial fibrillation (SAF) and complex atrial fibrillation (CAF). The number of nodes which provide intracavitary signals has been progressively reduced from the initial number (2039) to an eighth fraction (255). For these 3 models, the interpolation has been performed if 2 different places, using 2 different methods, as well as 2 alternative time windows to proceed with Bayes' regularization. Therefore, 8 different algorithms have been implemented and compared: interpolation performed in the electrogram (EG), or in an intermediate matrix used in Bayes' regularization (covariance matrix); interpolation method based on Nearest Neighbour (NN), or second spatial derivative (Laplacian); and finally temporal simultaneity between all nodes in the model, or in sets of 120 nodes.

The interpolation approach with the best performance depends on the mathematical model used. For SR and SAF, the algorithm which allows reducing the initial intracavitary activity the most, while at the same time maintaining or surpassing Tikhonov's performance is EGM Laplacian interpolation. CAF's model however, shows better results for EGM Nearest Neighbour interpolation method.

Keywords: Atrial fibrillation, computational simulation, electrocardiographic imaging, epicardial potentials, human atria, interpolation, intracavitary signal, inverse problem, reconstruction, regularization.

Acronyms

AF	Atrial Fibrillation
AV	Atrioventricular node
BEM	Boundary Element Method
BSPM	Body Surface Potential Mapping
CAF	Complex Atrial Fibrillation
CC	Pearson's Correlation coefficient
CCn	Spatial Correlation Coefficient
CCt	Temporal Correlation Coefficient
CRESO	Composite Residual and Smoothing Operator
CT	Computed Tomography
Cx	Epicardial Potentials' Covariance Matrix
DF	Dominant Frequency
DSVD	Damped Singular Value Decomposition
ECG	Electrocardiogram
ECGI	Electrocardiographic Imaging
EGM	Electrogram
FEM	Finite Element Method
FDM	Finite Difference Method
FVM	Finite Volume Method
FIRM	Focal Impulse Rotor Modulation
FRAW	Free Right Atrial Wall
GMRES	Generalized Minimal Residual
GS	Greensite
LA	Left Atrium
LV	Left Ventricle
MD	Mode Distance
NN	Nearest Neighbour
RA	Right Atrium
RDFE	Relative Dominant Frequency Error
RDMSn	Spatial Relative Difference Measurement Star
RDMSt	Temporal Relative Difference Measurement Star
RSPV	Right Superior Pulmonary Vein
RV	Right Ventricle
SA	Sinoatrial Node
SAF	Simple Atrial Fibrillation
SMF	Spatial Mass Function
SNR	Signal to Noise Ratio
SP	Singularity Point
SR	Sinus Rhythm
TSVD	Truncated Singular Value Decomposition
TV	Total Variation
WCT	Wilson Central Terminal

WOI	Weighted Over-estimation Indicator
WUI	Weighted Under-estimation Indicator

Contents of the Master's final project

- MASTER'S PROJECT

- BUDGET

UNIVERSITAT POLITÈCNICA DE VALÈNCIA

ESCUELA TÉCNICA SUPERIOR INGENIEROS INDUSTRIALES VALENCIA

MASTER'S PROJECT

Index of Contents

List of Figures

Index of Tables

1. Introduction

Most of the advances achieved in medicine in the last centuries have been possible due to the development of engineering technologies. The growth of basic scientific research has led to the appearance of new instruments, devices and techniques which have been applied in the medical field, especially in the diagnosis and treatment of diseases. These developments have defined a new concept of medicine, which implies that nowadays health diseases must be addressed both by doctors and engineers.

Cardiac diseases have been one of the most deeply studied since the discovery of electrocardiography by Einthoven [Einthoven 1906], which allowed to evaluate the heart's electrical activity and to establish links with a given cardiac disease. This relationship between a disturbance in the cardiac electrical activity and the appearance of pathology becomes evident in cardiac arrhythmias. Regarding these arrhythmias, atrial fibrillation (AF) is the most frequent type in the clinical practice. There are several treatments for AF, however, the optimum one requires the precise study of the atrial electrical activity to localize the source of the arrhythmia.

1.1. Motivation

Mapping technologies make use of catheters to record the atrial electrical activity once inside the atrial chamber. The use of such systems has allowed a better understanding of the nature of AF. To this respect, it has been discovered that certain regions in the atrial tissue act as sources of the fibrillation episode, causing the abnormal electrical activity in the rest of the atria. This theory has led to the appearance of new AF treatments which focus on the isolation of the fibrillation sources and have demonstrated to be very successful in some pilot studies [Narayan 2012, Haissaguerre 2014, Atienza 2014].

Despite the usefulness of mapping systems, distance between electrodes results in a loss of information from the atrial electrical activity. Also, the recording is only carried out once a patient has been diagnosed with AF and selected for an ablation procedure. These drawbacks have promoted the development of non-invasive technologies to map the atria, with the purpose of identifying AF sources to plan the ablation procedure in advance. These technologies use Body Surface Potential Mapping (BSPM) systems to record the atrial electrical activity which is projected on the torso [Guillem 2009, Guillem 2013]. These recordings can then be used to reconstruct the atrial activity by means of the electrocardiographic imaging (ECGI) technique [Messinger-Raport 1990]. This reconstruction process can be used to identify AF patterns as well as its sources, which in turn can serve to guide ablation procedures.

The reconstruction of epicardial potentials from signals recorded at the torso surface requires a regularization process which is very sensitive to noise. Several regularization methods have been compared using mathematical models of atrial fibrillation [Figuera 2016], demonstrating that Bayes

regularization is more precise than the results provided by the classical Tikhonov regularization. Bayesian Maximum a Posteriori Estimation is a regularization method which uses a priori information in the reconstruction process in combination with surface recordings. The a priori information used takes the form of a spatial covariance matrix between epicardial potentials recorded in the atria.

To this extent, the solution of the problem posed by ECGI previously requires the computation of the torso potentials provided the epicardial signal, thereby solving the forward problem. This step is crucial for establishing the mathematical relationship between atria and torso geometries needed to solve the inverse problem. Then, epicardial potentials can be estimated from the computed torso projections. Taking this into account, the clinical application of this new Bayesian regularization depends on the number of intracavitary recordings which are needed to reach the optimum precision in the reconstruction of epicardial activity. All in all, the minimum amount of spatial information to outperform Tikhonov method using Bayes regularization to solve the inverse problem needs to be determined.

1.2. Objectives

The hypothesis which was used to design this work is based on the assumption that Bayes regularization method is able to reconstruct the inverse problem of electrocardiography with more accuracy than the classical Tikhonov regularization without needing a large number of intracavitary signals.

Therefore, this work evaluates the efficiency of Bayes regularization method with a reduced number of intracavitary information in the reconstruction of the inverse problem. The target will be to establish the specific characteristics of the signals which are needed to achieve a correct performance, such as the number and positioning of intracavitary signals. As a reference, the classical Tikhonov's regularization method with the complete spatial information is used.

To do so, geometrical models of human atria and torso have been used, as well as 3 different mathematical models of epicardial activity, each one of them representing the most significant scenarios involved in the development of AF: sinus rhythm (SR), simple atrial fibrillation (SAF) and complex atrial fibrillation (CAF). The workflow to achieve the mentioned objective can be divided as follows:

- To evaluate the performance of all variants of Tikhonov regularization in solving the inverse problem with the complete spatial information from the models. Then, to choose the best for comparison purposes.
- To evaluate the reconstruction of epicardial activity provided all the intracavitary signals from the models, through Bayes regularization method. To compare results between Tikhonov and Bayes performance and confirm the hypothesis that Bayesian regularizations are superior.
- To progressively reduce the number of intracavitary information from the mathematical models. To do so, a criterion for node inclusion or exclusion within the models will have to be established.

- To interpolate the signals from the nodes which have been excluded so as to recover the initially provided spatial information. To so do, several approaches will be applied, differing in the place of interpolation, method of interpolation, as well as simultaneity or non-simultaneity between signals from different sets of 120 nodes in the model.
- To solve the forward problem, obtaining the mathematical relationship between the epicardial activity and torso potentials, as well as the projection on the body surface.
- To solve the inverse problem using Bayes regularization method, reconstructing the epicardial potentials with the original number of initially provided intracavitary signals.
- To compare the accuracy of this new method with the results provided by Tikhonov regularization algorithm with the whole set of nodes.
- To determine the minimum number of nodes needed for each model, as well as the optimum interpolation algorithm, which are needed to outperform Tikhonov regularization with the initial number of nodes.

2. State of the art

2.1. Atrial fibrillation

2.1.1. Cardiac anatomy and electrical activity

The heart is the main organ of the circulatory system, it is located at the centre of the thoracic cavity and its function is to pump oxygenated blood to all the cells in the body. It is formed by muscle tissue called myocardium and it is divided into 4 cavities: Left Atrium (LA), Right Atrium (RA), Left Ventricle (LV) and Right Ventricle (RV). Blood is transported to and from the heart through veins and arteries, respectively. The superior and inferior vena cava carry deoxygenated blood from the body to the RA. The pulmonary artery carries deoxygenated blood from the RV towards the lungs so that it can take up oxygen. The pulmonary veins then take oxygenated blood from the lungs to the LA. Finally, the aorta transports oxygen-rich blood from the LV to the systemic circulation. This process is illustrated in figure 2.1.

The atrial and ventricular cavities are separated by valves: the tricuspid valve is between the RA and RV, and the mitral valve separates LA and LV. Together with these two valves, there are also others which, as shown in figure 2.1, act as a barrier between ventricles and arteries: the pulmonary valve separating the pulmonary artery from the RV, and the aortic valve, located between the aorta and the LV. All in all, the function of these valves is to prevent blood retraction. Finally, the internal layer of the cavities is called endocardium, while the outer is known as epicardium.

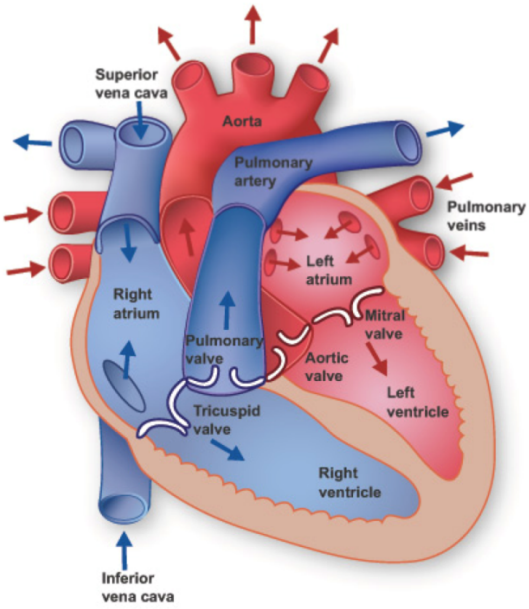

Figure 2.1: Cardiac anatomy.
Location of atrial cavities and valves within the heart. Extracted from: http://www.texasheart.org/HIC/Anatomy/anatomy2.cfm

The pumping activity of the heart is achieved through the contractions of the myocardium. These contractions appear due to the changes in transmembrane electric potentials taking place in each individual cell, which is generally triggered by the sinus node or sinoatrial (SA) node located in the RA. This process generates a signal which can be measured at the torso known as electrocardiogram (ECG).

The electrical signal propagates from the SA to the RA and LA provoking atrialdepolarization and subsequent contraction. This travelling impulse is reflected on the P wave of the ECG recording. The signal then reaches the atrioventricular (AV) node and experiences a delay which allows the ventricles to fill up with blood, which is observed in the ECG as the transition between the P and Q waves. The propagation is then produced towards the bundle of His and then to the right and left bundle branches, provoking the depolarization and contraction of the ventricles, leading to the ejection of blood to the whole body. This is represented in the QRS complex of the ECG. Finally, the ventricles repolarise and return to their resting state, represented in the T wave of the ECG. The whole process is illustrated in figure 2.2.

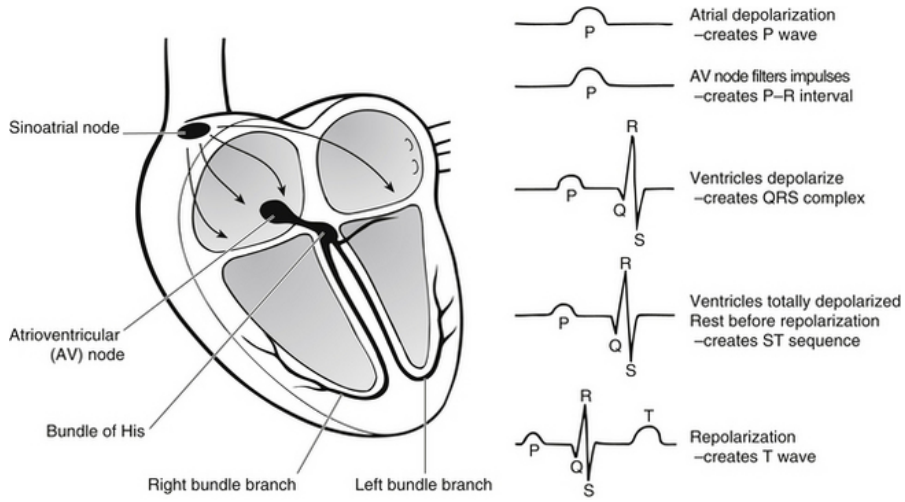

Figure 2.2: Cardiac electrical activity.
Propagation of the electrical signal within the heart and ECG recording resulting from it. Extracted from: https://clinicalgate.com/wp-content/uploads/2015/02/B9780702043154000279_f27-08-9780702043154.jpg

The electrical signal originating at the SA is the result of an autonomous stimulus which takes place from 60 to 100 times a minute in healthy patients. This normal rhythm is referred to as sinus rhythm. However, when the cardiac activation rate is out of this range, the rhythm is referred to as a cardiac arrhythmia.

2.1.2. Initiation and maintenance of atrial fibrillation

Atrial fibrillation is a supraventricular cardiac arrhythmia which originates in the atrial cavities of the heart. The cause underlying AF is the abnormal activation and propagation of electrical waves within the atria. This chaotic electrical activity implies an inefficient pumping of blood from the atria to the ventricles.

Atrial fibrillation may not cause death directly but it leads to the appearance of chronic patients. The inefficient pumping of blood between the atria and ventricles can result in the formation of clots which can travel to other parts of the body. Therefore, patients suffering from this condition generally have an increased risk of stroke and heart failure, which may lead, eventually, to death. There are many therapies to treat this condition, including the administration of anti-arrhythmic drugs, electrical cardioversion and catheter ablation [Guillem 2016]. Among the proposed therapies, catheter ablation seems to be the optimal treatment [Dobrev 2010, Wilber 2010, Parkash 2011].

The traditional treatment for AF focused on the isolation of the pulmonary veins, since they have been identified as anatomical regions prone to initiating atrial fibrillation [Haissaguerre 1998]. However, other approaches have been recently used, which are based on the identification and isolation of specific sources which play a role in activating and maintaining atrial fibrillation. This novel treatment has shown to be more effective than conventional therapies used for AF [Narayan 2012, Haissaguerre 2014].

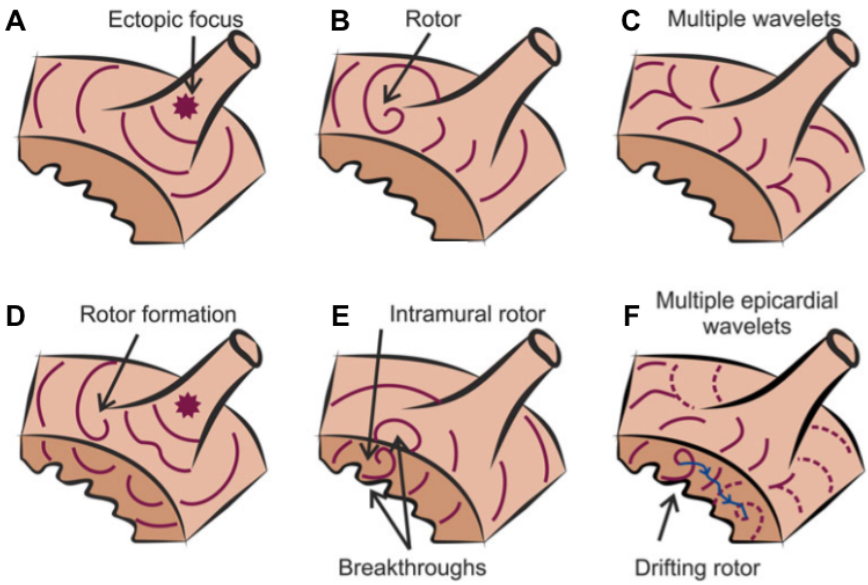

Figure 2.3: Theories for atrial fibrillation initiation and maintenance.
(A*) Ectopic focus (B) Rotors (C) Multiple wavelets. Co-existence of the different theories (D)Rotor appearance due to a wavebreak near an ectopic focus or (E)endocardial or epicardial breakthroughs. Also, rotor drift can lead to the appearance of wavelets (from Guillem et al. 2016).*

The specific cause of atrial fibrillation is still a topic of debate. Researchers have proposed many theories with respect to the mechanisms which lead to the initiation and maintenance of this

condition, illustrated in figure 2.3. Some argue that the cause lies in the existence of multiple wavelets which propagate randomly within the atria [Moe 1962]. As shown in figure 2.3C, this theory sustains that the presence of multiple wavelets leads to the characteristic disorganized electrical activity of fibrillation events, without the need of any arrhythmic trigger. Other researchers claim that the existence of electrically organized regions is the ones responsible for the fibrillation episode. These sources are classified either as ectopic foci or as rotors [Jais 1997, Jalife 2002], shown in figures 2.3A and 2.3B, respectively. Rotors are also termed functional re-entries [Cabo 1996] since they tend to surround atrial regions without exciting them, showing a characteristic action potential propagation wavefront.

These three theories, although they might seem contradictory at first, can actually be consistent with one another. As shown in figure 2.3D, an ectopic focus may cause a wavefront break in the vecinity, thereby leading to the formation of a rotor. Also, rotors with an intramural localization could be the cause of endocardial or epicardial breakthroughs, illustrated in figure 2.3E. Finally, in figure 2.3F it is shown that a drifting rotor could be the cause of multiple wavelets. Consequently, the rotor theory seems to be the most likely mechanism which causes and maintains atrial fibrillation.

2.1.3. Rotors

Rotors have been deeply studied in order to understand their nature, characteristics and implication in atrial fibrillation episodes. Langendorff-perfused isolated hearts, optical mapping technologies, as well as the use of mathematical models have helped to reach important findings with respect to rotors [Guillem 2016]. The most relevant features are, among others, the correlation between a rotor's rotation period and the dominant frequencies (DFs) at their localization [Mandapati 2000]. Other researchers have been able to identify not only the main characteristics of rotors, but also the region within the atria which has more probability of containing a rotor. To this respect, rotors have been detected with more frequency in the left atrium (LA).

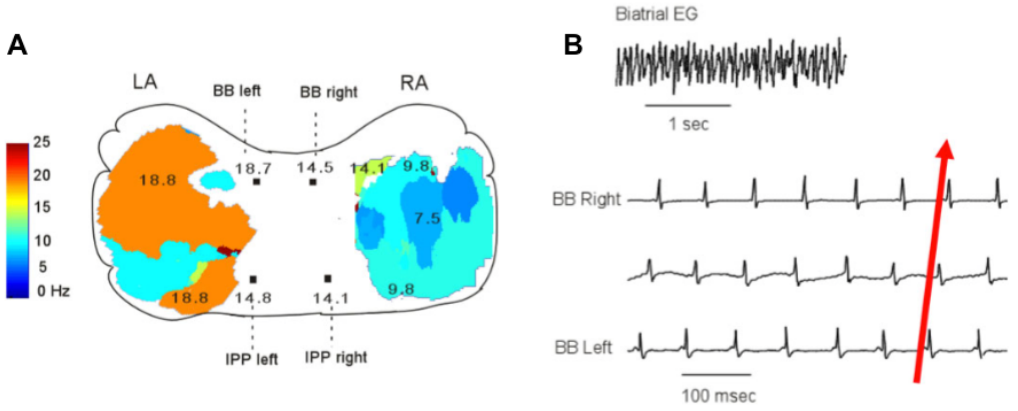

Figure 2.4: Dominant frequency distribution within the atria due to a rotor.
(A) Decrease in dominant frequency between the left and right atria. (B) Directionality of activation from the left to the right atrium. (From Mansour et al. 2001)

Since the presence of rotors is associated to the appearance of DF regions, the specific localization of a rotor at the LA generates a decreasing activation frequency gradient between the LA and RA, as illustrated in figure 2.4A. Furthermore, this also implies a propagation of the electrical wavefront from the LA to the RA [Mandapati 2000, Mansour 2001], as seen in figure 2.4B.

Regarding the propagation of rotors, two different patterns have been described. On the one hand, rotors can meander around a fixed region [Guillem 2016]. This propagation of rotors can be analysed by using the Hilbert transform and representing a phase map of action potential recordings [Zlochiver 2008], as illustrated in figure 2.5A. This phase map representation is a useful tool which serves to identify the electrical wavefront and its propagation direction, as well as singularity points (SPs), which are points within the wave to which all phases converge [Guillem 2016]. On the other hand, rotors can also show a propagation pattern within the atria which has been described as a drift through a given distance. In figure 2.5B,the fractionation of the electrogram (EGM) recordings during rotor drift is shown. This is explained by the fact that the local drifting direction changes with each beat and also by the Doppler Effect, which appears due to the acceleration of the wavefront ahead of the rotor [Guillem 2016].

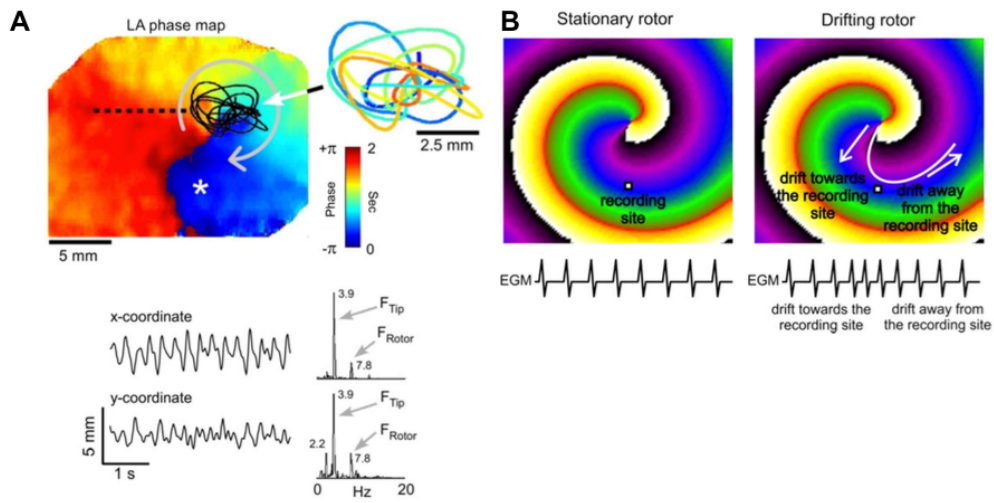

Figure 2.5: Phase maps and propagation patterns of rotors.
(A) Phase map of the left atrium of a sheep during atrial fibrillation. Trajectory of the tip and spectral peaks (from Zlochiver et al. 2008). (B) Comparison of the variation in activation times between a stationary and a drifting rotor (from Guillem et al. 2016)

To sum up, the most relevant features of rotors that have been described are one the one hand, the high frequency at the region where they are located, on the other hand the meandering or drifting propagation, and finally, the usefulness of phase maps to characterize them. The presence of DF zones, as well as the propagating rotors are responsible for the appearance of atrial fibrillation and consequently, irregular EGMs.

2.2. Mapping technologies for atrial fibrillation

2.2.1. Introduction

Electrocardiographic (ECG) signals recorded on the torso represent the electrical activity of the heart which is responsible for the efficient pumping of oxygenated blood to the whole body. Despite the simplicity of a healthy ECG signal, the study of the pattern can reveal important characteristics of the heart's activity. These recordings have been extensively used to diagnose cardiac diseases, especially those in which the electrical propagation within the heart is altered, such as atrial fibrillation.

The ECG signal is recorded by using 3 electrodes placed on the right arm, left arm and left foot, forming the so-called Einthoven's triangle [Einthoven 1906]. From these recordings, 6 different leads are calculated. The first 3 are computed as the potential difference between each pair of leads. The other 3 are augmented derivations (aV_R, aV_L, aV_F), and are calculated as the difference between each lead and the average of the remaining two leads. Then, six additional electrodes are placed on the anterior and left side of the chest and measured with respect to the Wilson Central Terminal (WCT). Therefore, the system, which is illustrated in figure 2.6, includes a total of 12 leads in the recording of the ECG signal.

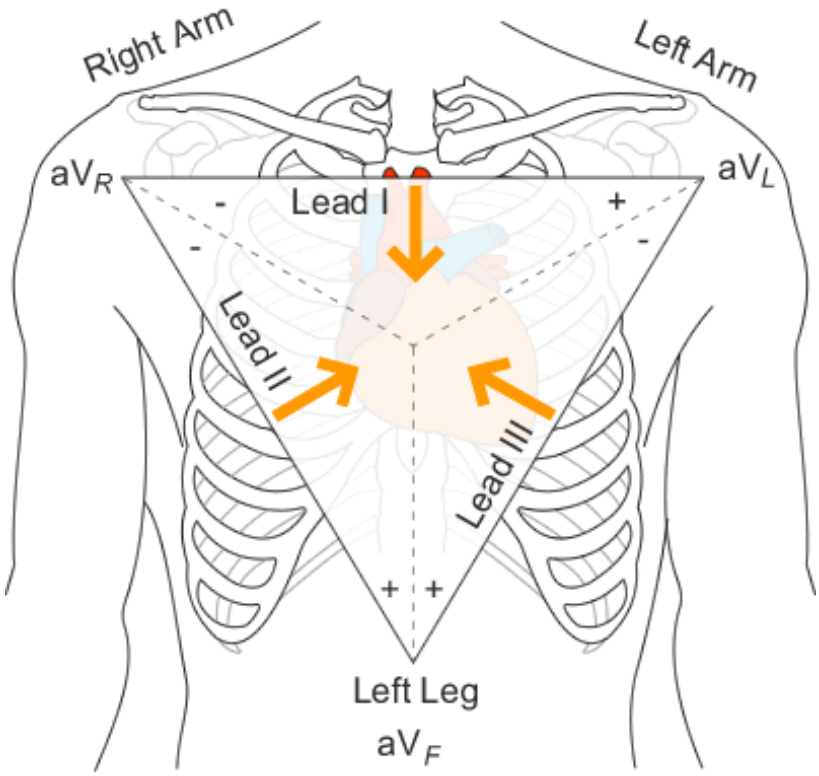

Figure 2.6: Traditional ECG recording system defined by Einthoven.
Extracted from: http://www.nottingham.ac.uk/nursing/practice/resources/cardiology/images/bipolar_triangle02.gif

Atrial fibrillation can be detected using this system and analysing the recorded ECG signal. The main features of an ECG signal from a patient suffering AF are, on the one hand, the absence of the P wave, representing atrial depolarization and contraction, as depicted in figure 2.7. On the other hand, the signal tends to be irregular and there is heart rate variability, this is observed through the RR intervals, which are not constant [Guillem 2008].

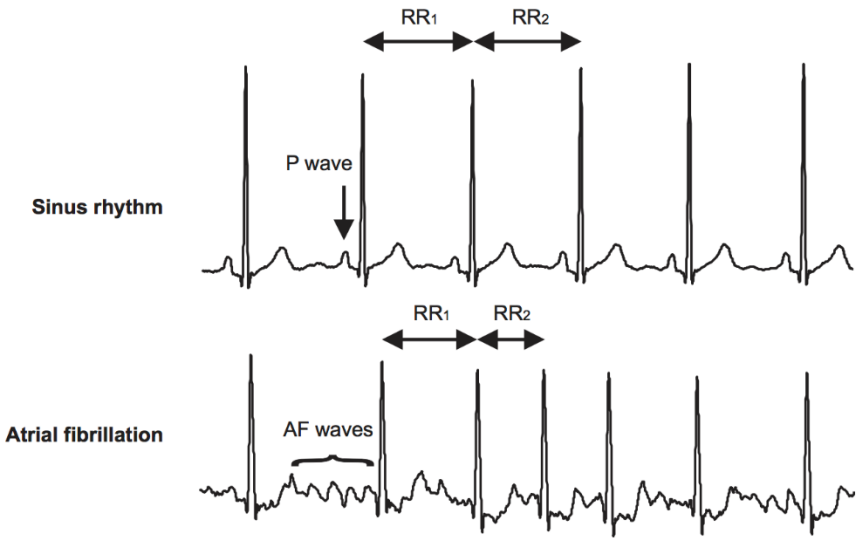

Figure 2.7: Differences in ECG between sinus rhythm and atrial fibrillation (from Guillem 2008).

Although the 12-lead ECG signal can be used to detect the global atrial fibrillation episode, the local characterization cannot be performed using this technique [Guillem 2013] due to the complexity of the fibrillation process and the limitations in recording both atria [Lankveld 2014].

2.2.2. Invasive mapping technologies

The complex nature of atrial fibrillation requires technologies different from the classical 12-lead ECG to be able to characterize the disease accurately. As described previously, rotors have been discovered to play an important role in initiating and maintaining AF. Therefore, the recording of AF episodes has been closely linked to the identification of rotors responsible for the fibrillation process.

The initial invasive mapping technology which was used to identify rotors was based on sequential or small regional mapping of a small number of sites. The technique for predicting the presence of rotors consisted on using the sequential recordings at 9 different sites. These measurements were then used to establish relationships between those regions having a high dominant frequency, fractionation, as well as a certain temporal regularity and stability [Berenfeld 2007]. This technology allowed observing the frequent localization of regions with high dominant frequency near the pulmonary veins, as well as a hierarchical pattern of activation rates [Sanders 2005]. Another

important finding with this technology was the effect of tissue remodelling in AF, which was shown to modify the dynamics of rotors [Atienza 2009], making more difficult the termination of the fibrillation event.

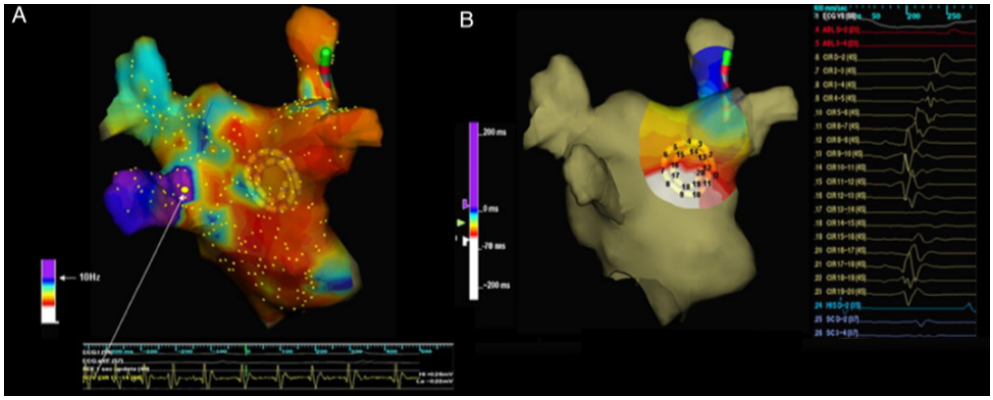

Figure 2.8: Atrial maps from multipolar spiral catheters with 20 electrodes.
(A) Dominant frequency map of the left atrium. (B) Activation map of the posterior left atrium showing an incoming wave travelling from the high dominant frequency site at the left inferior pulmonary vein (white) to the right (purple), which shows the relation between activation patterns and dominant frequency sites (from Atienza et al. 2011).

The second invasive mapping technology was based on the use of a multipolar spiral catheter with 20 electrodes. This technique allowed creatingfrequency and activation maps of the atria, as shown in figures 2.8A and 2.8B, respectively. These maps were able to illustrate, for the first time, rotational activity in the atria due to the presence of rotors [Atienza 2011]. However, the reduced number of electrodes implies that there is a high percentage of atrial tissue that is not being recorded. Consequently, this translates to an underestimation of the number of rotors that are being detected.

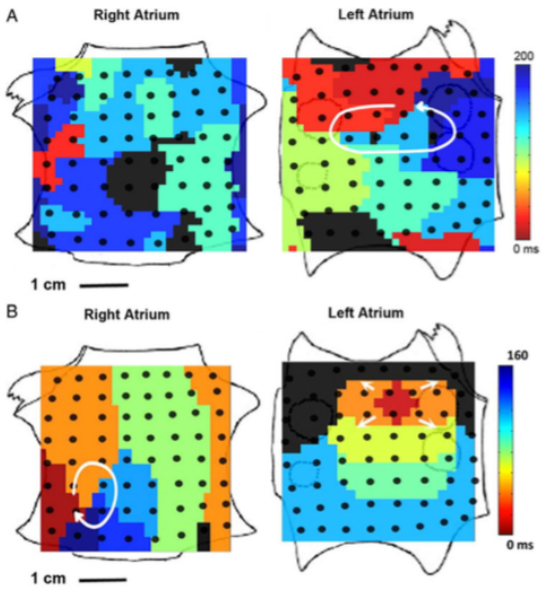

Figure 2.9: FIRM mapping of rotors during atrial fibrillation on two different patients.
(A) FIRM mapping of rotors for patient 1 and (B) patient 2 (from Narayan et al. 2012)

The limitations presented by the use of the previously described catheter lead to the use of a 64-pole catheter and phase based signal processing, giving rise to a technique known as focal impulse rotor modulation (FIRM) mapping [Narayan 2012]. The increased number of electrodes allows to map the entire atria. This is turn can enable the construction of activation maps, as illustrated in figures 2.9A and 2.9B, and consequently the observation of rotors or ectopic focus which act as sources for atrial fibrillation.

2.2.3. Non-invasive mapping technologies

Invasive mapping technologies for atrial fibrillation have shown to be useful tools for characterizing the electrical activity within the atria. However, non-invasive technologies are desired to be able to localize atrial fibrillation sources. In this sense, using this type of technology, the specific atrial activity of a patient could be observed in a non-invasive manner, rotors could be identified, and the ablation procedures could be planned in advance.

The most extensively used non-invasive technologies for mapping atrial fibrillation are Body Surface Potential Mapping (BSPM) and inverse-solution Electrocardiographic Imaging (ECGI) systems. BSPM makes use of a vest containing from 32 to 256 electrodes, which records the patient's ECG on the torso surface. The computation of the dominant frequency from these recordings has been shown to correlate with the ones in the atria [Guillem 2013], as shown in figures 2.10A and 2.10B, proving its usefulness in detecting atrial fibrillation episodes. Also, the use of this technology has allowed the identification of unstable and short re-entries by means of creating phase maps from TQ intervals of 64 surface potentials [Guillem 2009].

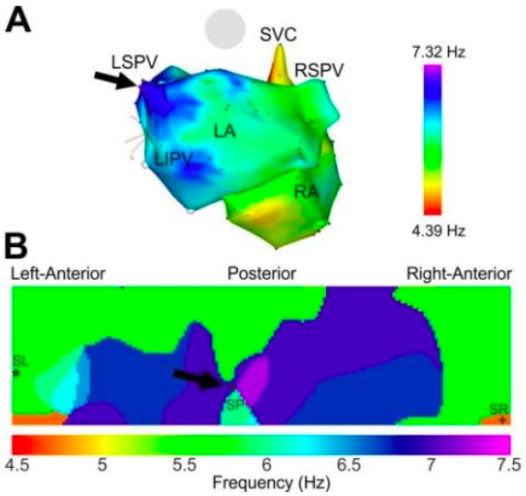

Figure 2.10: Correlation between intra-cardiac and BSPM dominant frequency maps.
(A) Dominant frequency map of the atria and (B) Dominant frequency map of the torso by BSPM (from Guillem et al. 2013).

ECGI allows to non-invasively obtain the atrial activity provided torso measurements. To do so, it makes use of a patient's torso and atria geometries provided by the segmentation of Computed Tomography (CT) images, or models of torso and atria. Recordings provided by BSPM are then used

to reconstruct the electrical activity of the atria. The reconstruction process requires the use of the inverse solution to compute the virtual potentials on the epicardial layer of the atria from measurements on the torso [Cuculich 2010], giving rise to the inverse problem of electrocardiography. The forward problem would be the computation of the torso's electric potentials provided the activity in the atria.

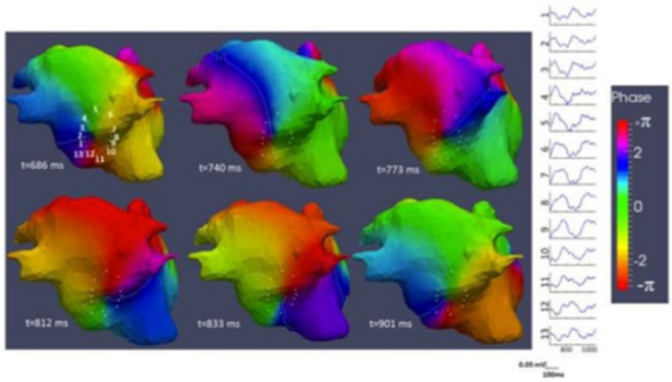

Figure 2.11: Atrialphase map of the reconstructed signal by ECGI.
Identification of atrial fibrillation sources by ECGI (from Haissaguerre et al. 2014)

The computed virtual potentials, estimated by means of ECGI, can be used to build phase and activation maps during atrial fibrillation, as illustrated in figure 2.11. This process allows the identification of wavelets and rotors, which serve to guide ablation procedures. Nevertheless, this process is conditioned by the loss of information from signals propagating from the atria to the torso, which gives rise to a problem that is ill-posed [Rodrigo 2014].

The ill-conditioned problem posed by ECGI requires regularization techniques to be able to perform the reconstruction of epicardial potentials from torso measurements. The use of such regularization methods has allowed to identify activation sequences, arrhythmogenic substrates and regions with high dominant frequencies within the atria [Milanic 2014, Van Dam 2009, Rudy 2013, Pedrón-Torrecilla 2016]. Furthermore, the use of signal processing such as filtering, wavelet transform and phase mapping has allowed researchers to observe unstable rotors and pulmonary vein foci [Haissaguerre 2013]. Although the technique has not been yet validated for identifying rotors using simultaneous panoramic intracardiac mapping, it is a valid technique for high dominant frequency sites and dominant frequency gradients [Guillem 2013].

2.3. Models in atrial fibrillation

The advance of technology has allowed to use mathematical models in computer simulations to study cardiac arrhythmias. This has provided a deeper insight into the analysis of different pathologic conditions. The better understanding of atrial fibrillation in particular has been incredibly enhanced by the use of such simulations. In order to do so, different models and geometries of the atria and torso have been developed.

2.3.1. Atrial models

Several models of the atria have been developed in order to study the initiation and maintenance of atrial fibrillation. The building of these models aims at fitting the electrical activity of cardiac myocytes into the three dimensional geometry of the atria. The facts that have been considered in creating realistic tissue properties for atria models can be summarized as follows:

- The potential difference between adjacent myocytes leads to the flow of ionic currents through gap junctions that connect neighbouring cells.
- The inward flow of current into these cells causes their depolarization.

These tissue properties can be simulated by means of a reaction-diffusion model, which takes into account not only the inward and outward flow of currents through each cell, but also the anisotropy of the medium. Regarding the reaction-diffusion models which have been built, they can be classified into two categories, depending on the considerations taken:

- Monodomain model: only takes into account the cells membrane potential in the electrical propagation and despite their simplicity, have been very useful [Dössel 2012].
- Bidomain model: considers the differences between the intracellular ionic concentrations and potentials and the extracellular ones [Trayanova 2006]. This model is more complex to solve but allows the study of other phenomena.

Once the electrical properties of the atrial tissue have been defined, they have to be fitted into the geometry of the atria in order to model the organ's activity. For this purpose, different geometries have been developed, which can be broadly classified as follows:

- Non-inclusion of the atrial wall: these models neglect the effect of the atrial wall thickness, and they are built with triangular meshes and a single face [Jacquement 2006].
- Inclusion of the atrial wall: these models take into account the atrial wall thickness, and they are built by tetrahedrons or cubes by means of extracting information from medical images [Krueger 2011, Aslanidi 2011]. Also, they may include anisotropic properties or, as shown in figure 2.12, they may divide the model into regions with different properties [Dössel 2012, Tobón 2013].

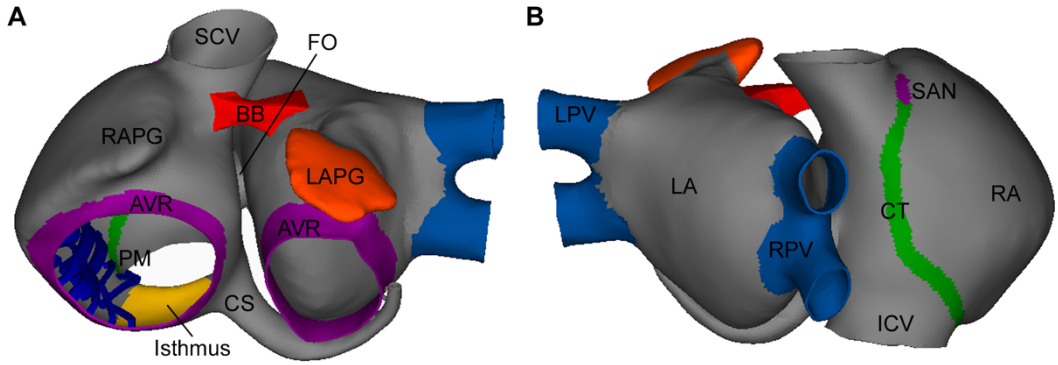

Figure 2.12: 3D Atrial model including areas with different conductivities.
(A) Frontal and (B) Dorsal view of a 3D atrial model used to study atrial fibrillation. Coloured regions represent different conductivities and tissue heterogeneity. (Extracted from Tobón et al. 2013)

2.3.2. Torso models

The activity of the atria gives rise to the appearance of an electric potential on the torso, which can be obtained by solving the forward problem if a torso model is provided. This forward problem can be described in the following manner:

$$Y = A \cdot X \tag{1}$$

where Y is the potential at the torso created by the electrical activity of the atria (X) and A is a transfer matrix which depends on the geometry of both atria and torso. Since the electric potentials which are projected on the torso due to the atrial activity can be directly measured, solving the forward problem does not have a straightforward application. However, it is an essential step for solving the inverse problem posed by ECGI, since the reconstruction process requires knowing the transfer matrix A relating atria and torso electrical activity.

The problem poses a set of differential equations which can be solved with several numerical approaches which differ in the way the torso is treated:

- Finite difference method (FDM): this method divides the torso into a set of nodes and it aims to solve Kirchoff's law at each node. To do so, it uses tissue conductivity and anisotropy to determine the conductivity between de nodes at the torso [Walker 1987]. The results obtained are the electric potentials both at the torso surface and entire volume.
- Finite element method (FEM): this method divides the torso into volume elements and uses continuous functions to solve the equations in each one of them, producing results with high accuracy [Fischer 2000].
- Finite volume method (FVM): this method also treats the torso as a set of volume elements, and the equations are solved for a point located at the centre of each of them [Abboud 1994].

- Boundary elements method (BEM): this method uses Green's theorem and solves the equations for surface elements instead of volume elements. The use of this method is illustrated in figure 2.13, and it requires the volumes inside each surface to be homogeneous and isotropic [Seger 2005].

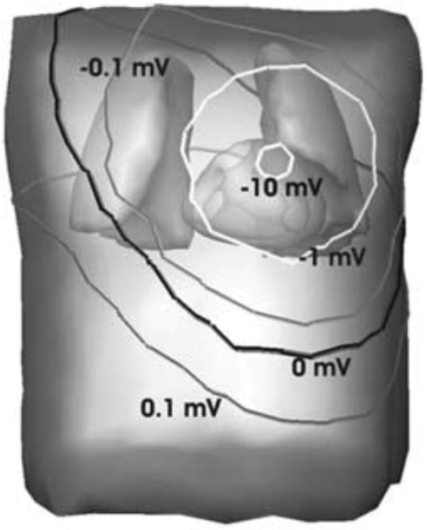

Figure 2.13: Torso model.
Computed body surface potentials using BEM method (Extracted from Seger et al. 2005)

2.4. Regularization methods to solve the inverse problem of electrocardiography

2.4.1. Inverse problem formulation

The electrical activity in the atria gives rise to the appearance of electric potentials on the torso which result from the projection of such activity. The inverse problem of electrocardiography consists on estimating the source epicardial activity (X) given the measurements of torso potentials (Y) and the transfer matrix (A) relating atria and torso geometries. The solution requires the prior knowledge of the transfer matrix A, which is obtained by first solving the forward problem through the methods described in the previous section. Then, the inverse problem aims at solving the following equation:

$$X = A^{-1} \cdot Y \tag{2}$$

This problem is ill-conditioned, since the values of the resulting epicardial potentials are very sensitive to perturbations in the initial conditions, for example changes in geometries or the presence of electrical noise in the torso potentials. Also, the transfer matrix A is either non-invertible or its inverse form contains so many errors that the computation of the epicardial potentials is highly inaccurate.

Traditionally, two main approaches have been implemented to solve this inverse problem. The first one consists on numeric regularization methods where atrial activity is reconstructed in form of surface or volumetric sources and accepts all possible potential distributions [Wang 2010]. The second approach limits the solution to certain a priori constraints which are chosen with different basis [Rahimi 2016]. However, for the case of atrial fibrillation, electrophysiological constraints cannot be established, therefore, the first approach is the most used, where the reconstruction of electrical potentials does not imply any restriction [Wang 2010, Pedrón-Torrecilla 2016].

2.4.2. Regularization parameter

Numerical regularization methods aim to modify the matrix A which relates atria and torso geometries in order to obtain an invertible matrix, which implies that the solution will incorporate certain errors. This regularization process depends on a regularization parameter(λ) which helps to choose a value that will imply the smallest amount of errors introduced into the solution due to the implementation of the method. Therefore, the regularization parameter controls the aggressiveness of the technique by choosing the degree of regularization that balances the errors introduced by the

non-reversibility of A and the regularization itself [Rodrigo 2016]. Some of these regularization methods are summarized in section 2.4.3.

There exist a number of mathematical methods to choose the appropriate regularization parameter. These methods are needed because for small values of λ, the computed epicardial potentials are very sensitive to perturbations (under-regulated), whereas for high values of λ, the potentials are over smoothed (over-regulated) [Rodrigo 2016]. The most popular approaches in bioengineering for choosing the optimal λare the composite residual and smoothing operator (CRESO) [Colli-Franzone 1985], which is based on a mathematical formulation, and the L-curve method [Hansen 1993], which uses a graphical approach.

The L-curve represents the logarithm of the solution error norm $||L\cdot X(\lambda)||^2$ as a function of the logarithm of the residual error norm $||A(\lambda)\cdot X(\lambda)-Y||^2$. These norms measure, respectively, the error due to the non-reversibility of the transfer matrix A, which increases with decreasing values of λ, and the error caused by the regularization itself, which is higher for increasing values of λ [Rodrigo 2016]. Such graphical representation places the optimal regularization parameter on the corner of the curve, as shown in figure 2.14, and is usually found by measuring the curvature at each point of the graph [Horácek 1997].

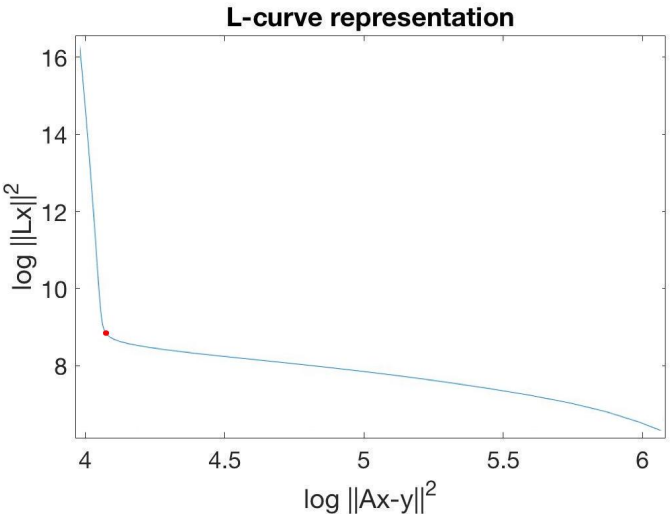

Figure 2.14: L-curve representation.
Logarithmic representation of the errors introduced due to the non-invertibility of the transfer matrix A (vertical axis) as a function of the errors introduced due to the regularization itself (horizontal axis). The optimal regularization parameter is located at the point of maximum curvature of the curve (represented with a red circle)

The choice of the optimal regularization parameter λ through the L-curve approach can be performed for each different time instant λ_t, or it can be computed globally for the whole set of time instants λ_g. For the global regularization parameter case, a constant λ_g is used for the reconstruction of epicardial potentials at all time instants. For the instantaneous λ_t case, each time instant of the epicardial potentials is computed using a different value of λ, which would be the optimum value for that instant in particular, as shown in figure 2.15.

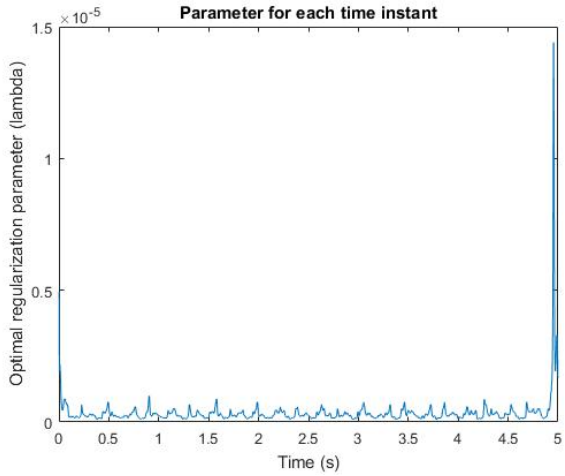

Figure 2.15: Example of optimal choice of instantaneous λ for a model of simple atrial fibrillation.
Optimal λ at each time instant for zero-order Tikhonov's algorithm with instantaneousλ.

Finally, the value of the optimal regularization parameter, whether global or instantaneous, varies with the level of input noise carried in the input signal. In this sense, for increasing values of signal to noise ratio (SNR), the value of the optimal λ decreases. This means that for decreasing noise content within the signal, the value for the regu

larization parameter decreases, as shown in figure 2.16.

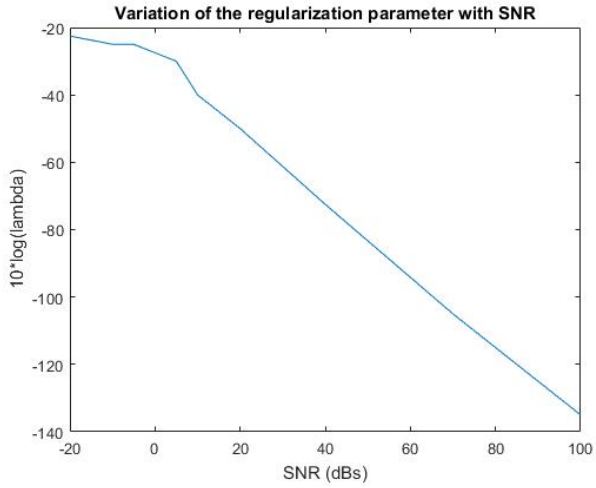

***Figure 2.16**: Example of the relationship between the value of the optimal regularization λ chosen and the SNR of the input signal.*
Variation of the optimal λ with the signal to noise ratio from the input signal.

2.4.3. Regularization techniques

As mentioned in previous sections, regularization techniques are used to modify the transfer matrix A which relates atria and torso geometries to make it invertible. These methods commonly use a regularization parameter (λ) which helps to decide the amount of errors that will be incorporated into the solution. The use of the regularization methods described in this section has helped in solving the inverse problem posed by ECGI, thereby leading to the estimation of epicardial potentials provided measurements at the torso.

Tikhonov regularization

The first regularization method to solve the inverse problem was developed by Tikhonov [Tikhonov 1963]. Tikhonov regularization helps to stabilize the solution of inverse problems by penalizing their complexity [Figuera 2016]. The regularization consists on minimizing the following function:

$$\|Y - A \cdot X\|_{Fro}^2 + \lambda \|L \cdot X\|_2^2 \tag{3}$$

Where Y is an M x T matrix containing the torso recordings on M different places for T time instants and X is an N x T matrix containing the reconstructed epicardial potentials at N nodes for T time instants, λ is the regularization parameter and L is an N x N spatial regularization matrix which can adopt three different forms. Finally, $\|\cdot\|_{Fro}$ stands for the Frobenius norm and $\|\cdot\|_2$ is the L_2 norm, which are computed as follows:

$$\|Y - A \cdot X\|_{Fro}^2 = \sqrt{\sum_{i=1}^{M} \sum_{i=1}^{T} \left|(y - ax)_{ij}\right|^2} \tag{4}$$

$$\|L \cdot x_t\|_2^2 = \sqrt{\sum_{i=1}^{N} L \cdot {x_t}_i^2} \tag{5}$$

where x_t represents each time instant in matrix X.As described previously through the explanation of the L-curve, the first part of the function to minimize $\|Y - A \cdot X\|_{Fro}^2$ quantifies the error caused by the non-invertibility of matrix A, and the second part $\lambda_g \|L \cdot X\|_2^2$ makes reference to the regularization error. The different forms of the spatial regularization matrix L determine the order of the method [Figuera 2016], and they are the ones summarized below:

1. Identity matrix (zero-order Tikhonov, which minimizes the L_2 norm of the solution).
2. Gradient operator (first-order Tikhonov, which favours constant solutions and penalizes gradients).
3. Laplacian operator (second-order Tikhonov, which favours constant gradient solutions).

Once the function in Equation 3 has been minimized, the solution of the problem becomes:

$$\hat{X} = (A^T \cdot A + \lambda \cdot L^T \cdot L)^{-1} \cdot A^T \cdot Y \quad (6)$$

Where suffix ^{T} denotes the transpose operator. Hence, the non invertible A^{-1} matrix is replaced by $A(\lambda)=(A^T \cdot A + \lambda \cdot L^T \cdot L)^{-1}$, which becomes invertible for high values of λ.

Truncated and damped singular value decomposition (TSVD and DSVD) regularization

The transfer matrix A can be decomposed into singular values, giving rise to three matrices following the formula:

$$A = U\Sigma V^* \quad (7)$$

With respect to equation 7, A is the transfer matrix relating torso and heart potentials, and has dimension of M x N, where M is the number of nodes at the torso and N the number of nodes at the atria. In the singular value decomposition, U and V are unitary matrices, each with dimensions of M x M and N x N, respectively. The suffix * denotes the conjugate transpose of V. Finally, matrix Σ is a diagonal M x N matrix, whose entries are positive and real, and are known as the singular values σ of A.

Taking this into account, zero-order Tikhonov regularization can be modified by expressing the transfer matrix A in its singular value decomposition form [Figuera 2016]. With this formulation, both TSVD and DSVD regularization processes act as a high pass filter, since they have the effect of attenuating the smallest singular values σ contained in matrix Σ. The filtering function was described by Hansen and co-workers [Hansen 2007] as:

$$H = \frac{\sigma}{\sigma+\lambda} \quad (8)$$

where σ represents each singular value in the diagonal of matrix Σ. The difference between both methods lies on the fact that DSVD smoothly filters the smallest singular values and TSVD directly ignores the smallest ones [Hansen 2007]. Both methods require a priori information, λ for DSVD and the number of ignored singular values for TSVD [Hansen 2007]. Since TSVD uses Tikhonov's formulation to solve the inverse problem, this regularization technique was later modified. This was performed so that TSVD could also be performed with the three different orders of Tikhonov's algorithm depending on the nature of the spatial regularization matrix L (zero order for identity matrix, first order for Gradient operator and second order for Laplacian) [Hansen 1992].

Total variation (TV) regularization

Total variation regularization method is a slight variation of first order Tikhonov regularization, where the spatial regularization matrix L is the gradient operator. The modifications which are made are based on the use the L_1 instead of the L_2 norm on the term which makes reference to the regularization error, $L \cdot X$. Also, the L_2 instead of the Frobenius norm is performed on the error introduced due to the non-invertibility of matrix A, $Y - A \cdot X$. With this technique, it is possible to obtain more detailed and less smoothed solutions than the original method [Ghosh and Rudy 2009]. The function to minimize becomes:

$$\|Y - A \cdot X\|_2 + \lambda \|L \cdot X\|_1 \tag{9}$$

where the L_1 norm is computed as follows:

$$\|L \cdot x_t\|_1 = \sum_{i=1}^{N} \left|L \cdot x_{t_i}\right| \tag{10}$$

Bayesian maximum a posteriori estimation (Bayes) regularization

Bayesian regularization method uses a priori information in the estimation of epicardial potentials from torso measurements [Serinagaoglu 2005]. Particularly, the information that needs to be known a priori for this regularization is the epicardial potentials' spatial covariance matrix. This matrix is estimated either using measurements from multielectrode coronary venous catheters [Serinagaoglu 2006], or using results from the forward problem as a priori information [Hanna 2009]. Once one of these two types of a priori information is available, the computation of the epicardial potentials' covariance matrix follows the equation:

$$C_x = \frac{1}{N_{samples}} (X - X_{mean})(X - X_{mean})^T \tag{11}$$

To calculate the covariance matrix, C_x, first of all, a given number of the atrial signal's time instants, $N_{samples}$, are used for the matrix X. A different time window, typically containing 1 second of the signal, is used to calculate X_{mean}. Among the samples to compute the X_{mean} matrix, 150 are randomly selected, and the mean is then calculated for this 150 random samples. Finally, the covariance matrix is computed following Equation 11, and it represents the spatial correlation between epicardial potentials within the atria. The reconstructed signal can then be estimated by the following formula:

$$\hat{X} = (C_x \cdot A^T)(A \cdot C_x \cdot A^T + C_n)^{-1} \cdot Y \tag{12}$$

where C_x represents the epicardial potentials' and C_n the noise's covariance matrix. This regularization method has, so far, been identified as the one with the best performance in the reconstruction of epicardial potentials from torso measurements [Figuera 2016].

Greensite (GS) regularization

Greensite's regularization method modifies Bayes', and introduces not only the spatial correlation of the epicardial potentials, but also the temporal correlation by assuming isotropic conditions [Greensite 2003]. This spatial-temporal covariance matrix can be calculated with the following formula:

$$C_X = C_t \otimes C_x \tag{13}$$

where C_x is the spatial covariance matrix and C_t is the temporal covariance matrix. The dimensions of this matrix can be very large, therefore, the problem is commonly simplified by means of applying a whitening filter to the data [Onal and Serinagaoglu 2009] or filtering together with a Tikhonov approach [Figuera 2016].

Generalized minimal residual (GMRES) regularization

Generalized minimal residual (GMRES) regularization is an iterative method which, unlike Tikhonov, TV and MAP, does not use any a priori constraint or assumption. The objective of this regularization is to obtain the optimum number of iterations that will give a solution with the least amount of errors [Ramanathan 2003].

3. Materials and methods

3.1. Geometrical models

For the purpose of this work two different atria and torso geometrical models were provided. These were needed for the reconstruction of the inverse problem. To this respect, geometrical models were not only needed for the mere purpose of visualizing the estimated atrial activity, but also in the specific characterisation of atrial fibrillation as well as in further steps for interpolation purposes, as will be described in following sections.

3.1.1. Atrial models

The three dimensional geometries of the atria for both models consisted on a volume formed by triangular meshes. One of the models, shown in figure 3.1A (Atria model 1), contained nodes in the atria holes. This type of geometry is needed to calculate the specific location of the atrial fibrillation's rotors. The other model, shown in figure 3.1B, (Atria model 2) has empty atrial holes, and was used for visualization purposes. This model was also used in the algorithms that selected nodes for the interpolation steps.

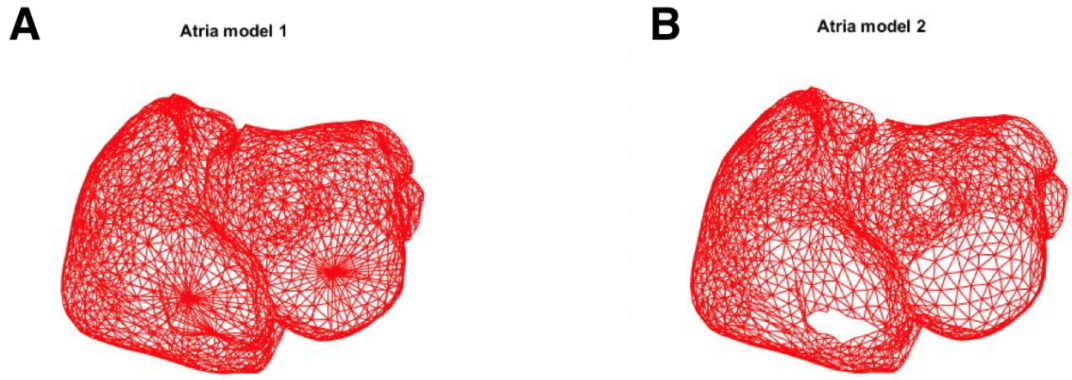

Figure 3.1:Three-dimensional geometries of atrial models.
(A) Atria model with filled geometry and (B) Atria model without a filled geometry.

Regarding the specifications of these models, Atrial model 1 includes the coordinates of each triangle's vertices, indexes and norms. Atrial model 2 also contains the distances between each triangle's vertices as well as the areas of the triangles. Despite being the same three dimensional models, the fact that Atrial model 1 is the filled geometry of Atrial model 2 explains why the first one contains a larger number of vertices and triangles, as can be seen in table 3.1.

Table 3.1: Variables specified in the two atrial models used.

	Atria model 1 (filled geometry)	Atria model 2
Vertices	[2048x3]	[2039x3]
Faces	[4092x3]	[3860x3]
Norms	[2039x3]	[2039x3]
Areas		[2039x1]
Distances		[2039x2039]

3.1.2. Torso model

A single model was used for the torso. The three dimensional geometry of such model also consisted on a volume defined by triangular meshes. The specifications contained within the model were, once again, the triangle´s vertices, and faces. Unlike the atrial models, a filled geometry of the torso model was not needed, since the computation of the rotor's location is performed directly on the estimated epicardial potentials in the atria. The three dimensional geometry of the torso model can be seen in figure 3.2A, while the torso enclosing the atrial geometrical model is shown in figure 3.2B. The specifications of the torso model are shown in table 3.2.

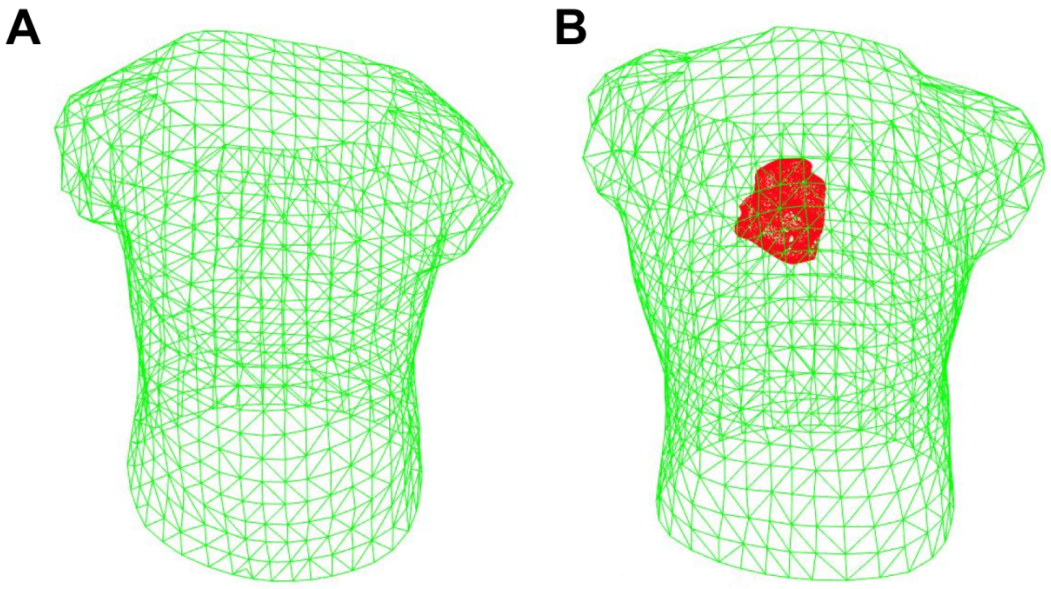

Figure 3.2: Three dimensional geometry of torso model.
Torso geometry (A) and torso enclosing atria geometry (B).

Table 3.2: Variables specified in the torso model used.

Torso model 1	
Vertices	[659x3]
Faces	[1255x3]

Together with these atrial and torso model, a transfer matrix (A) relating both geometries was also provided to be able to solve both the forward and inverse problem of electrocardiography. This transfer matrix was originally obtained by using the Boundary Element Method (BEM) in the propagation of the atrial signal towards the torso surface [Figuera 2016]. Taking into account the dimensions of the atria and torso models, this transfer matrix had dimensions of M x N, being M the nodes at the torso (659), and N the nodes at the atria (2039).

3.2. Mathematical models of epicardial activity

Three different mathematical models of monopolar epicardial activity were provided, consisting on spatio-temporal signals representing different electrical propagation patterns within the atria. Provided the EGMs, a set of target parameters can be computed from these potentials. These additional target parameters are useful in the characterization of atrial fibrillation episodes and can be computed from the provided epicardial potentials as follows:

- Dominant frequency: it is computed from the epicardial potentials. To do so, the power spectral density of the signal as a function of the frequency is estimated using Welch's periodogram. The specifications for this estimation were a 2 Hamming window for evaluation with 50% overlap and a sampling frequency of 500Hz [Figuera 2016]. Upon obtaining the periodogram estimation, the frequency with the maximum density is selected after having eliminated the harmonics [Guillem 2013]. This procedure is performed one by one for each node.

  This parameter is an important target, since the localization of regions in the atria with a common dominant frequency can be a key factor in the successful performance of ablation procedures which end with atrial fibrillation episodes [Guillem 2013].
- Instantaneous phase: this parameter is also computed from the epicardial potentials. The procedure is performed first of all by band pass filtering the signal between a specified low pass frequency and a high pass frequency. The low pass frequency is the same as the filtering step described in previous sections, 0 Hz for the model of sinus rhythm and 3 Hz for the models of simple and complex atrial fibrillation. Regarding the high pass frequency, its value varies for each node, and it is equal to the dominant frequency at the node whose phase is being evaluated. Also, the DC component is removed from the reconstructed and band pass filtered signal.

  The Hilbert transform is then performed to this processed signal, so that it is expressed as a contribution of a real and imaginary part. Finally, the angle between the imaginary part and

the signal is computed and stored as the instantaneous phase for each node and time instant. These phases can then be used to create phase maps, which can in turn be used to detect re-entrant activity in the atria and potential ablation targets [Rodrigo 2014].

- Singularity Point (SP) location: it is identified using the phase maps described previously. SP are, by definition, regions within a phase map which are surrounded by 0 and 2π and whose duration is larger than two full rotations [Rodrigo 2016]. Among these SP, the dominant singularity points are the ones within the region of the atria with the highest dominant frequency [Figuera 2016].
  Just like the other parameters, the identification of singularity points can serve to localize ablation targets which can eventually terminate the fibrillation episodes.

The first model was the simplest one, sinus rhythm (SR), which corresponds to the normal atrial activity. The characteristics of this atrial activity are a periodical activation with a frequency of 1.2 Hz (Hz), a planar propagation wavefront, and the absence of dominant frequency regions and singularity points. This model can be observed in figure 3.3. In figure 3.3A the distribution of epicardial potentials in the atria at second 1.652 of the signal is shown, as well as the instantaneous phase (figure 3.3B).

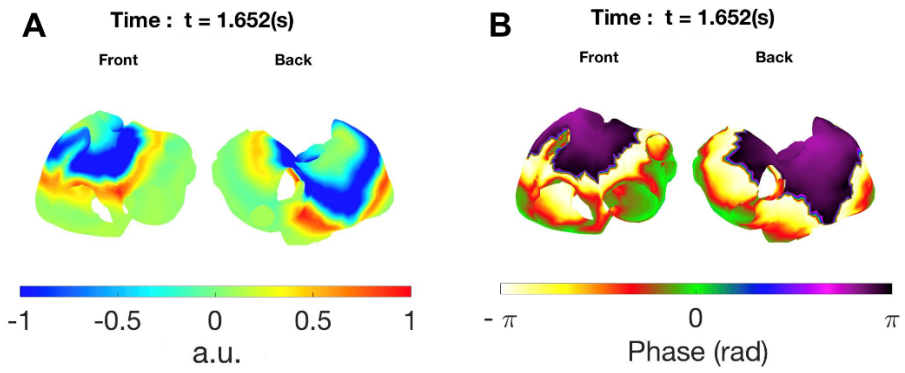

Figure 3.3: Representation of sinus rhythm model propagation wavefront and instantaneous phase in the atria.
(A) Epicardial potentials distribution in the atria at t=1.652 seconds. (B)Instantaneous phase in the atria at t=1.652 seconds.

The second mathematical model corresponded to an episode of simple atrial fibrillation (SAF). The propagation pattern of this model, as seen in figure 3.4, is different from planar and slightly more complex. The SAF model used has a dominant frequency gradient from the right to the left atrium which leads to the appearance of different DF regions (figure 3.4C). The underlying cause is the presence of a rotor in the RA, which can be seen in figure 3.4D. The functional re-entry rotates at 7.3 Hz, while the rest of the atria has a periodical activation frequency at 4.7 Hz. All these facts explain the distribution of potentials at second 3.446 being different from planar (figure 3.4A), as well as for the instantaneous phase (figure 3.4B).

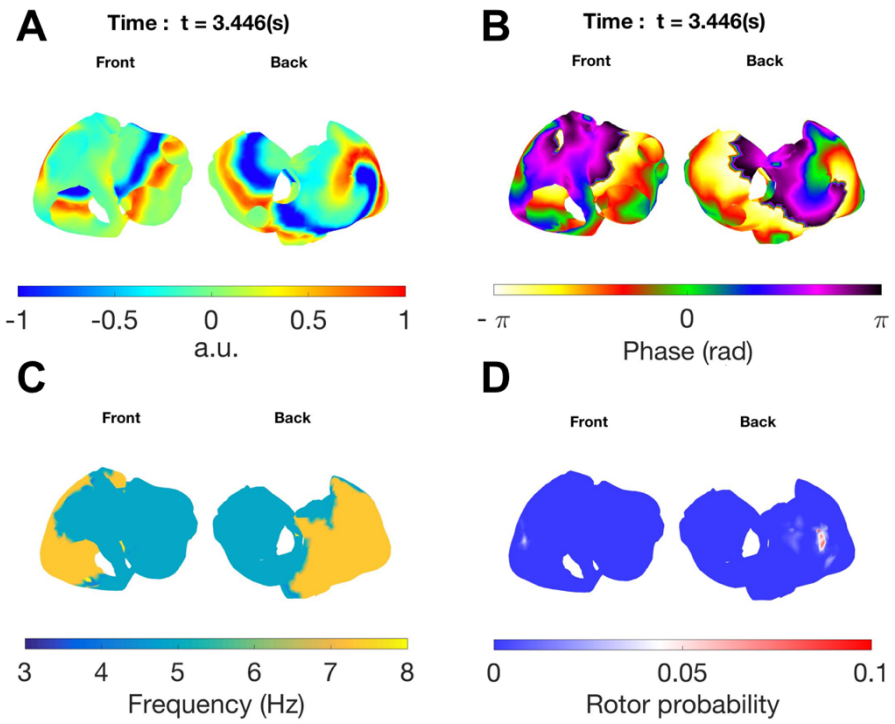

Figure 3.4: Representation of simple atrial fibrillation model propagation wavefront, instantaneous phase, frequency and singularity point distribution in the atria.
(A) Epicardial potentials in the atria at t=3.446 seconds. (B) Instantaneous phase at t=3.446 seconds. (C) Dominant frequency map (D) Location of singularity points.

Finally, the third mathematical model represented a case of complex atrial fibrillation (CAF). This type of atrial activity is represented by a chaotic electrical propagation within the atria. The underlying cause is the same as that for the SAF model, but now the model makes reference to a more severe and complex condition of atrial fibrillation with slightly different constants in the model, as well as a percentage of fibrosis to account for a remodelled state in the atria. In particular, the CAF model includes a 25% of atrial cells under fibrotic conditions [Rodrigo 2016], as well as a rotor located at the LA (figure 3.5D). The rotation frequency of this rotor is of 6.8 Hz, and the activation at the rest of the atria takes place at 5.4Hz. In figure 3.5A the distribution of epicardial potentials at second 2.426 is shown, which is completely different from planar, and the same applies to the instantaneous phase (figure 3.5B). Also, the presence of a rotor in the LA gives rise to the appearance of different dominant frequency regions (figure 3.5C). The specific features of the three models are summarized in table 3.3.

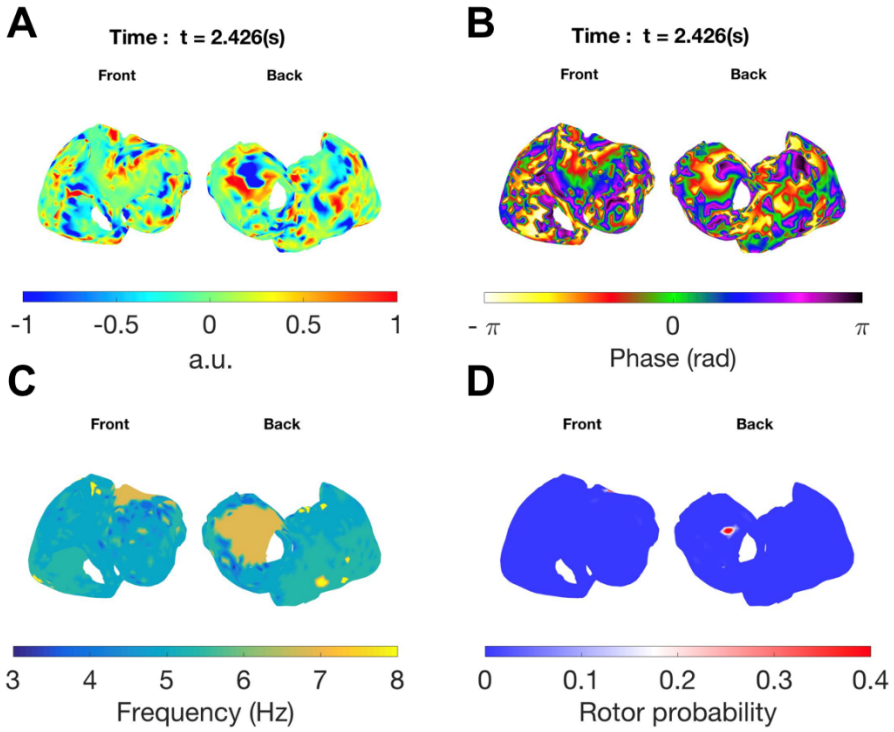

Figure 3.5: Representation of complex atrial fibrillation model propagation wavefront, instantaneous phase, frequency and singularity point distribution in the atria.
(A) Epicardial potentials in the atria at t=2.426 seconds. (B) Instantaneous phase at t=2.426 seconds. (C) Dominant frequency map. (D)Location of singularity points.

Table 3.3: Characteristics of the three models of epicardial activity.

	Sinus rhythm	Simple atrial fibrillation	Complex atrial fibrillation
Nodes	2039	2039	2039
Samples	2500	5000	5000
Sampling Frequency (Hz)	500	500	500
Time (s)	5	10	10
Mean Frequency (Hz)	1.2	4.7	5.4
Singularity Point Location	None	Right atrium	Left atrium
Nearest point to SP	None	FRAW	RSPV
Rotor Frequency (Hz)	None	7.3	6.8
Fibrosis (%)	0	0	25

As shown in table 3.3, the three models of epicardial activity included different electrical signals for 2039 nodes distributed in the atria, and the location of these nodes coincided with those provided in the atria geometrical model. The number of samples that were provided differed from one model to another. For the SR model, 2500 samples were included in the model, whereas the SAF and CAF models contained a total of 5000 samples. Since the sampling frequency is set to 500 Hz, this translates, respectively, to 5 and 10 seconds of electrical activity. The mean activation frequency of each model was of 1.2, 4.7 and 5.4 Hz for the SR, SAF and CAF models, respectively. The SR model did not contain any singularity points (SPs) whereas the SAF model contained one in the RA, near the Free Right Atrial Wall (FRAW) with a rotation frequency of 7.3 Hz. Finally, the CAF model included 25% of fibrotic cells and a rotor at the LA with a rotation frequency of 6.8 Hz, whose nearest clinically-relevant point was the Right Superior Pulmonary Vein (RSPV).

Regarding the samples for the SAF and CAF models, not all of them were used for the performance of the forward problem, interpolation, and inverse problem. This has two different reasons. The first, is the fact that if the SR model contained only 5 seconds of signals, then the same time interval must be used for the other two models, or at least a similar one. The second reason is the time needed for the signals to stabilize and the fibrillation episodes to begin for the SAF and CAF models. This translates to the presence of signals which are initially either very close to zero (figure 3.6B), or with very different patterns to the middle transients of the same signal, which lasted for a certain amount of time, depending on the model. Also, the end transients were irregular and different from the rest of the signal for some of the registered nodes, as shown in figure 3.6A. Therefore, the initial and end transients were removed from the SAF and CAF models so that only the nonzero and stable signals were used in further steps, and to ensure that the number of samples was more or less the same for all of the models. The samples eliminated and used in each model are summarized in table 3.4.

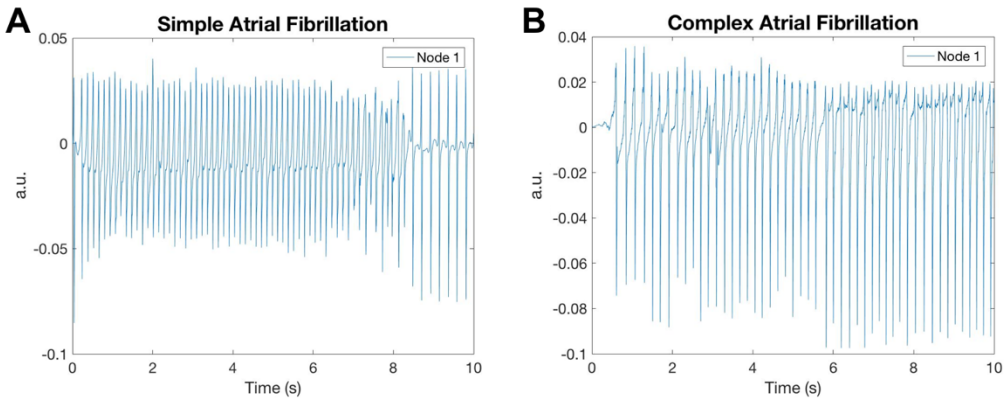

Figure 3.6: Presence of irregular transients in the simple and complex atrial fibrillation models.
(A) Unstable end transients in the SAF model and (B) close to zero initial transients in the SAF model.

Table 3.4: Samples eliminated and used for each of the models.

	Sinus rhythm	Simple atrial fibrillation	Complex atrial fibrillation
Number of samples	2500	5000	5000
Removed initial transients	1	1:1001	1:501
Removed end transients	None	3501:5000	3001:5000
Samples used	2:2500	1002:3500	502:3000

The samples described in table 3.4 can be used to calculate the forward problem in order to obtain the projection of the epicardial potentials on the torso surface. As mentioned in previous sections, the computation of the forward problem requires a matrix relating atria and torso geometry. This transfer matrix was also provided, and was calculated originally through BEM.

In order to proceed with the forward problem, the epicardial potential signals were first filtered. The filtering method depends on the model that is being used. For sinus rhythm, the Direct Current (DC) component of the signal is removed and then it is filtered by means of a 4^{th} order low pass filter which is built using Matlab®. For the other two models, the DC component is also eliminated, and then the signal is band pass filtered using a 4^{th} order filter, also built with Matlab®. The cut-off frequencies and filtering methods are summarized in table 3.5, as well as the sampling frequency which is used to build the filters.

Table 3.5: Filtering specifications for each of the models.

	Sinus rhythm	Simple atrial fibrillation	Complex atrial fibrillation
Type of filter	Low pass	Band pass	Band pass
Cut-off frequencies (Hz)	0-30	3-30	3-30
Sampling frequency (Hz)	500	500	500

Once the epicardial potentials for the models are filtered, an additional step needs to be performed before proceeding with the forward problem. This step consists on modifying the transfer matrix (A) relating atria and torso geometries to refer the computed surface potentials to the Winston's Central Terminal (WCT), as used as reference in the patients. In order to do so, a new matrix is created. This matrix is squared, and has dimensions of the N number of nodes present at the torso. The entries of the matrix are the inverse of the number of nodes at the torso, following equation 14:

$$M_{wct} = \frac{1}{N} \times \begin{bmatrix} 1 & \cdots & 1 \\ \vdots & \ddots & \vdots \\ 1 & \dots & 1 \end{bmatrix}_{NxN} \tag{14}$$

Where N is the number of nodes at the torso and M_{wct} is the matrix used in Winston's Central Terminal correction. Upon obtaining this matrix, the transfer matrix A is corrected using equation 15:

$$A_{corr} = (A - (M_{wct} \times A)) \tag{15}$$

The corrected transfer matrix A is then multiplied times the filtered epicardial potentials to obtain the projected potentials at the torso's surface. For the purpose of making the situation as realistic as possible, white Gaussian noise is added to these computed torso potentials, and then they are filtered in the same manner as the epicardial potentials, which has been described previously. These final torso potentials for each of the models available can be visualized in figure 3.7. In this figure, the torso projections of SR (figure 3.7A), SAF (figure 3.7B) and CAF (figure 3.7C) are shown. All in all, it is these torso potentials the ones that are going to be used when proceeding with the inverse problem.

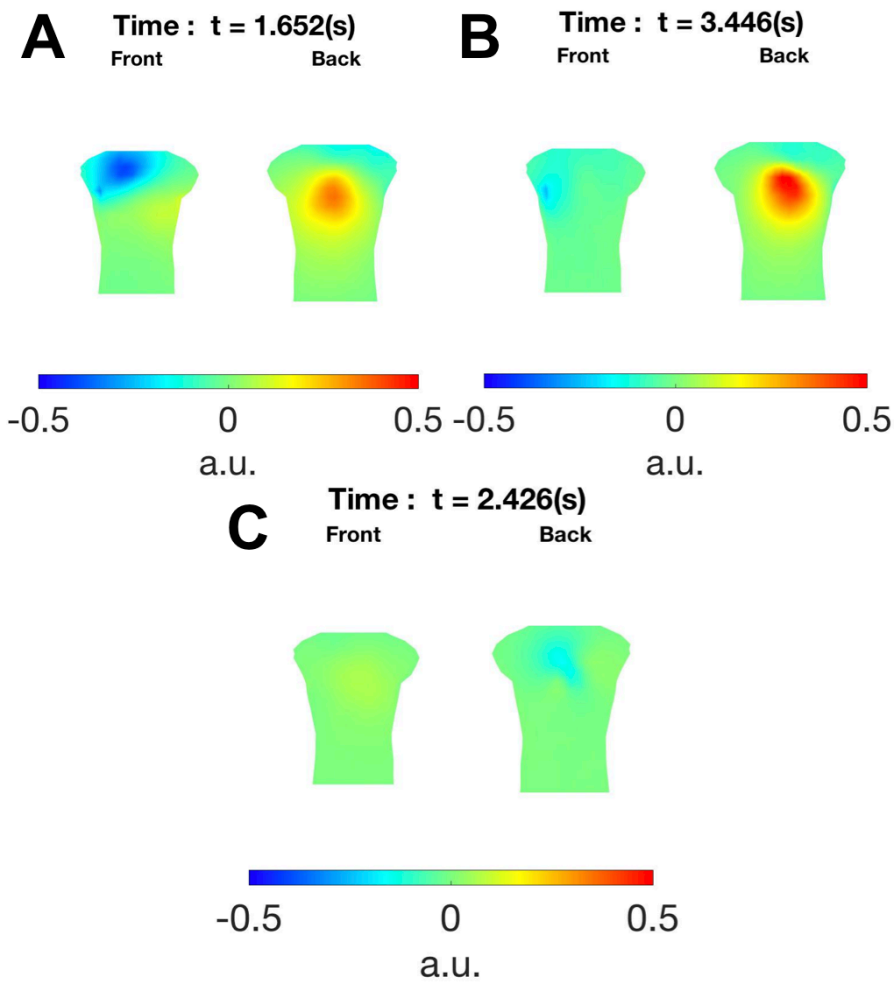

Figure 3.7: Torso potentials for each of the models computed through the forward problem.
Potentials at the torso computed for a sample time instant through the forward problem for the models of (A) sinus rhythm, (B) simple atrial fibrillation and (C) complex atrial fibrillation.

3.3. Reconstruction of epicardial potentials

The purpose of computing the forward problem and obtaining the potentials at the torso's surface for each of the models is to perform the inverse problem. Upon proceeding with the inverse problem, the epicardial activity can be estimated using the information on the torso as well as the transfer matrix relating atria and torso geometries. In this work, the reconstruction of epicardial potentials was performed using Bayes and Tikhonov regularizations, which have been described in previous sections. Tikhonov reconstruction was performed on the models with all the available spatial information, and the results were used for comparison purposes. Bayes regularization however, was applied to the provided models but also to a modified version of the original data. This modified version consisted on the models with reduced intracavitary information, with the aim of reconstructing the original number of epicardial signals provided a reduced number of initial data. This will be explained in further detail in section 3.4.

Computing the inverse problem allows to obtain epicardial potentials. In this work, these potentials are computed directly by using torso potentials, the transfer matrix, and two different regularization methods: Tikhonov and Bayes. Tikhonov regularization method was used on the raw data and the results obtained were used for comparison purposes. Bayes regularization method was used on a modified version of the original data, where the amount of spatial information from the signals was reduced. The purpose was to interpolate such signal and reconstruct the problem by Bayesian methods to obtain the original amount of spatial information. Also, it was desired to obtain a better resolution than Tikhonov regularization with the raw data.

As well as reconstructing the epicardial potentials, the target parameters described in section 3.2 can also be computed from the estimated potentials: dominant frequency, instantaneous phase and singularity point, as depicted in figure 3.8. The calculation of these target parameters follows the same procedure as the one described in section 3.2, but using the estimated potentials instead of the real ones.

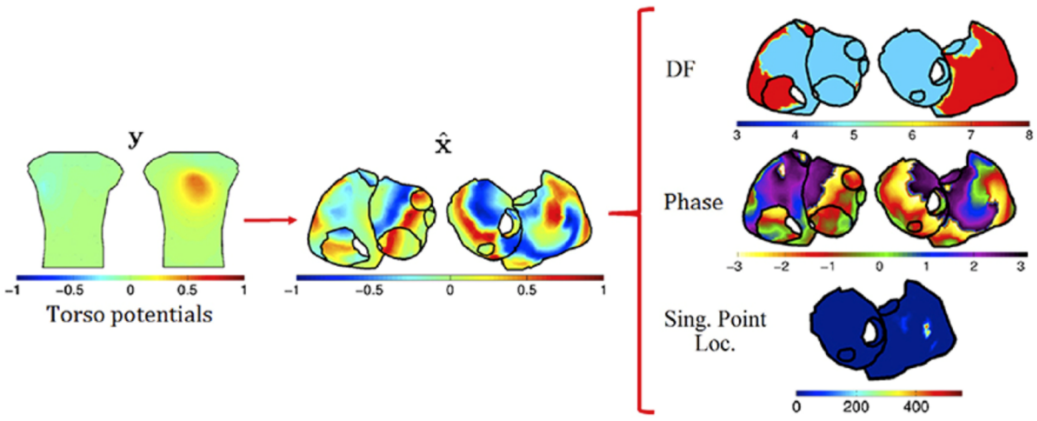

Figure 3.8: Schematic representation of the inverse problem procedure to compute the target parameters.
Target parameters computed from reconstructed epicardial potentials, which are estimated from torso potentials. Extracted from Figuera et al. (2016)

3.3.1. Performance metrics

The efficiency of the reconstruction of epicardial activity was assessed using different performance metrics. These metrics were used to compare the degree of similarity between the computed target parameters after the reconstruction and the target parameters calculated from the models of epicardial potentials. To this respect, on the one hand, the reconstructed epicardial potentials were compared with the actual epicardial potentials after applying the same filtering procedure that has been described in section 3.2. On the other hand, the estimated dominant frequencies, phases, and location of singularity points were compared with these same measurements computed directly from the actual epicardial potentials.

Depending on the value of each metric, the performance of each regularization method could be analysed in a straightforward manner. The application of these performance metrics was not only to evaluate Tikhonov and Bayes regularization on the original data, but also on the data with reduced spatial information reconstructed through Bayes regularization. For such purpose, each of the previously described target parameters was treated differently and assessed with a different performance metric, focusing either on temporal or spectral features.

The performance metrics used for each target parameter were:

- Epicardial potentials: the similarity between the estimated and actual epicardial potentials was assessed with two different metrics. The first one is Pearson's Correlation Coefficient (CC), which is the covariance between two variables divided by the multiplication of the variance of each one of them, as described by the following formula:

$$CC_x = \frac{cov\,(x,\hat{x})}{\sigma_x \sigma_{\hat{x}}} \tag{16}$$

  Taking into account the formulas for the covariance and the variance between two variables, the definition for CC can be rewritten as:

$$CC_x = \frac{(k\sum x\hat{x}) - (\sum x)(\sum \hat{x})}{\sqrt{[k\sum x^2 - (\sum x)^2][k\sum \hat{x}^2 - (\sum \hat{x})^2]}} \tag{17}$$

  Where x and $\hat{x}$ represent, respectively, the actual and the reconstructed epicardial potentials. The measurement can be computed in two different manners to obtain either the temporal or the spatial version. The temporal version consists on using all time instants and obtaining the correlation between nodes on the actual and estimated epicardial potentials. The spatial version however, uses all nodes and the correlation between time instants is obtained. Therefore, the k-sum specified in the formula depends on whether the temporal or spatial version is being computed. For the temporal case, since matrix x and $\hat{x}$ have dimensions of NxT, being N the number of nodes and T the number of time instants, the sum is performed for each time instant across all nodes, and k is the total number of nodes. For the spatial case however, the sum is performed for each node across all time instants, and k is the total number of time instants.

The second performance metric is the Relative Difference Measurement Star (RDMS) which is calculated using the following formula:

$$RDMS_x = \sqrt{\sum_k \left(\frac{x_k}{\|\boldsymbol{x}^2\|} - \frac{\hat{x}_k}{\|\hat{\boldsymbol{x}}^2\|}\right)^2} \tag{18}$$

Once again, x and $\hat{x}$ make reference to the actual and estimated epicardial potentials, and analogously to the first metric, there exists a temporal and a spatial version for the RDMS. The temporal version, just like the CC, implies a sum over the nodes for each time instant of the signal, and in the spatial version, the sum over the time instants for each node is performed.

- Dominant frequency: the performance metric used to evaluate the difference between the dominant frequency computed from the estimated and actual epicardial potentials is the relative dominant frequency error (RDFE). This metric is calculated by averaging the relative error for each node through the equation:

$$RDFE(\%) = \frac{100}{N}\sum_{n=1}^{N}\frac{|DF_n - \widehat{DF}_n|}{DF_n} \tag{19}$$

Where DF_n and $\widehat{DF}_n$ represent, respectively, the dominant frequencies at node n from the actual and estimated epicardial potentials.

- Phase: the performance metrics used to evaluate the accuracy between the phases computed from the actual and estimated potentials are the same as those used for the epicardial potentials, the CC and RDMS. The formulas for their calculation is the same as the one described above but substituting the epicardial potentials matrix by the phase vector:

$$CC_{\varphi} = \frac{(k\sum\varphi\hat{\varphi}) - (\sum\varphi)(\sum\hat{\varphi})}{\sqrt{[k\sum\varphi^2 - (\sum\varphi)^2][k\sum\hat{\varphi}^2 - (\sum\hat{\varphi})^2]}} \tag{20}$$

$$RDMS_{\varphi} = \sqrt{\sum_k \left(\frac{\varphi_k}{\|\boldsymbol{\varphi}^2\|} - \frac{\hat{\varphi}_k}{\|\hat{\boldsymbol{\varphi}}^2\|}\right)^2} \tag{21}$$

Where φ and $\hat{\varphi}$ represent, respectively, the phase computed from the real and estimated epicardial potentials.

- Singularity Point (SP) location: the similarity between the location of singularity points from the real and estimated epicardial potentials was assessed by means of 4 different performance metrics. The preliminary step in computing such metrics is to know the probability of a singularity point being at a specific site, since it has been shown that this is more clinically relevant than knowing the location of SPs for every time instant [Haissaguerre 2014]. This probability of SP location can be obtained by means of creating a normalized spatial histogram representing the frequency of SP occurrence at each node, obtaining a Spatial Mass Function (SMF). Then, the SP regions will be those nodes where the SMF is

different from zero. Taking this into account, the performance metrics used for SP location will assess the SMF computed from the real and reconstructed epicardial potentials.
The first metric is the Weighted Under-estimation Indicator (WUI), which measures the percentage of true SP regions that are not detected from the whole true SP region [Figuera 2016]. The WUI can be calculated by using equation 22:

$$WUI(\%) = 100 \cdot \frac{\sum_{n \in FN} p(n) A_n}{\sum_{n \in FN} p(n) A_n + \sum_{n \in TP} p(n) A_n} \tag{22}$$

where A_n is the area of the faces surrounding node n and $p(n)$ is the probability of having a SP in that node. FN stands for False Negative, and it represents the nodes that are not present in the SP region of estimated potentials but actually belong to a SP region in the real potentials. Finally, TP stands for True Positive and it represents the set of nodes belonging to the true SP region, therefore they are present in both the real and estimated potentials.
The second metric is the Weighted Over-estimation indicator (WOI) which measures the percentage of erroneous SP regions from the entire SP region through equation 23:

$$WOI(\%) = 100 \cdot \frac{\sum_{n \in FP} p(n) A_n}{\sum_{n \in FP} p(n) A_n + \sum_{n \in TP} p(n) A_n} \tag{23}$$

Once again, A_n represents the area of the faces surrounding node n and $p(n)$ is the probability of having a SP in that node. FP stands for False Positive, and it represents the nodes that do not belong to the SP region for the real potentials but are identified as SP regions for the inverse-estimated ones. Analogous to the previous case, TP stands for True Positive and it represents the set of nodes belonging to the SP regions for both the real and estimated potentials.
The third metric is the Correlation Coefficient (CC) between the real Spatial Mass Function (SMF) and the SMF computed from the estimated potentials. This parameter is computed through equation 24:

$$CC_{SMF} = \frac{(n \sum p(n)\hat{p}(n)) - (\sum p(n))(\sum \hat{p}(n))}{\sqrt{[n \sum p(n)^2 - (\sum p(n))^2][n \sum \hat{p}(n)^2 - (\sum \hat{p}(n))^2]}} \tag{24}$$

Where $p(n)$ and $\hat{p}(n)$ represent, respectively, the probability of having a SP from the real and estimated potentials in node n. This measure effectively compares both spatial mass distributions and is able to include information from the previously mentioned metrics (WUI and WOI).
Finally, the fourth performance metric is the mode distance (MD) between the modes of the Spatial Mass Functions from the real and estimated potentials. The MD is calculated as the Dijkstra distance; so that it is assured that the distance between both modes will be the minimum length of vertices connecting them. This metric is useful when the real and estimated SMFs are near but do not overlap.

3.4. Interpolation

As mentioned in previous sections, one of the objectives of this project has been to reduce the number of spatial information available from the different models of epicardial activity. Once this data had been eliminated, different interpolation techniques were used to recover the original amount of spatial information before proceeding with the reconstruction of epicardial potentials through Bayes regularization algorithm. The aim was to identify the amount of initial spatial information from the signals that was needed to reconstruct the inverse problem using Bayes regularization with at least the same accuracy (if not better) than Tikhonov reconstruction with all the original spatial information.

Regarding the interpolation techniques, different approaches have been used. The difference between them lies either in the place where the interpolation is performed, the method that is used for interpolating, and simultaneity between all signals' nodes or just in sets of 120 nodes. These approaches are described in detail in the following sections.

3.4.1. Place of interpolation

Reducing the spatial information from the models of epicardial activity amounts to dividing the set of nodes of the atrial model into two groups: those whose signals are going to be included and those whose signals are going to be excluded. Among the excluded nodes, the set of signals belonging to this group are eliminated, while the set of signals from the included nodes are kept in the model. Then, this truncated signal has to be interpolated to recover the information for the original number of nodes, so that the reconstruction of epicardial potentials could be performed with the same spatial resolution as if all nodes had been present.

Two different approaches were used for the place of interpolation of the truncated signal: the electrogram (EGM) itself and the Covariance matrix (Cx) used in the reconstruction of epicardial potentials through Bayes regularization. The first approach consisted on eliminating the EGM signal from a set of nodes, and then assigning to the excluded nodes a certain EGM value which depended on the method of interpolation used, and will be described in this section. Then, once the EGM had been reconstructed and the total number of nodes had been restored, Bayes algorithm proceeded in its usual manner, and the covariance matrix of epicardial potentials was built with the information of the interpolated EGM. The second approach consisted on eliminating the EGM signal from a set of nodes, and then proceeding with the computation of the covariance matrix of epicardial potentials with the information of the truncated signal. Then, before the reconstruction of the epicardial potentials through Bayes regularization, the covariance matrix was interpolated to recover the dimensions it should have had according to the original EGM with all nodes. Again, the covariance value that was assigned to the missing nodes depended on the interpolation method used, and will be described in section 3.4.2.

The detailed performance of each approach is as follows:

- EGM interpolation. This approach was performed following a number of steps. The first step consisted on selecting which nodes from the atrial model were going to be used. To do so, the fraction of nodes that was going to be used needed to be set a priori. To this respect, 8 different sets of nodes were selected, which corresponded, respectively to the 8^{th}, 7^{th}, 6^{th}, 5^{th}, 4^{th}, 3^{rd},2^{nd}, and 1.5^{th} fraction of the original number of nodes. Having set the number of spatial information that was going to be used, the criteria for node selection was the following:
    1. First node: node which is farthest apart from the whole set of nodes.
    2. Second node: node which is farther away from the first selected node.
    3. Rest of nodes: node which is farther away from all the previous ones.

  Since the geometrical atrial model provided included a matrix for the distances between all nodes, this could be implemented in a straightforward manner. Initially, the distances from all nodes to the rest are sorted in descending order, so that the highest distances are located in the first positions inside a matrix. The nodes corresponding to each distance are also stored.

  Then, the first node is selected, which is the one which is farthest away from the general set of nodes. This was performed by means of adding, for each node, all the distances to the rest of nodes. The location within the matrix for which the maximum value of such sum was obtained was identified as the node which, in general terms, was the farthest away from the whole set. Upon selecting the first node, the second one is simply the one whose distance is the highest from the first. This can be obtained in a straightforward manner since all distances for all nodes were previously sorted in descending order.

  Once the first two nodes have been selected, a loop is created to select the rest of nodes. For the first iteration (the algorithm is looking for the third node), all the distances from the first node to the others are evaluated in descending order. The program takes the node which corresponds to the distance under study, and evaluates the distance from the second node to the node under study. Then, the distances from both nodes the new node is added, and this sum is stored in a vector, as well as the node corresponding to the sum. Once the whole vector has been built (all the distances from the first node to the others have been evaluated), the program takes the maximum entry in such vector, and the selected node will be the one corresponding to this maximum. The identified node will be the one which is, simultaneously, the farthest from the two previous nodes.

  Upon finding the third node, the distances between this new node and all the others are added to the previous vector, entry by entry, so that each entry corresponds to the sum of distances of a different node. To ensure that there are no duplicated nodes, a security-check loop is also created. This loop will find any coincidences between a new node and the previously selected ones. If there are any repetitions, that entry is put to zero and a new maximum is looked for. Finally, the nodes which are going to be included in the model are stored in ascending order, as well as the nodes which are not going to be used. The program then stores from the original EGM, the signals which correspond to the chosen nodes.

  Now the EGM contains a fraction of the initial nodes, which has been set a priori, and all the initial samples from the nodes that have been included. At this point, the first approach performs the EGM interpolation through different methods to reconstruct the EGM and ensure that it has the initial dimensions. The different algorithms used to perform the

interpolation on the EGM will be described in section 3.4.2. The interpolated EGM is then used to build the spatial covariance matrix, and Bayes regularization algorithm and reconstruction of epicardial potentials proceeds normally.

- Cx interpolation. The covariance matrix interpolation approach begins just like the EGM approach, by eliminating the information belonging to a set of nodes from the original EGM signal. The choice of the nodes that will be included and those that will be excluded was performed in the same way as for the previous case. Also, the elimination of spatial information from the original EGM signal proceeds in the same way as the EGM approach described previously. However, this time the algorithm will return the truncated EGM signal only with the selected nodes, as well as the set of nodes that have been included and the ones that have been excluded from the original model. Furthermore, the function returns the neighbours from the nodes that are not used, which will be used for one of the interpolation methods that will be described in the following section. These variables will be used later to interpolate the covariance matrix appropriately.
  The code continues executing normally, and the covariance matrix is created with the specified fraction of the original EGM information. After this, before reconstructing the epicardial potentials using Bayes regularization method, a function is introduced to interpolate Cx and restore the dimensions of the covariance matrix that corresponds to the dimensions of the initially provided EGMs. This function is different depending on the method of interpolation and will be described in the following section.

3.4.2. Method of interpolation

Two different interpolation methods were applied, both on the EGM and Cx interpolation approaches, to restore the initial number of spatial information from the truncated data. The first approach was Nearest Neighbour (NN) interpolation, which basically consists on giving to the missing nodes values corresponding to their nearest neighbour within the atrial geometrical model. The second approach was based on using the second spatial derivative (Laplacian) between a missing node and its connected neighbours. For this last approach, an interpolation matrix is created, which multiplied by the truncated EGM or Cx, restores the dimensions of the original data. The detailed description of these interpolation methods is as follows:

- Nearest Neighbour (NN) interpolation. The adequate performance of this method requires a preliminary step which consists on finding the nearest nodes to the ones that have been excluded from the signal. As described previously, the atrial model included a variable with the distances between all nodes. Hence, by sorting the distances for each node to the rest of nodes in ascending order, and taking into account that the minimum distance of all nodes will be the one with itself, the closest node will be the one in the second entry.
  However, this is not so straightforward. For most of the cases, especially when a high number of nodes are excluded, the nearest neighbour is also going to belong to the excluded set. Therefore, it was necessary to check whether the nearest node to a missing node belonged to the set of included nodes. If a given node was not in the set, even if its distance to an excluded node was the minimum, it was discarded, and the next nearer neighbour was

taken. Once the loop ended, it returned a vector containing the neighbours from the excluded nodes from which the information was going to be copied.

At this point, the nearest neighbour interpolation method differs slightly depending on the interpolation approach used previously, whether EGM or Cx. This is simply because of the values that the covariance matrix represents. For EGM interpolation, the dimensions were restored first of all by creating an empty EGM with the same dimensions as the original one, with all the spatial information. A loop is created which fills each node in the EGM with the following criteria:

- For each node in the new EGM, if it belongs to the set of included nodes in the truncated EGM, the node is given the same values as the reduced EGM.
- If the node does not belong to the set of included nodes, then it is given the values in the reduced EGM from its nearest neighbour.

Once the dimensions of the EGM have been recovered, the covariance matrix is computed through equation 11 and the epicardial potentials are estimated through Bayes regularization method, following equation 12.

For the covariance matrix interpolation approach, this algorithm works slightly different. This is due to the fact that the covariance matrix is a squared matrix which represents the covariance values between all nodes. Therefore, the first step requires building an empty squared matrix which will have the same dimensions of the original number of nodes in the atrial geometrical model. These are the dimensions that the matrix should have had if no spatial information has been reduced from the EGMs.

Then, for each entry in such matrix, the code checks whether the row and column are within the set of included nodes. If they are, then the value of the empty covariance matrix at such point will be the one of the truncated covariance matrix at the corresponding pair of nodes. If either the row, or column, or both of them, are not within the set of nodes, the code gets the nearest neighbour to the missing row, column or both, as well as the covariance value in the truncated Cx for each row-column pair. Finally, each selected entry in the interpolated Cx is given values that either belong to covariance values of included nodes, or to the nearest neighbours.

Once the covariance matrix has restored its original dimensions, Bayes formula for the reconstruction, defined by equation 12, is applied, and the epicardial potentials are estimated.

- Laplacian interpolation. The first step in the Laplacian method of interpolation consists on computing the second spatial derivative of the irregular triangular meshes defined within the atrial geometry, as well as the linear distances between vertices belonging to the same face in the atrial geometrical model. The Laplacian is calculated by initializing an empty square matrix which will have the dimensions of the total number of nodes in the atrial model. Then, for each node, the direct neighbours are stored, which are the nodes which share a face with the node under evaluation. The Laplacian is then computed for that node and itself and for its direct neighbours according to the formulas that are shown below, while its value is zero for indirect neighbours.

$$Lap(i,i) = -\left(\frac{4}{h_i}\right) \times \left(\frac{1}{n_i}\sum_{k=1}^{n_i}\frac{1}{dist(i,k)}\right) \quad (25)$$

$$Lap(i,k) = \left(\frac{4}{h_i \times n_i}\right) \times \frac{1}{dist(i,k)} \quad (26)$$

Where $Lap(i,i)$ is the Laplacian of node i and itself, $Lap(i,k)$ is the Laplacian of node i and its k direct neighbours, h_i is the mean distance from a node to all its connected neighbours and $dist(i,k)$ is the distance from node i to its connected neighbour k. Finally, n_i is the number of direct neighbours for node i.

Once the Laplacian is calculated, it is used together with the set of nodes that have been included in the truncated signal to calculate an interpolation matrix. This interpolation matrix will include the coefficients that will contribute to the computation of the values, whether from the EGMs or the covariance matrix, for the excluded set of nodes, given the known values at the set of included nodes.

The Laplacian matrix calculated previously is reshuffled, so that the entries belonging to the set of included nodes are located in the first entries, and those belonging to the set of excluded nodes are the last entries of the matrix. Then, this reshuffled Laplacian matrix is separated into 2 different matrices depending on whether the values belong, or not, to the set of included nodes. Finally, the interpolation matrix is computed as:

$$M_{int} = -A^{\dagger}B \tag{27}$$

Where $A^{\dagger}$ is a E x N matrix representing the pseudoinverse of A, being A the matrix with the values of the Laplacian at the excluded set of nodes, N is the total number of original nodes in the model and E is the number of excluded nodes, B is an N x I matrix representing the values of the Laplacian at the included set of nodes and I is the number of included nodes in the model.

The computed interpolation matrix, M_{int}, has dimensions of E x I. Since this matrix also has to take into account the values that are known from the truncated signal without modifying them, and identity matrix is appended to M_{int}. Finally, the rows and columns of the interpolating matrix are reshuffled taking into account the order of the nodes.

Once the Laplacian interpolation matrix has been calculated, the interpolation proceeds in a straightforward manner. For the EGM approach, the matrix is multiplied by the truncated signal:

$$EGM_{int} = M_{int} \times EGM_{trc} \tag{28}$$

Where EGM_{int} is the interpolated signal that includes all the original spatial information, M_{int} is the interpolation matrix and EGM_{trc} is the EGM signal with reduced spatial information.

For the covariance matrix approach, since it has squared dimensions, it has to be multiplied twice by the interpolating transfer matrix.

$$C_{x_{int}} = \left(M_{int} \times \left(M_{int} \times C_{x_{trc}}\right)^{t}\right)^{t} \tag{29}$$

Where $C_{x_{int}}$ is the interpolated covariance matrix that includes all the original spatial information, M_{int} is the interpolation matrix and $C_{x_{trc}}$ is the covariance matrix that has been computed from the EGM with reduced spatial information.

Upon performing each of the interpolation methods, whether on the electrogram or the covariance matrix, the estimation of epicardial potentials proceeded. The results from the execution of the inverse problem contained the same spatial information as the original signal. This is because due to the interpolation steps, the original problem could be solved using a reduced amount of the initial information.

3.4.3. Alternatives

Taking into account the described interpolation approaches, which differed on either the place of interpolation or the method, a total of 4 different alternatives were applied onto the data according to the methodology described so far. These were: Nearest Neighbour (NN) interpolation of the EGMs, NN interpolation of the Covariance Matrix, Laplacian interpolation on the EGMs and Laplacian interpolation on Cx. However, an additional alternative method was also used, which will be described in this section.

As described in previous sections, not all the samples from the signals of each model are used in the reconstruction of epicardial activity. It has been explained that, for the sinus rhythm model, all the samples from the model are used excluding the first one (from the 2nd to the 2500th sample). The simple and complex atrial fibrillation models contain a total of 5000 samples, from which a number of initial and end transients are removed. The SAF model uses from the 1002nd sample to the 3500th and the CAF model uses from the 502nd to the 3000th.

The computation of the covariance matrix which is used in Bayes regularization method requires a 1 second window from the signal, which, at a sampling frequency of 500Hz, translates into 500 samples. However, the samples used must be different from the ones used in the reconstruction of the signal itself. The location of this time window used to compute the covariance values for the matrix differed from one model to another. For the sinus rhythm model, since all the samples (except the first) are originally used for the reconstruction of potentials, a given number of samples must be left out when proceeding with Bayes regularization. Therefore, the last 500 samples are used for computing the covariance matrix and the rest of samples are used for the inverse problem. For the simple and complex atrial fibrillation models, since a large number of samples are removed for the reconstruction of potentials, the 1 second window is chosen from a stable region among these removed samples. In this sense, for the simple atrial fibrillation model, the covariance matrix is calculated with samples from 500 to 999. Finally, the complex atrial fibrillation model uses samples from 3500 to 4000. This is summarized in table 3.6.

Table 3.6: Samples used originally from all the models for the first interpolation alternative: computation of the covariance matrix used in Bayes regularization method and reconstruction of the inverse problem.

	Sinus rhythm	Simple atrial fibrillation	Complex atrial fibrillation
Total number of samples	2500	5000	5000
Removed initial transients	1	1:1001	1:501
Removed end transients	2001:2500	3501:5000	3001:5000
Samples used for the inverse problem	2:2000	1002:3500	502:3000
Samples used for computing the covariance matrix	2001:2500	500:999	3500:4000

From these 500 sample windows, 150 are randomly selected, and the mean is computed for each node using the 150 time instants. Finally, the covariance matrix is calculated with equation 11.

The time windows described so far, both for the matrix used in the reconstruction of the inverse problem and the computation of the covariance matrix constitute the first alternative among the two that were used in the four different interpolation approaches. The second alternative consisted on using simultaneous time instants for a maximum of 120 nodes when calculating Cx. This was performed in order to mimic a more realistic clinical situation, where no more than 120 points in the atria can be measured simultaneously.

Taking into account that the original time window for calculating Cx contained 1 second of signals (500 samples), of which, 150 samples were randomly selected, if a maximum of 120 nodes were going to be taken at simultaneous instants, then a larger time window is needed to calculate the covariance matrix. However, the choice of such additional time window is not arbitrary, and it cannot be taken from the samples that have been eliminated from the original models due to the presence of unstable transients. Therefore, taking into account that the valid samples of each model are the ones described in table 3.6, these must be rearranged to create a larger time window for computing the covariance matrix.

The solution was achieved by reducing the number of samples used for the reconstruction of the inverse problem, and using such samples to enlarge the time window used for the covariance matrix. This was performed by taking the last 750 samples of each model from the ones used for the reconstruction process and using them together with the ones established originally to compute Cx. In this sense, for the model of sinus rhythm, the samples from 2 to 1250 were used for the inverse problem and from 1251 to 2500 for the Covariance Matrix. The simple atrial fibrillation model now used samples from 1002 to 2750 for the reconstruction of potentials and samples from 500 to 999 concatenated with the samples from 2751 to 3500 for calculating Cx. Finally, the complex atrial fibrillation model used samples from 502 to 2250 for the inverse problem and samples from 2251 to 3000 concatenated with samples from 3500 to 4000 for the covariance matrix. This is summarized in table 3.7 where concatenation of matrices is denoted as $\cup$.

Table 3.7: Samples used from all the models for the second interpolation alternative: computation of the covariance matrix used in Bayes regularization method and reconstruction of the inverse problem.

	Sinus rhythm	Simple atrial fibrillation	Complex atrial fibrillation
Total number of samples	2500	5000	5000
Removed initial transients	1	1:1001	1:501
Removed end transients	1251:2500	3501:5000	3001:5000
Samples used for the inverse problem	2:1250	1002:2750	502:2250
Samples used for computing the covariance matrix	1251:2500	500:999 ∪ 2751: 3500	2251:3000 ∪ 3500:4000

The time windows described in table 3.7 were the ones used in the second interpolation alternative. The 1250 samples used in this second variant to calculate the covariance matrix, were taken in groups of 120 nodes and 500 samples. Then, for each set, 150 were randomly selected, the mean of such 150 samples was computed and the covariance matrix was calculated as described above. In this sense, the covariance matrix was computed using non-simultaneous time instants.

In conclusion, 8 different approaches were applied onto the data. 4 for computation of covariance matrix using simultaneous time instants: Nearest Neighbour interpolation on the EGMs, NN interpolation on Cx, Laplacian interpolation on the EGMs and Laplacian interpolation on Cx; and the same 4 approaches were applied using a non-simultaneous computation of Cx, making a total of 8. Finally, the number of nodes from the models was reduced to an 8^{th}, 7^{th},6^{th}, 5^{th}, 4^{th}, 3^{rd}, 2^{nd} and 1.5^{th} fraction of the original number, leading to results for 255, 291, 340, 408, 510, 680, 1020 and 1359 nodes, respectively. Taking into account that 3 different models of atrial activity were used, this lead to set of 192 different results.

4. Results

This section shows the results obtained after performing the inverse problem on the simulates surface potentials and estimating the epicardial activity. Two different regularization methods were used: Tikhonov and Bayes. Tikhonov's regularization method was used to solve the inverse problem with the data containing all the spatial information available. The results obtained on the three mathematical models available were used as gold standards for comparison purposes. Bayes' regularization method was also used in the reconstruction of epicardial activity with no reduced spatial information. The purpose of doing so was to verify the hypothesis that this regularization showed a better performance than Tikhonov and therefore could be used in subsequent steps when the spatial information was reduced. Finally, Bayes regularization was used to solve the inverse problem on the interpolated data with reduced spatial information.

4.1. Tikhonov regularization

Tikhonov regularization method to solve the inverse problem has different variants. As mentioned in previous sections, the method can be zero order, first order or second order. The zero order variant uses an identity matrix for the spatial regularization matrix, first order uses the Gradient operator and second order uses the Laplacian operator. Also, each order of the method can be executed either using a constant regularization parameter (λ) or an instantaneous λ. The former is used globally to reconstruct all time instants of the signal, whereas the latter varies in the reconstruction of each time instant.

Taking this into account, the preliminary step in defining a gold standard for comparison purposes was to evaluate the performance of the each of the variants of Tikhonov regularization in each of the models available. This performance is summarized in tables 4.1-3. The performance metrics in the reconstruction of epicardial potentials using all variants of Tikhonov's regularization for the sinus rhythm, simple atrial fibrillation and complex atrial fibrillation models are shown in these tables.

For the sinus rhythm model, using a global λ the temporal performance of the regularization decreases for increasing orders of the method, whereas the spatial performance increases for increasing orders, as shown in table 4.1. This is justified, on the one hand, by the decrease in the temporal correlation coefficients (CCt) and the decrease in the temporal relative difference (RDMSt) for increasing orders. On the other hand, the spatial correlation coefficient (CCn) and relative difference (RDMSn) show a better performance for increasing orders of the method, since the first measures slightly increases and the second slightly decreases. These differences in performance between spatial and temporal measures do not occur when using an instantaneous λ. For this case, increasing the order of the method decreases the accuracy of the reconstruction both for the temporal and spatial correlation coefficient and relative difference, as shown in table 4.1. To this respect, both CCt and CCn decrease for increasing orders and both RDMSt and RDMSn increase for increasing orders. Furthermore, it can be seen that in general terms, within the same order, the

method shows a better performance when using an instantaneousλinstead of a global one. Therefore, it can be concluded that among all variants of Tikhonov's regularization, the one which is able to reconstruct epicardial potentials with the highest accuracy is zero order with instantaneous λ.

Table 4.1: Performance metrics in the reconstruction of epicardial potentials for the model of sinus rhythm using all variants of Tikhonov regularization.

Model: Sinus rhythm

	Tik-0	**Tik-1**	**Tik-2**
		Global λ	
CCt	0.655 ± 0.340	0.530 ± 0.345	0.517 ± 0.337
CCn	0.403 ± 0.210	0.520 ± 0.263	0.539 ± 0.261
RDMSt	0.763 ± 0.328	0.914 ± 0.325	0.929 ± 0.319
RDMSn	1.076 ± 0.194	0.938 ± 0.284	0.915 ± 0.290
		Instantaneousλ	
CCt	0.698 ± 0.337	0.698 ± 0.336	0.592 ± 0.286
CCn	0.518 ± 0.148	0.518 ± 0.148	0.496 ± 0.151
RDMSt	0.704 ± 0.329	0.705 ± 0.328	0.868 ± 0.253
RDMSn	0.971 ± 0.147	0.971 ± 0.147	0.993 ± 0.149

The performance metrics computed after reconstructing the epicardial potentials from the model of simple atrial fibrillation using all of the variants of Tikhonov regularization are shown in table 4.2. For this model, the performance of the inverse problem decreases for increasing orders of the method when using a global λ. Unlike the sinus rhythm model, this time both the temporal and spatial measures show a loss of accuracy in the reconstruction for increasing orders and constant λ. This is also the case when using an instantaneousλ, where it can be seen that the CCt and CCn decrease for increasing orders and the RDMSt and RDMSn increase for increasing orders. Finally, it can be seen that, within the same order, the value of the metrics show a better performance when using an instantaneous instead of a global λ. Hence, just like the previous case, it can be concluded that the variant among Tikhonov's algorithm with shows the best performance for the model of simple atrial fibrillation is zero order with instantaneousλ.

The performance metrics for the model of complex atrial fibrillation are shown in table 4.3. In general terms, this model shows the same conclusions as the case of simple atrial fibrillation. When using a global λ, there is a general trend of loss of accuracy in the performance metrics for increasing orders of the method. This is also the conclusion for the instantaneousλcase. Just like all the other models, the performance for the model of complex atrial fibrillation is better for zero order Tikhonov's regularization with instantaneous λ.

Table 4.2: Performance metrics in the reconstruction of epicardial potentials for the model of simple atrial fibrillation using all variants of Tikhonov regularization.

Model: Simple atrial fibrillation

	Tik-0	Tik-1	Tik-2
	Global λ		
CCt	0.542 ± 0.294	0.485 ± 0.252	0.380 ± 0.283
CCn	0.480 ± 0.072	0.448 ± 0.093	0.376 ± 0.077
RDMSt	0.917 ± 0.277	0.987 ± 0.253	1.083 ± 0.260
RDMSn	1.017 ± 0.070	1.047 ± 0.087	1.115 ± 0.069
	Instantaneousλ		
CCt	0.553 ± 0.287	0.553 ± 0.287	0.478 ± 0.242
CCn	0.498 ± 0.077	0.498 ± 0.077	0.441 ± 0.107
RDMSt	0.906 ± 0.271	0.906 ± 0.280	1.000 ± 0.207
RDMSn	1.000 ± 0.076	1.000 ± 0.076	1.052 ± 0.100

Table 4.3: Performance metrics in the reconstruction of epicardial potentials for the model of complex atrial fibrillation using all variants of Tikhonov regularization.

Model: Complex atrial fibrillation

	Tik-0	Tik-1	Tik-2
	Global λ		
CCt	0.170 ± 0.364	0.125 ± 0.359	0.116 ± 0.356
CCn	0.235 ± 0.021	0.152 ± 0.038	0.153 ± 0.037
RDMSt	1.256 ± 0.289	1.293 ± 0.280	1.301 ± 0.277
RDMSn	1.237 ± 0.017	1.302 ± 0.029	1.301 ± 0.028
	Instantaneousλ		
CCt	0.189 ± 0.358	0.189 ± 0.358	0.159 ± 0.306
CCn	0.250 ± 0.026	0.250 ± 0.026	0.207 ± 0.065
RDMSt	1.241 ± 0.286	1.241 ± 0.286	1.275 ± 0.236
RDMSn	1.224 ± 0.021	1.224 ± 0.021	1.258 ± 0.051

4.1.1. Reconstruction of epicardial activity

Having shown that the best performance in Tikhonov regularization is achieved through the zero order method with instantaneous λ, now the goal is to use this method to reconstruct not only the epicardial potentials, but also the rest of target parameters. As mentioned in previous sections, these target parameters include the instantaneous phase and dominant frequency distribution within the atria, as well as the location of singularity points. Upon performing such reconstructions, the performance metric for each parameter will be used as a gold standard for comparative purposes in the following sections.

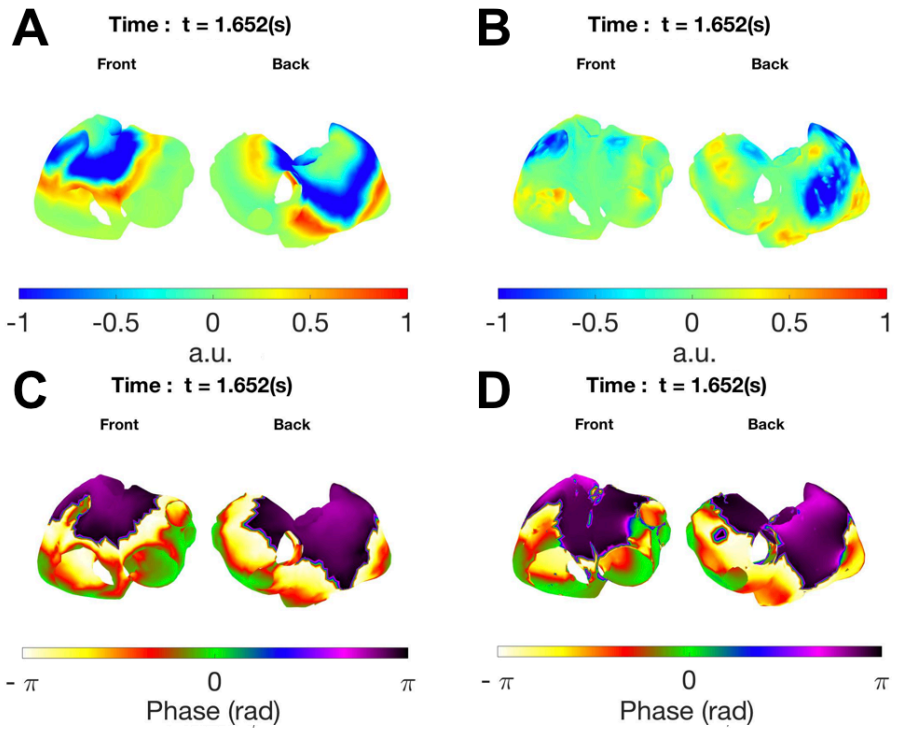

Figure 4.1: Sinus rhythm reconstruction through zero order Tikhonov regularization with instantaneous λ.
Real (A) and reconstructed (B) epicardial potentials, real (C) and reconstructed (D) instantaneous phase at the 1.652nd second of the signal from the model of sinus rhythm using zero order Tikhonov regularization with instantaneous λ.

The first model that was estimated with the described method was SR. As seen in the Materials and method section, this model lacks dominant frequency regions and singularity points. This is due to the fact that the model represents normal cardiac activity, where the frequency distribution is the same for all the atria as is equal to the frequency of activation. Also, the model lacks any rotors. Therefore, the reconstruction aims at estimating the epicardial activity and then computing from these potentials, the associated instantaneous phase.In figure 4.1A the real epicardial potentials from the SR model are shown and the estimated potentials are illustrated in figure 4.1B.The estimation of these potentials is performed using zero-order Tikhonov regularization with instantaneous λ, and both of them are illustrated at the 1.652nd second of the signal. In figure 4.1C,

the real instantaneous phase from the SR model is represented for the same time instant as the potentials, and in figure 4.1D the reconstructed instantaneous phase is shown.

The use of zero order Tikhonov regularization with instantaneous λ in the estimation of SR epicardial activity allows reconstructing both epicardial potentials and instantaneous phase. As shown in figure 4.1, the technique can be used to obtain a smooth distribution of the real parameters. Although the results obtained are not extremely precise, they are useful in identifying the overall atrial activity.

The second model that was reconstructed corresponded to the one of simple atrial fibrillation. In this case, the presence of a fibrillation episode translates to the appearance of different dominant frequency regions within the atria. Also, as mentioned in previous sections, the condition is associated to the presence of a singularity point guiding the fibrillation pattern. This can be observed in figures 4.2 and 4.3, where not only the epicardial potentials have been depicted, but also the instantaneous phase, dominant frequencies and singularity points, which could be calculated from the potentials. In figure 4.2A, the distribution of real epicardial potentials from the SAF model is shown for the 3.446th second of the signal, and the reconstructed potentials can be seen in figure 4.2B, also at the same time instant. The real instantaneous phase from the SAF model is seen in figure 4.2C, whereas the reconstructed instantaneous phaseis shown in figure 4.2D, both at the same time instant as the epicardial potentials, 3.446 seconds.

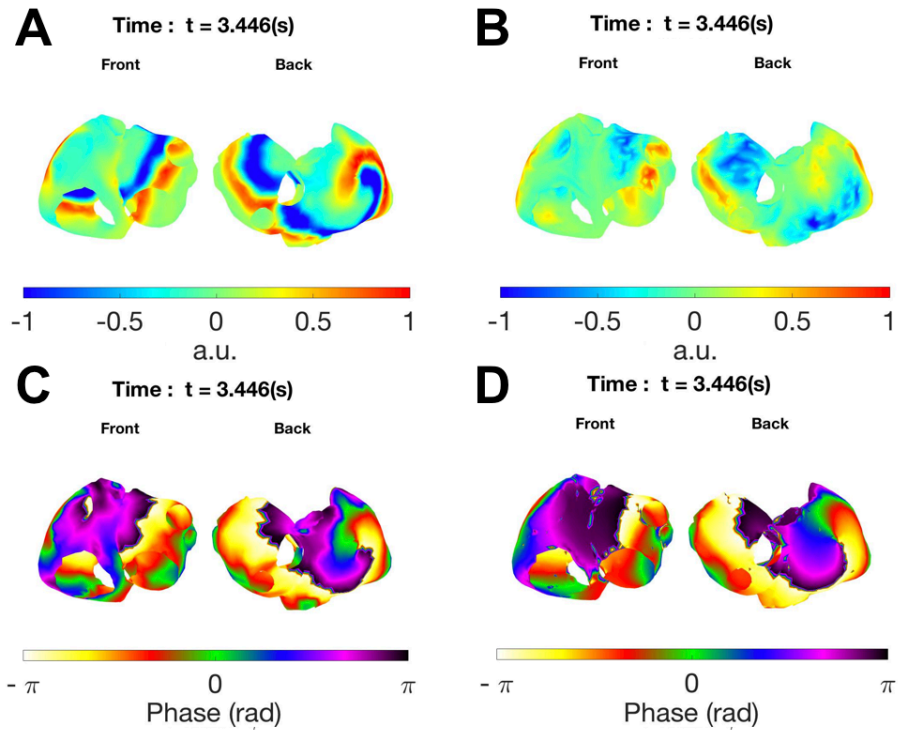

Figure 4.2: Simple atrial fibrillation reconstruction through zero order Tikhonov regularization with instantaneousλ.
Real (A) and reconstructed (B) epicardial potentials, real (C) and reconstructed (D) instantaneous phase at the 3.446th second of the signal from the model of simple atrial fibrillation using zero order Tikhonov's regularization with instantaneousλ.

The other two target parameters from the SAF model are shown in figure 4.3. The real dominant frequency map from the SAF model is shown in figure 4.3A, while the reconstructed parameter is illustrated in figure 4.3B. Finally, the last parameter to reconstruct from the SAF model is the location of singularity points. The real probabilities of rotor location (SMF) are shown in figure 4.3C, whereas the reconstructed ones are represented in figure 4.3D.

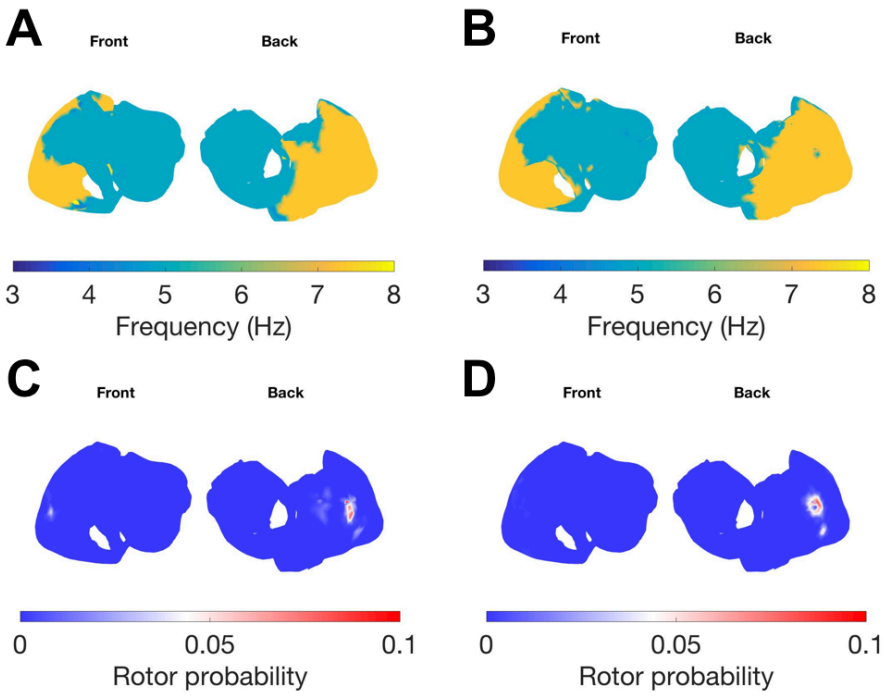

Figure 4.3: Simple atrial fibrillation reconstruction through zero order Tikhonov regularization with instantaneous λ.
Real (A) and reconstructed (B) dominant frequencies, real (C) and reconstructed (D) singularity point occurrences in the atria from the model of simple atrial fibrillation using zero order Tikhonov regularization with instantaneous λ.

Tikhonov regularization method is a useful tool for identifying not only epicardial potentials, but also the instantaneous phase, dominant frequencies and the presence of singularity points from models of SAF. As seen in the figures, the accuracy in the reconstruction process is not perfect, but it is good enough to identify the main features of the fibrillation episode.

Finally, the third model to estimate was the one of complex atrial fibrillation. Analogously to the previous case, this type of model requires the computation of dominant frequencies and singularity points as well as epicardial potentials and the instantaneous phase. These are shown in figure 4.4 and 4.5. It can be seen that the reconstruction is not very accurate for this type of model. This is due to the complexity of the fibrillation activity, which is extremely chaotic, as well as the presence of fibrosis, which makes the estimation less accurate. The distribution of real epicardial potentials from the CAF model is shown in figure 4.4A at the 2.426thsecond of the signal. In figure 4.4B, the reconstructed potentials using zero order Tikhonov with instantaneous λ are shown for the same time instant.

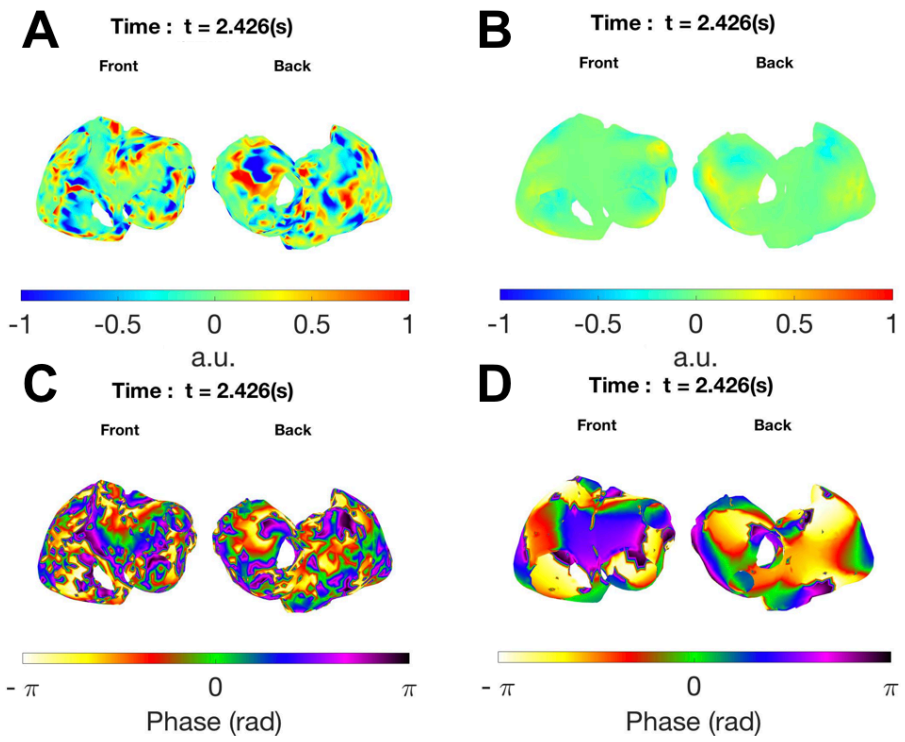

***Figure 4.4**: **Complex atrial fibrillation reconstruction through zero order Tikhonov regularization with instantaneousλ.** Real (A) and reconstructed (B) epicardial potentials, real (C) and reconstructed (D) instantaneous phase at the 2.426th second of the signal from the model of complex atrial fibrillation using zero order Tikhonov regularization with instantaneousλ.*

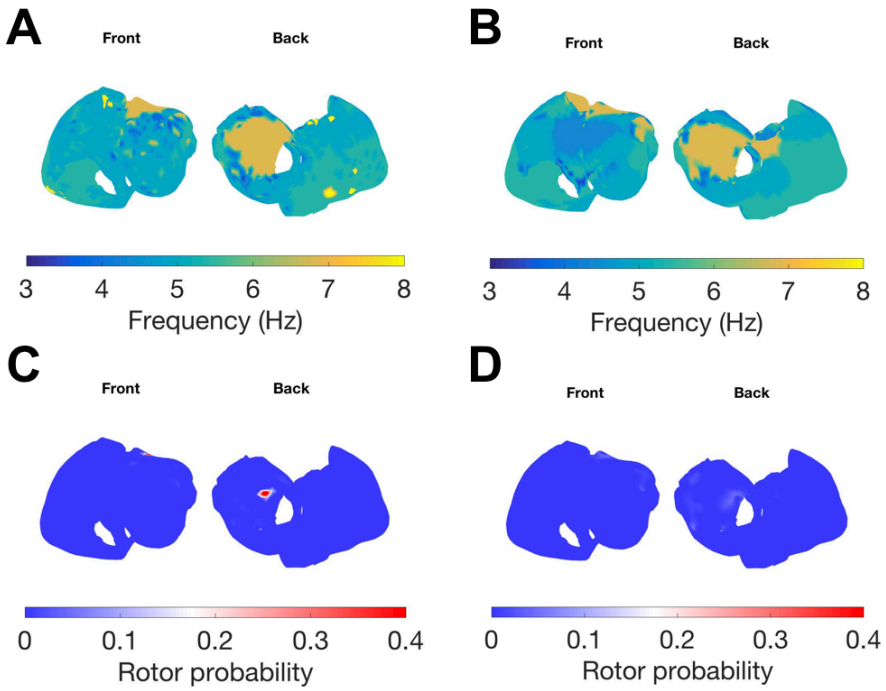

***Figure 4.5: Complex atrial fibrillation reconstruction through zero order Tikhonov regularization with instantaneousλ.** Real (A) and reconstructed (B) dominant frequencies, real (C) and reconstructed (D) singularity point occurrences in the atria from the model of complex atrial fibrillation using zero order Tikhonov regularization with instantaneous λ.*

The real and reconstructed instantaneous phase from the model is shown, respectively, in figures 4.4C and 4.4D, both at the same time instant as the epicardial potentials. Just like the SAF case, there are DF regions and rotors in the CAF model, as shown in figure 4.5. The real atria DF map is shown in figure 4.5A, whereas the reconstructed parameter is illustrated in figure 4.5B. Finally, the real probabilities of finding a rotor in the atria for the CAF model are represented in figure 4.5C, whereas the probabilities of rotor location for the reconstructed model are shown in figure 4.5D.

4.1.2. Performance metrics

This section contains the results obtained for the performance metrics of the target parameters in the reconstruction of each of the models using zero order Tikhonov regularization with instantaneous λ. In addition to the tables containing the mean and standard deviation values for the performance metric of each of the target parameters, the values of these measures in the geometrical atrial model are also shown in figures.

The first set of results corresponds to the performance of the reconstruction from the model of sinus rhythm. The temporal performance metrics for the estimated potentials and the instantaneous phase are shown in figure 4.6. Despite the fact that the accuracy of the estimated epicardial potentials can be measured with both temporal and spatial performance metrics (temporal and spatial correlation coefficient and relative difference), only the temporal ones are illustrated. This is explained by the lack of spatial metrics to measure the performance of the instantaneous phase's reconstruction. Hence, to be able to compare effectively the accuracy between the estimated potentials and instantaneous phase, only the temporal versions of the correlation coefficient (CCt) and relative difference (RDMSt) are shown.

The distribution of the values of the correlation coefficient and relative differences within the atria are shown in figure 4.6, both for the reconstruction of epicardial potentials (4.6A and 4.6B, respectively) and instantaneous phase (4.6C and 4.6D). The distribution of CCt values of potentials and instantaneous phase, shown infigures 4.6A and 4.6C, respectively, is slightly better for the reconstruction of potentials than for the instantaneous phase. This can be observed through the presence of more blue regions in figure 4.6C than in figure 4.6A, representing smaller correlation values. This is also the case for the relative difference (RDMSt). The distribution of RDMSt values in the atria for the reconstruction of epicardial potentials and instantaneous phase are shown in figures 4.6B and 4.6D, respectively. The mean correlation and relative difference values for all nodes in the atria are summarized in table 4.4, as well as their standard deviation. The values of this metric within the atrial geometrical model are also better (>10%) for the epicardial potentials than for the instantaneous phase. This is visualized by means of the greater appearance of yellow zones in figure 4.6D than figure 4.6B. This conclusion makes sense, since the instantaneous phase is computed from the reconstructed potentials. Hence, the error introduced in the solution of the inverse problem is not only maintained in the reconstruction of the instantaneous phase, but may be actually increased in the subsequent computation of this target parameter. These mean values once again confirm the better performance of the method in the reconstruction of epicardial potentials than instantaneous phase.

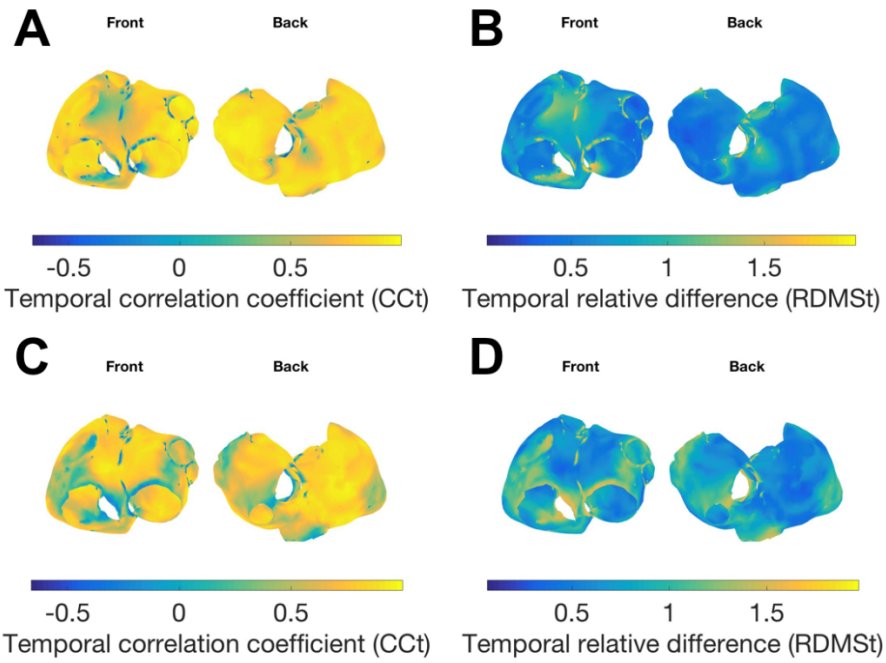

Figure 4.6: Performance metrics in sinus rhythm's reconstruction through zero order Tikhonov regularization with instantaneousλ.

Performance metrics in the reconstruction of sinus rhythm's epicardial potentials and instantaneous phase within the atria using zero order Tikhonov regularization with instantaneousλ. Epicardial potentials' (A) temporal correlation coefficient (CCt) and (B) temporal relative difference measurement star (RDMSt). Instantaneous phase's (C) CCt and (D) RDMSt.

In general terms, the correlation values for the SR model are close to 1, and the relative difference values are close to 0 for most of the atrial tissue. However, as seen in figure 4.6, the CCt values of both the reconstructed potentials (figure 4.6A) and instantaneous phase (figure 4.6C) decrease notably for the atrial model's spatial discontinuities. The opposite takes place for the relative difference values, which decrease near the model's orifices and concavities (figure 4.6B and figure 4.6D). For this case in particular, the anatomical regions with the lowest CCt (and highest RDMSt) values is the right atrial appendage, as well as the atrial holes.

Table 4.4: Temporal performance metrics in the reconstruction of epicardial potentials and instantaneous phase for the model of sinus rhythm using zero order Tikhonov regularization with instantaneous λ.

Model: Sinus rhythm

	Epicardial potentials	**Instantaneous phase**
CCt	0.698 ± 0.337	0.584 ± 0.322
RDMSt	0.704 ± 0.329	0.852 ± 0.327

The second set of results corresponds to the performance metrics in the reconstruction of the simple atrial fibrillation model, once again using zero order Tikhonov regularization with instantaneous λ. All the values obtained are summarized in table 4.5. Analogously to the previous case, only the temporal metrics are shown for the reconstruction of epicardial potentials, as well as for the instantaneous phase. The mean and standard deviation for the CCt and RDMSt is shown in the table for all the values obtained from the whole atrial geometrical model.

Table 4.5: Performance metrics in the reconstruction of epicardial potentials and instantaneous phase for the model of simple atrial fibrillation using zero order Tikhonov regularization with instantaneous λ.

Model: Simple atrial fibrillation

	Epicardial potentials	**Instantaneous phase**
CCt	0.553 ± 0.287	0.561 ± 0.299
RDMSt	0.906 ± 0.271	0.892 ± 0.289

Regarding table 4.5, the mean values obtained for the metrics in the reconstruction of epicardial potentials and instantaneous phase show that, the performance in the estimation of potentials and instantaneous phase is almost the same. However, compared to the model of sinus rhythm, it can be seen that the reconstruction method is less precise when the atrial activity is different from the normal one and slightly more complex due to a fibrillation event.

The performance in the reconstruction of the simple atrial fibrillation model is also shown in figure 4.7. However, the distribution, and not only the mean values, within the atrial model for each of the metrics are shown in each figure. Regarding the temporal correlation coefficient (CCt), the distribution for the reconstructed potentials (figure 4.7A) and instantaneous phase (figure 4.7C)is very similar, as seen previously in the mean values shown in table 4.5. This is also the case for the distribution of the temporal relative difference (RDMSt) of potentials and instantaneous phase, shown in figures 4.7B and 4.7D.Hence, the potentials and instantaneous phasewithin the atria are reconstructed with almost the same precision, and differ only 1%. With respect to the dominant frequency's metric, it can be seen that in general terms, the value of the relative dominant frequency error is low. This can be observed in the predominant dark blue-painted portions in figure 4.7E, which correspond to a low value for the RDFE. However, there are a small number of regions which have a very high value of this metric, which are painted in light blue, green and yellow in the figure.

Analogously to the SR model, the CCt shows high values (and RDMSt low values) for most of the atrial tissue, both for the reconstruction of epicardial potentials and instantaneous phase. Nevertheless, these metrics tend to show lower accuracy near the atrial model's holes and cavities. For SAF model in particular, the anatomical region which is reconstructed with the least precision is the septum.

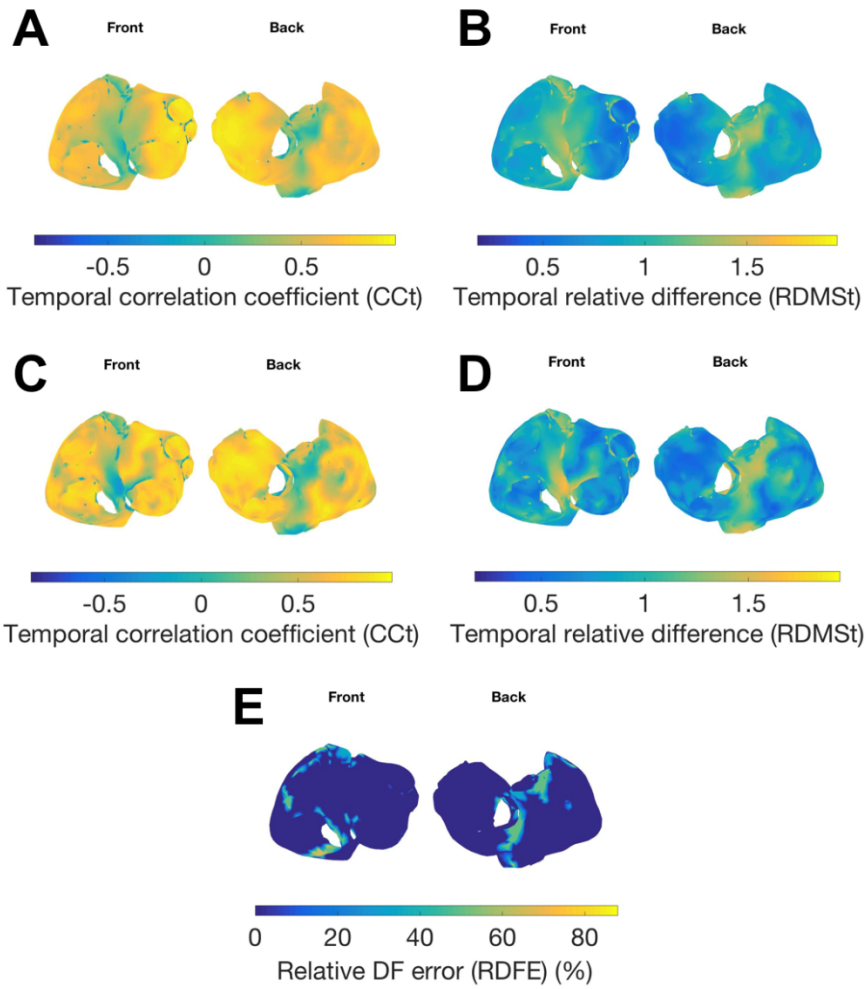

Figure 4.7: Performance metrics in simple atrial fibrillation's reconstruction through zero order Tikhonov regularization with instantaneous λ.

Performance metrics in the reconstruction of simple atrial fibrillation epicardial potentials, instantaneous phase and dominant frequencies within the atria using zero order Tikhonov regularization with instantaneousλ. Epicardial potentials' (A) temporal correlation coefficient and (B) temporal relative difference measurement star. Instantaneous phase's (C) temporal correlation coefficient and (D) temporal relative difference measurement star. Dominant frequencies (E) relative error.

The third set of results corresponds to the performance metrics in the reconstruction of the complex atrial fibrillation model through zero order Tikhonov regularization with instantaneous λ. The mean and standard deviation values obtained for the temporal correlation coefficient and relative difference for the potentials and instantaneous phase are shown in table 4.6.Analogously to the simple atrial fibrillation, the complex atrial fibrillation model shows similar mean values of performance metrics for potentials and instantaneous phase, as represented in table 4.6. Also, the distribution within the atrial model for each of the metrics is very similar both for the epicardial potentials and instantaneous phase, as shown in figure 4.8 from A to D. The temporal CC for the reconstructed potentials is illustrated in figure 4.8A, which is very similar to the CCt distribution of the reconstructed instantaneous phase, shown in figure 4.8C. Analogously, the temporal relative difference in the reconstructed potentials is represented in figure 4.8B, which once again, is very similar to the RDMSt distribution of the reconstructed instantaneous phase, as shown in figure 4.8D.

Table 4.6: Performance metrics in the reconstruction of epicardial potential and instantaneous phase for the model of complex atrial fibrillation using zero order Tikhonov regularization with instantaneous λ.

Model: Complex atrial fibrillation

	Epicardial potentials	Instantaneous phase
CCt	0.189 ± 0.358	0.187 ± 0.364
RDMSt	1.241 ± 0.286	1.239 ± 0.304

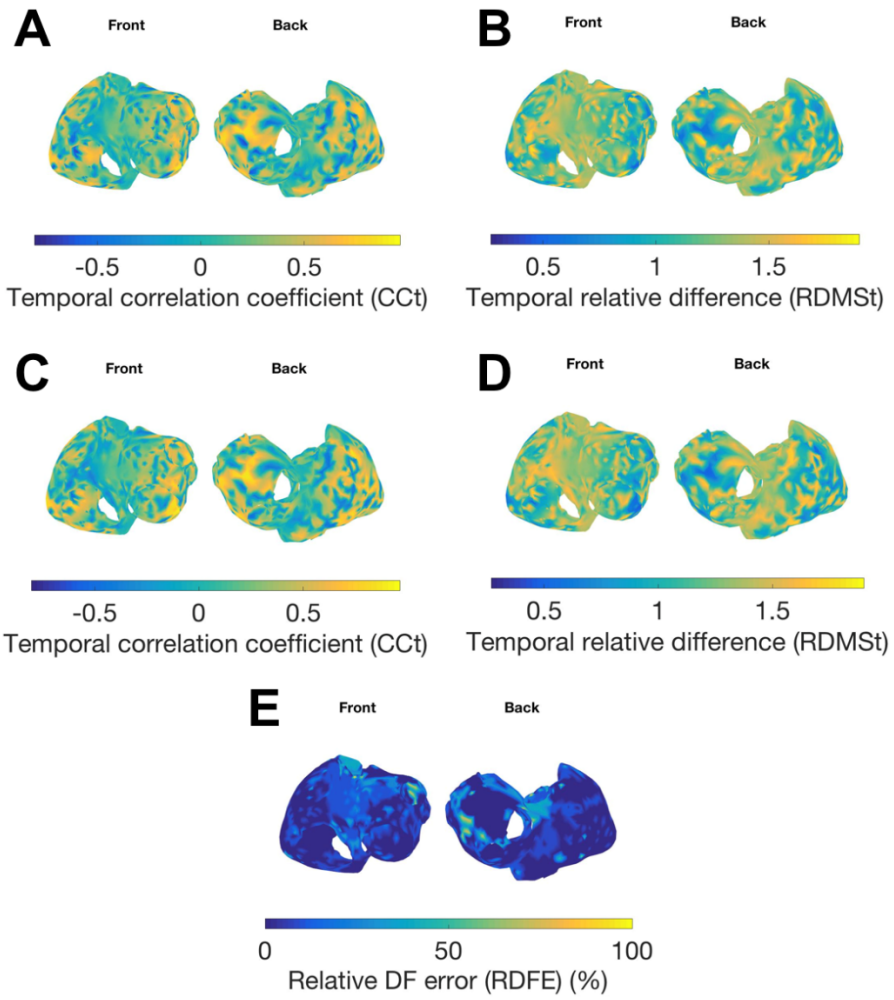

Figure 4.8: Performance metrics in complex atrial fibrillation's reconstruction through zero order Tikhonov regularization with instantaneous λ.
Performance metrics in the reconstruction of complex atrial fibrillation's epicardial potentials, instantaneous phase and dominant frequencies within the atria using zero order Tikhonov regularization with instantaneousλ. Epicardial potentials' (A)temporal correlation coefficient and (B) temporal relative difference measurement star. Instantaneous phase's (C) temporal correlation coefficient and (D) temporal relative difference measurement star. Dominant frequencies (E) relative error.

Regarding the performance metric for the reconstruction of dominant frequencies, there are many regions with a small RDFE value, which means a good performance. However, there are many regions

in the atria which have a high value for the relative dominant frequency error, as shown in figure 4.8E. Contrary to the previous models, where the error in the reconstruction of epicardial potentials and instantaneous phase was localized in certain anatomical regions, CAF shows no specific area where the errors are concentrated. Hence, the values of the performance metrics for all the target parameters vary in all atrial regions, as seen in figures from 4.8A to 4.8E.

4.2. Bayes regularization

Bayesian Maximum a Posteriori Estimation (Bayes) is a regularization method to solve the inverse problem of electrocardiography which uses a priori information. As mentioned in previous sections, this a priori information used is the epicardial potentials' covariance matrix, whose computation has been already discussed.

This regularization method was the one used not for comparison purposes like Tikhonov, but actually as the reconstruction technique with the reduced spatial information models. Among the interpolation approaches used, one of them focused on the interpolation of the covariance matrix. Hence it is necessary to perform an analysis and interpretation of this matrix in order to interpolate in an appropriate manner in subsequent steps. Therefore, this section presents an analysis of the epicardial potential's covariance matrix used in Bayes regularization method, as well as the results of this reconstruction technique with the originally provided models (without reducing spatial information).

4.2.1. Analysis of the epicardial potential's Covariance Matrix

The epicardial potentials' covariance matrix is a squared matrix with dimensions of the total number of nodes in the model which are used in the calculation. It represents the covariance values for the potentials at each node and the rest of nodes. By selecting a random node and plotting the covariance values on a coloured scale on top of the atrial geometrical model, it can be seen that the actual distribution of covariance values is similar to the distribution of potentials within the atria. This can be seen in figure 4.9. The covariance values for the three models of epicardial activity at the 500^{th} node in the atria with respect to the rest of nodes are shown in this figure. The models of sinus rhythm, simple atrial fibrillation and complex atrial fibrillation are represented, respectively, in figures 4.9A, 4.9B and 4.9C. Despite having different values to the potentials, as well as the different colour scale which is used to represent them, the distribution is very similar to the potentials themselves. Hence, the interpolation of this covariance matrix in further steps is similar, in terms of distribution within the atria, to interpolation of the electrogram itself.

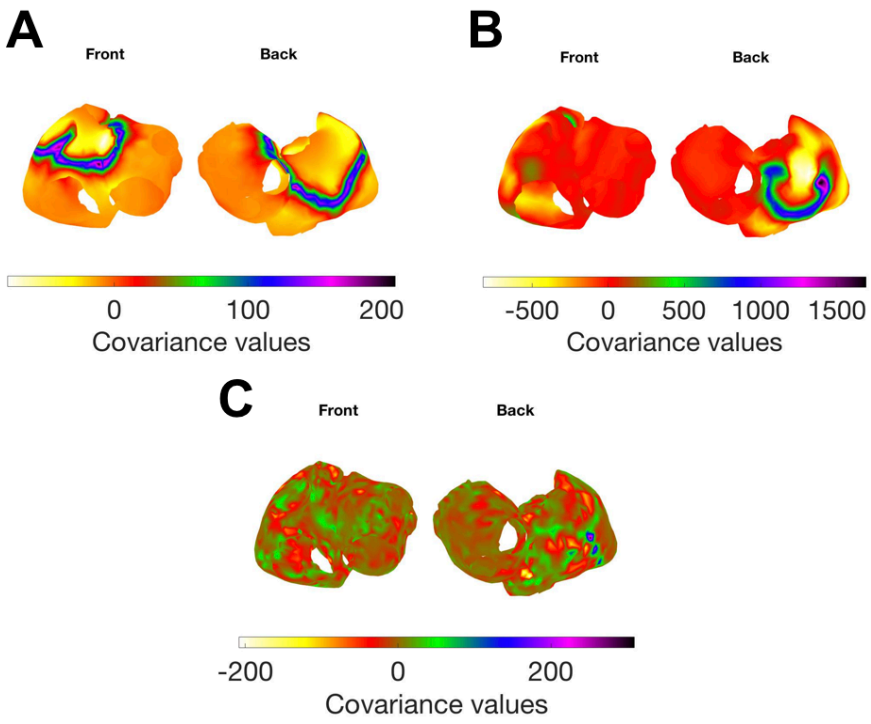

Figure 4.9: Covariance values between a random node (Node 500) and the rest of nodes within the atria.
(A) Sinus rhythm model. (B) Simple atrial fibrillation model. (C) Complex atrial fibrillation model.

As mentioned in previous sections, the location of the time window to calculate the covariance matrix differed from one model to the other. Therefore, another feature of this matrix to take into account was the variation of covariance values depending on the location of this time window within the electrogram. To analyse this, a 500 sample window was moved along the electrogram of each of the models, in intervals of 250 samples, and different covariance matrices were computed.

The variation, for each of the models, of the different covariance values between a random node (node 500) and the rest of nodes depending on the location of the time window is shown in figure 4.10.The results for the sinus rhythm model are shown in figure 4.10A. As shown in this figure, the location of the time window to compute the covariance values is irrelevant for this model, since the covariance values for node 500 and each of the other nodes are almost constant when moving the time window through the EGM. The results for the simple atrial fibrillation model are shown in figure 4.10B, where it can be seen that for this model, the variation among covariance values is slightly greater depending on the location of the time window. Still, these variations are small, and it can be concluded that the covariance values are not affected by moving the time window along the EGM. Finally, the results for complex atrial fibrillation are shown in figure 4.10C. For this case, the variation of covariance values is affected by the location of the time window, as shown in the plot, especially if it is placed between in the second half of the signal (between the middle and end transients). However, these particular middle and end transients from the CAF model are not used, neither for the computation of the covariance matrix nor for the reconstruction of the inverse problem in any of the interpolation approaches.

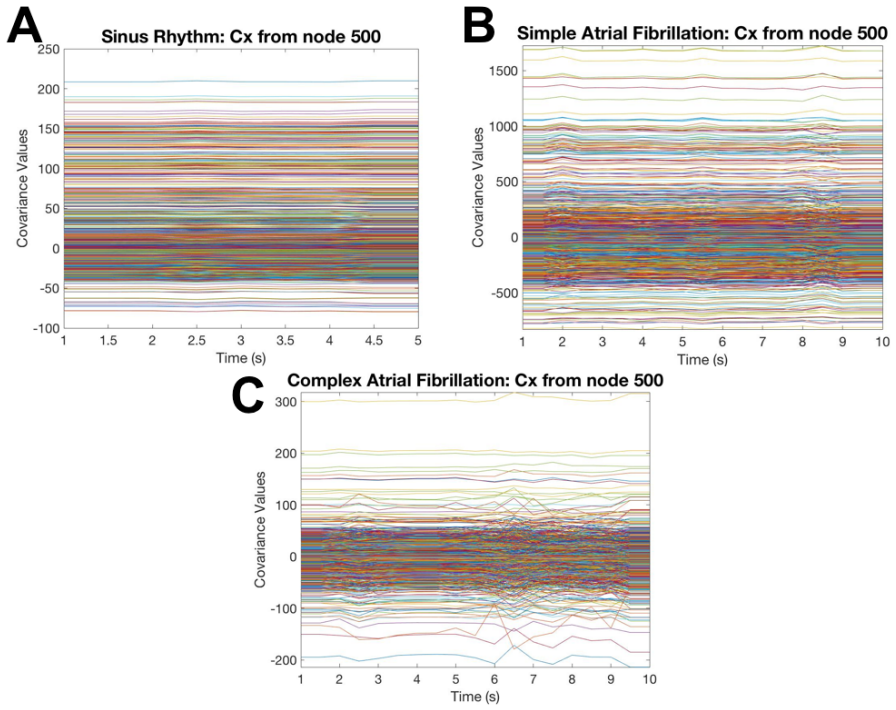

Figure 4.10:Variation of covariance values for a random node (Node 500) and the rest of nodes within the atria depending on the location of the time window used to compute the Covariance Matrix.
(A) Sinus rhythm model. (B) Simple atrial fibrillation model. (C) Complex atrial fibrillation model.

In conclusion, the distribution of covariance values for a random node in the atria and the rest of nodes is very similar to the distribution of epicardial potentials for a given time instant,as shown in these figures. Therefore, interpolating the covariance matrix has a similar meaning to interpolating the electrogram, in terms of distribution of values. Also, it has been shown that the location of the time window to compute the matrix affects the values of the matrix in the CAF model, but not in the SR or SAF models. However, the two different alternatives of time windows that have been used in the interpolation steps for computing Cxare not located within the samples in which the covariance values vary.

4.2.2. Reconstruction of epicardial activity

This section shows the results corresponding to the reconstruction of epicardial activity for the three models available using Bayes' regularization method. The models used for this set of results contained all the spatial information that was originally provided. Also, the time windows used both for the estimation of potentials and for the computation of the covariance matrix correspond to the ones used originally, described previously in materials and methods.

The reconstruction of epicardial activity for the sinus rhythm model is shown in figure 4.11. The distribution in the atrial model of the real epicardial potentials from the SR model is shown in figure

4.11A for second 1.652 of the signal. The reconstructed potentials in the atrial model using Bayes regularization method are shown in figure 4.11B, again for the same time instant as the real potentials. The real and reconstructed instantaneous phase from the SR model are illustrated, respectively, in figures 4.11C, and 4.11D, both for the same time interval as the epicardial potentials. The normal electrical propagation in the atria which is represented in this model explains the absence in dominant frequency regions as well as singularity points. In fact, the frequency distribution is the same for the whole atrial geometry, and is equal to 1.2 Hz, as mentioned in previous sections.

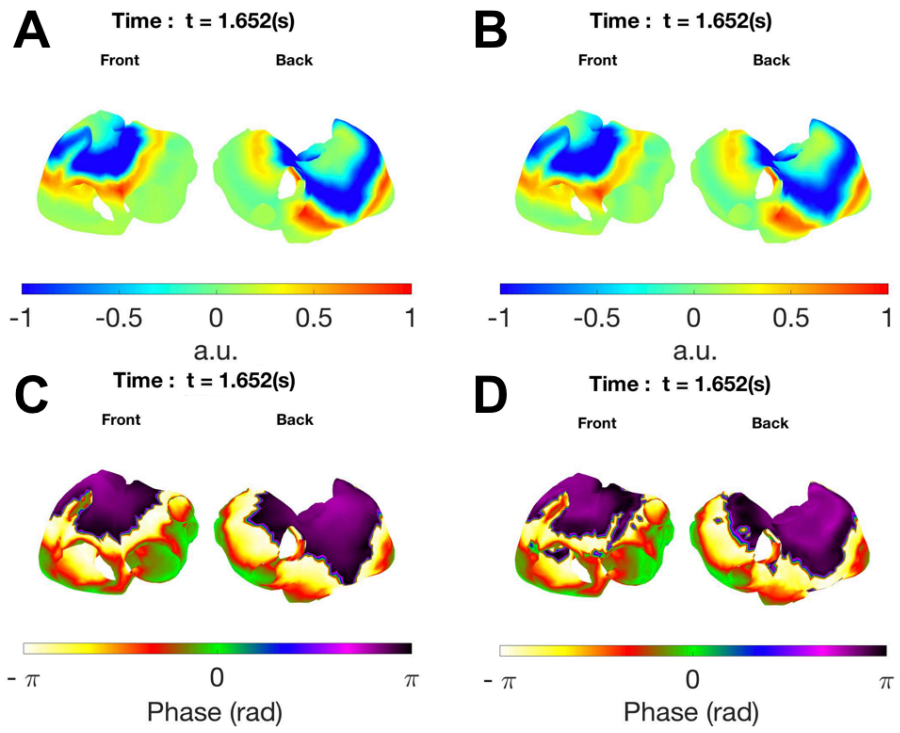

Figure 4.11: Sinus rhythm reconstruction through Bayes regularization method.
Real (A) and reconstructed (B) epicardial potentials at second 1.652 of the signal, real (C) and reconstructed (D) instantaneous phase at second 1.652 of the signal from SR model using Bayes regularization.

Regarding the reconstruction of target parameters from SR model through Bayes regularization, it is more accurate than Tikhonov. In fact, the differences between the real and estimated epicardial activity is negligible, as shown in figure 4.11, especially for the epicardial potentials. Overall, the SR model is reconstructed in detail with Bayes regularization.

The estimated epicardial activity for the model of simple atrial fibrillation can be seen in figures 4.12 and 4.13. The distribution of real epicardial potentials from the SAF model is shown in figure 4.12A, during second 3.446 of the signal. The reconstructed potentials for the same model and time instant using Bayes' regularization method are shown in figure 4.12B. The real instantaneous phase of the SAF model is represented in figure 4.12C, whereas the reconstructed oneis shown in figure 4.12D, both for the same time instant as the epicardial potentials. The presence of fibrillation activity means that there are also dominant frequency regions which can be computed from the potentials, as well

as probabilities of finding rotors, which are illustrated in figure 4.13. The real dominant frequency map for the SAF model is shown in figure 4.13A, and the reconstructed DFs can be seen in figure 4.13B. Finally, the probabilities of finding a singularity point at each node in the atria for the real SAF model is shown in figure 4.13C, and this same probability for the reconstructed model can be seen in figure 4.13D.

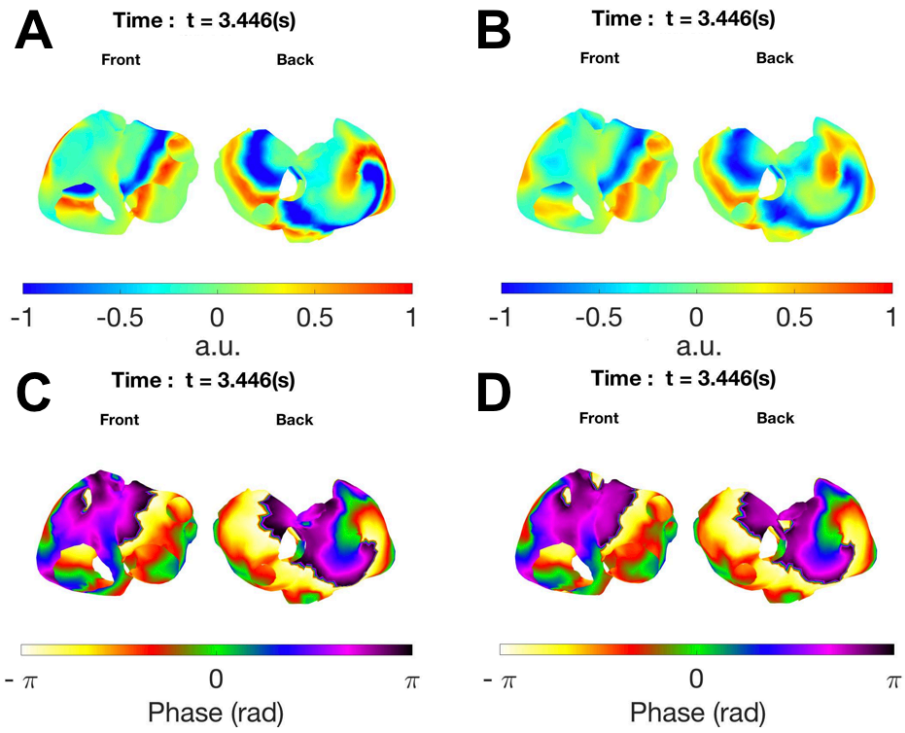

Figure 4.12: Simple atrial fibrillation reconstruction through Bayes regularization method.
Real (A) and reconstructed (B) epicardial potentials at second 3.446 of the signal, real (C) and reconstructed (D) instantaneous phase at second 3.446 of the signal from SAF model using Bayes regularization.

Bayes regularization is also useful for estimating SAF epicardial activity, as shown in figures 4.12 and 4.13. Analogously to the previous model, more detailed and less smoothed results are obtained, compared to Tikhonov regularization. This accuracy in the reconstruction of parameters translates in an easier identification of wavefronts and rotors, as shown in the figures.

The last set of results corresponds to the complex atrial fibrillation model, and is illustrated in figures 4.14 and 4.15. Analogously to the previous model, the estimated epicardial potentials from this model can also be used to create instantaneous phase and dominant frequency maps, as well as for the detection of singularity points. The distribution of real epicardial potentials in the atria at second 2.426 from the CAF model is shown in figure 4.14A, and the reconstructed potentials for the same time instant using Bayes regularization method are illustrated in figure 4.14B. The real and reconstructed instantaneous phase can be seen, respectively, in figures 4.14C and 4.14D, both for the same time instant as the epicardial potentials.

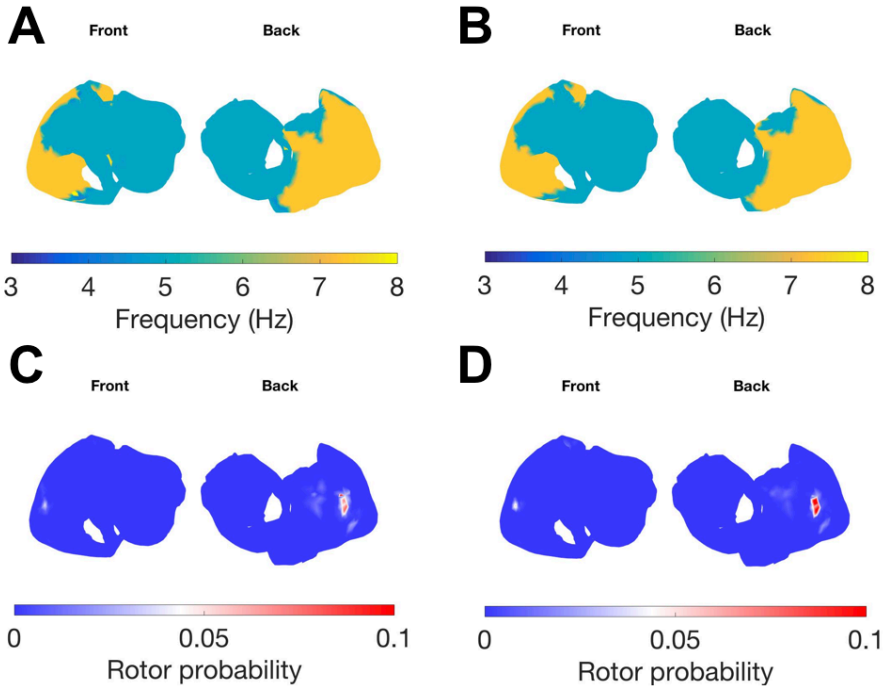

Figure 4.13: Simple atrial fibrillation reconstruction through Bayes regularization method.
Real (A) and reconstructed (B) dominant frequency maps, real (C) and reconstructed (D) probabilities of singularity point location in the atria from SAF model using Bayes regularization.

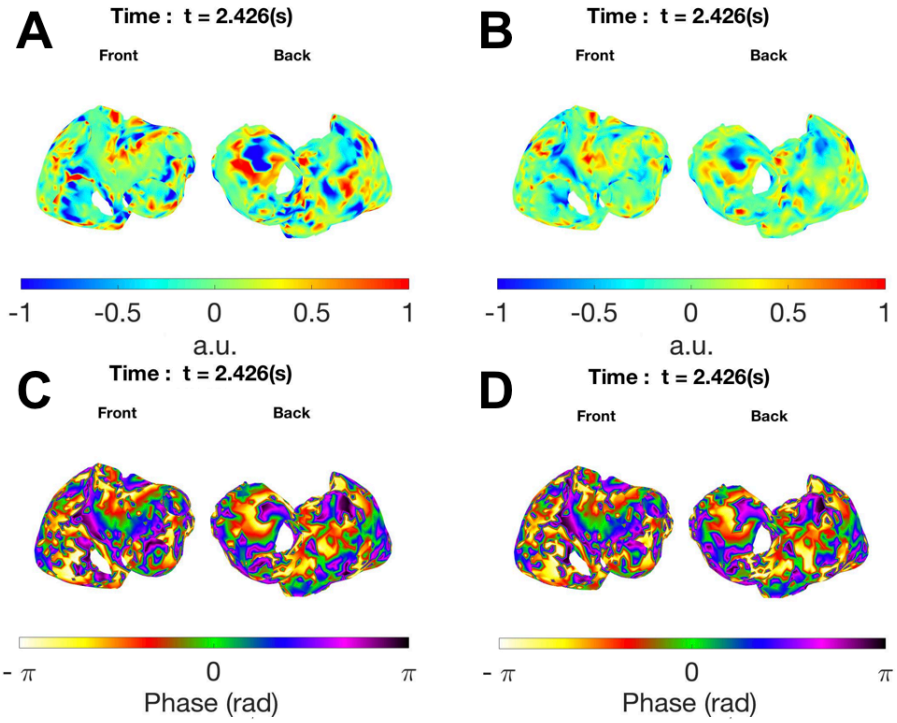

Figure 4.14: Complex atrial fibrillation reconstruction through Bayes regularization method.
Real (A) and reconstructed (B) epicardial potentials at second 2.426 of the signal, real (C) and reconstructed (D) instantaneous phase at second 2.426 of the signal from CAF model using Bayes regularization.

The other target parameters which can be computed in the CAF model are illustrated in figure 4.15. The real dominant frequency map is shown in figure 4.15A, and the reconstructed DF map using Bayes' regularization method is represented in figure 4.15B. Finally, the probability of finding a singularity point at each node in the atria for the real CAF model is shown in figure 4.15C, and the same probability for the estimated model can be seen in figure 4.15D.

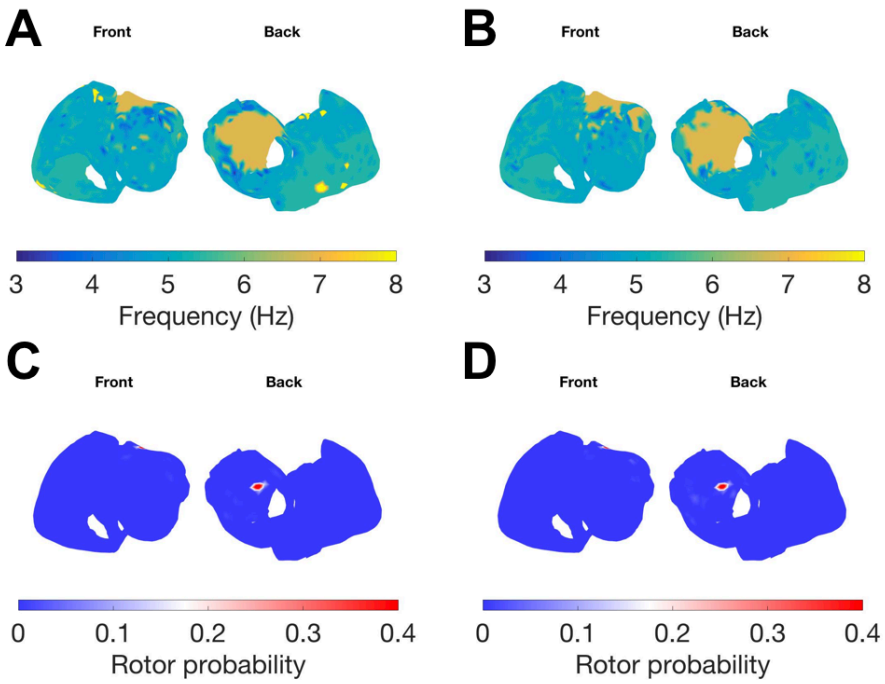

Figure 4.15: Complex atrial fibrillation reconstruction through Bayes regularization method.
Real (A) and reconstructed (B) dominant frequency maps, real (C) and reconstructed (D) probabilities of singularity point location in the atria from CAF model using Bayes regularization.

Analogously to the previous models, CAF epicardial activity is reconstructed in detail through Bayes regularization, as shown in figures 4.14 and 4.15. Despite the complexity of the model, the reconstructed target parameters are more accurate than the ones obtained through Tikhonov's approach.

4.2.3. Performance metrics

This section shows the results obtained for the performance metrics in the reconstruction of epicardial activity for each of the models using Bayes regularization method. Analogously to the results presented in Tikhonov's section, the values for each node in the atrial model are shown in figures, and the mean and standard deviation values for the entire atria are shown in tables.

The performance metrics in the estimation of potentials and instantaneous phase for the model of sinus rhythm are shown in figure 4.16. Only the temporal correlation coefficient (CCt) and relative difference (RDMSt) are shown for the reconstructed potentials, and not the spatial versions. As explained in previous sections, this is due to the lack of these spatial versions for the reconstructed instantaneous phase. Therefore, in order to compare both parameters, only the temporal metrics are included.

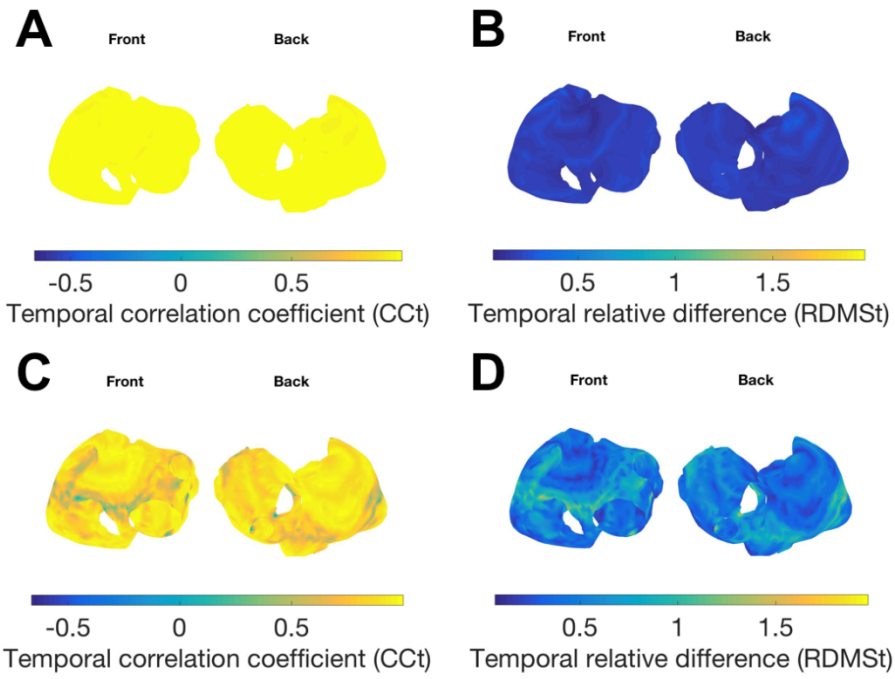

Figure 4.16: Performance metrics in the reconstruction of the sinus rhythm model through Bayes regularization method. *Performance metrics in the reconstruction of epicardial potentials and instantaneous phase within the atria using Bayes regularization. Epicardial potentials (A)temporal correlation coefficient (CCt) and (B) temporal relative difference measurement star (RDMSt). Instantaneous phase (C) CCt and (D) RDMSt.*

Table 4.7: Values of the performance metrics obtained in the reconstruction of the sinus rhythm model.

Model: Sinus rhythm

	Epicardial potentials	**Instantaneous phase**
CCt	0.982 ± 0.006	0.842 ± 0.161
RDMSt	0.188 ± 0.032	0.505 ± 0.250

The distribution of temporal correlation coefficients for the estimated potentials and instantaneous phase, are represented in figure 4.16A and 4.16C, respectively. The performance is better for the reconstruction of epicardial potentials than for the instantaneous phase, as shown in these figures. This can be seen in the completely yellow-painted atria in figure 4.16A, representing high correlation values for all nodes, whereas the presence of certain areas which are green or blue coloured in figure

4.16C demonstrates lower correlation values for those nodes. This fact can also be observed in table 4.8. In this table, the mean and standard deviation for the performance metrics' values within the atria is shown. Regarding the mean CCt values for the epicardial potentials and instantaneous phase, the reconstruction is better (>10%) for the potentials than for the instantaneous phase. In the same manner, the relative differences in the atria for the estimated potentials and instantaneous phase, which can be seen, respectively, in figures 4.16B and 4.16D, are lower for the potentials than for the instantaneous phase. Again, this can be seen in the almost completely dark blue coloured atria with low relative difference values in figure 4.16B, whereas a lighter blue colour as well as areas tending towards yellow, representing higher RDMSt values, is shown in figure 4.16D. This is clarified in table 4.8 with the mean and standard deviation values for this metric, where it can be seen than the epicardial potentials' and instantaneous phase's RDMSt differ more than 30%.

Comparing Bayes and Tikhonov performance for SR model, it can be seen than Bayes regularization is superior to Tikhonov. In fact, reconstructing SR epicardial activity through Bayes regularization method does not lead to the appearance of atrial regions where the errors are concentrated. Unlike Tikhonov's approach, the presence of holes and cavities in the atrial model does not imply a poorer performance when using Bayes regularization. Furthermore, the correlation coefficient for the estimated potentials is nearly 30% greater for Bayes regularization compared to Tikhonov (0.982±0.006 vs 0.698±0.337).

The results obtained for the performance metrics in the reconstruction of the simple atrial fibrillation model are illustrated in figure 4.17 and table 4.9. The distribution of CCt values within the atria in the estimated potentials and instantaneous phase are shown, respectively, in figure 4.17A and 4.17C. The accuracy in the reconstruction process is very similar for the potentials and for the instantaneous phase, as shown in table 4.9. The complexity of this cardiac activity with respect to the previous one introduces more errors in the estimation process, meaning an overall loss of precision in the SAF model compared to the SR model, as seen in table 4.9. This fact is also seen through observation of the values of RDMSt in figures 4.17B and 4.17D, which correspond to the potentials and instantaneous phase, respectively. Again, the distribution is very similar for both of them, in figure 4.17B and figure 4.17D. Also, the mean RDMSt values of table 4.9 reaffirm this hypothesis.

Table 4.8: Values of the performance metrics obtained in the reconstruction of the simple atrial fibrillation model.

Model: Simple atrial fibrillation

	Epicardial potentials	**Instantaneous phase**
CCt	0.851 ± 0.093	0.838 ± 0.076
RDMSt	0.517 ± 0.174	0.555 ± 0.123

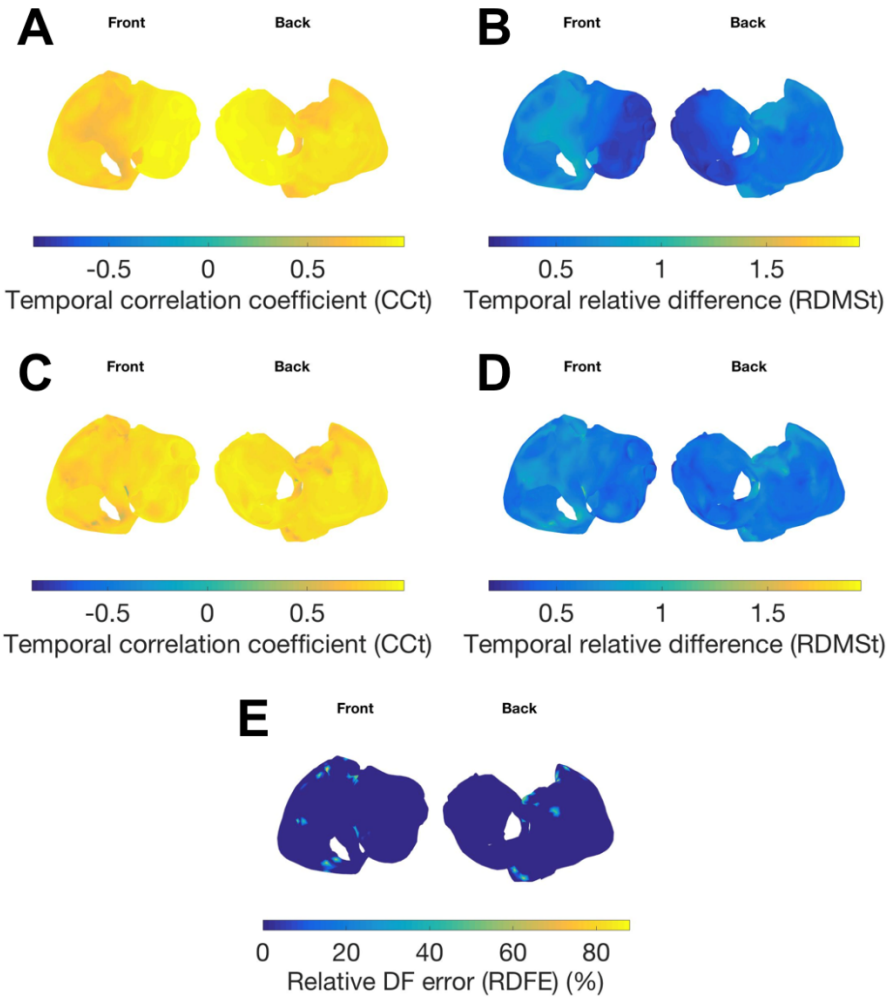

Figure 4.17: Performance metrics in the reconstruction of simple atrial fibrillation model through Bayes regularization method.

Performance metrics in the reconstruction of epicardial potentials,instantaneous phase and dominant frequencies within the atria using Bayes regularization. Epicardial potentials (A)CCt and (B) RDMSt. Instantaneous phase (C) CCt and (D) RDMSt. Dominant frequencies (E) relative dominant frequency error (RDFE).

The dominant frequency regions are detected with great accuracy, especially compared to the results seen previously with Tikhonov's approach. The distribution of the values obtained for the dominant frequency's performance metric, the relative dominant frequency error (RDFE), is shown in figure 4.17E. In general terms, the error committed in the reconstruction process is almost zero, except a number of small regions in the atria, as shown in this figure.

Analogously to the previous model, Bayes regularization has a better performance than Tikhonov in the reconstruction of SAF model. Once again, there are no localized regions where the values of the performance metrics are worse than the rest of the atrial tissue. The results obtained through Bayes regularization for SAF are more detailed than Tikhonov, in fact, the correlation coefficient for the reconstructed epicardial potentials is once again nearly 30% higher for Bayes (0.851±0.093 vs 0.553±0.287).

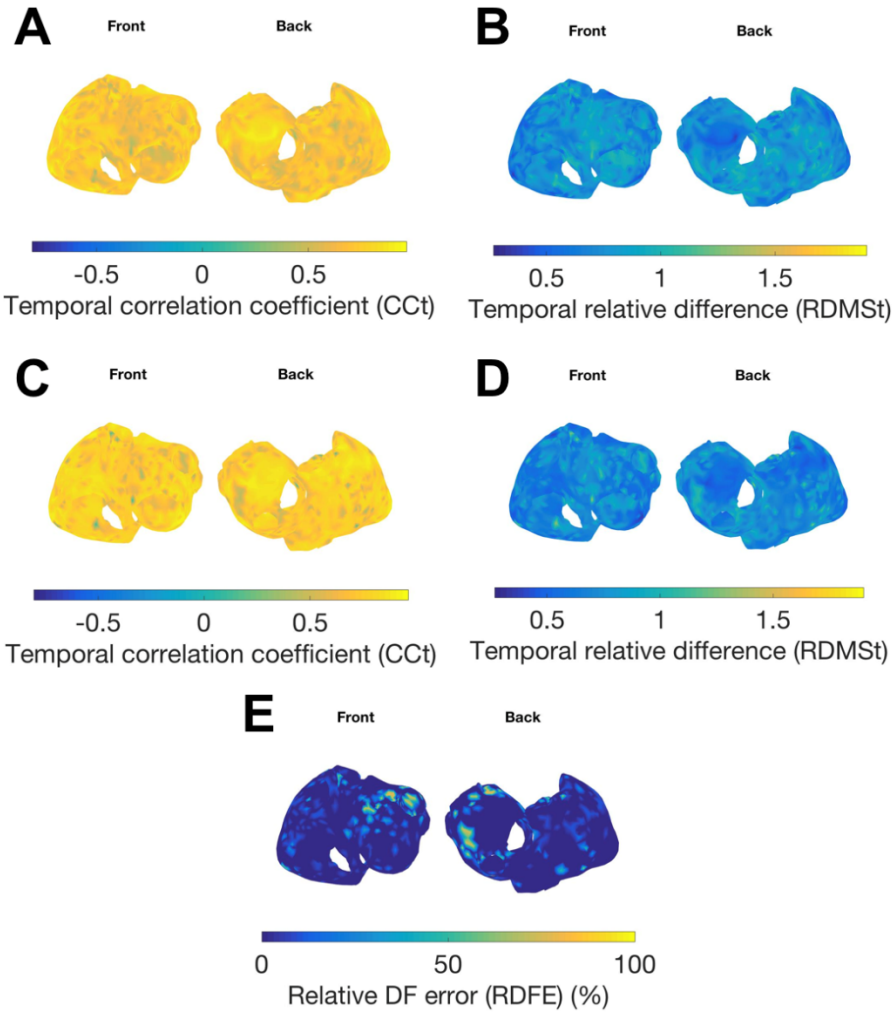

Figure 4.18: Performance Metrics in the reconstruction of the complex atrial fibrillation model through Bayes regularization method.

Performance metrics in the reconstruction of epicardial potentials, instantaneous phase and dominant frequencies within the atria using Bayes regularization. Epicardial potentials (A)CCt and (B) RDMSt. Instantaneous phase (C) CCt and (D) RDMSt. Dominant frequencies (E) RDFE.

The last set of results for this section corresponds to the performance metrics in the reconstruction of the complex atrial fibrillation model, which are shown in figure 4.18 and table 4.10. In general terms, there is an overall loss of precision in the reconstruction of all target parameters compared to the previous models. This makes sense, since the fibrillation event is more complex and the model considers the presence of fibrotic tissue. The distribution of CCt values within the atria for the estimated potentials and instantaneous phase, are shown, respectively, in figure 4.18A and figure 4.18C. Again, the RDMSt for potentials and instantaneous phase can be seen in figure 4.18B and figure 4.18D. The distribution of RDFE in the reconstruction of dominant frequencies is represented in figure 4.18E. As it can be seen, the accuracy in the detection of this parameter is worse than for the model of simple atrial fibrillation.

Table 4.9: Values of the performance metrics obtained in the reconstruction of the complex atrial fibrillation model.

Model: Complex atrial fibrillation

	Epicardial potentials	Instantaneous phases
CCt	0.707 ± 0.111	0.750 ± 0.117
RDMSt	0.751 ± 0.146	0.691 ± 0.152

Once again, a superior performance is achieved when using Bayes regularization instead of Tikhonov for reconstructing CAF epicardial activity. The location of atrial regions with errors is randomly distributed, just like Tikhonov's case. However, this time the values of the performance metrics is notably better. In fact, the correlation coefficient for the reconstructed epicardial potentials is over 50% better for Bayes regularization (0.707±0.111 vs 0.189±0.358).

In conclusion, the results shown in this section demonstrate the superior performance of Bayes regularization in comparison to Tikhonov for solving the inverse problem of electrocardiography. Hence it is adequate to use this method while reducing the models' spatial information and at the same time aiming to achieve a performance equal or greater than the one obtained through Tikhonov regularization.

4.3. Interpolation

This section shows the results obtained for the performance metrics on the interpolated and reconstructed models. As described in previous sections, the goal of this work was to reduce the spatial information from the different models of epicardial activity and perform the inverse problem using Bayes regularization method. The overall objective was to achieve a performance superior that Tikhonov's approach, provided a reduced number of intracavitary signals. In this sense, figures are included in this section both for Tikhonov and Bayes performance on the raw data, as well as Bayes results obtained with the subsequent elimination of spatial information from the models.

For each of the figures shown, Tikhonov and Bayes performance on the models with all the spatial information (2039 nodes) are represented, respectively, with black and red dashed lines on the graphs. Interpolation of the covariance matrix is represented by diamonds joined by lines, and electrogram interpolation is represented by joined circles. The different colours represent the different interpolation methods: dark blue for nearest neighbour and cyan for laplacian. Finally, the second alternative in which the covariance matrix was calculated with different time windows for sets containing of a maximum of 120 nodes is also represented with different colours. For this alternative, nearest neighbour interpolation is shown in green and laplacian's method is magenta.

The first set of results corresponds to the sinus rhythm's model, which are shown on figures from 4.19 to 4.22. In figure 4.19, the temporal correlation coefficient between the reconstructed epicardial potentials and the real ones for different interpolation approaches is shown. The performance of Cx interpolation versus EGM interpolation using Nearest Neighbour method and the same time window for all nodes can be seen in figure 4.19A. As seen in this figure, EGM interpolation has a superior performance than interpolating the covariance matrix. In figure 4.19B, EGM Nearest Neighbour interpolation versus Laplacian is shown, and the same two interpolation methods over Cx are seen in figure 4.19C, both of them using the same time window for all nodes when calculating the covariance matrix. For SR model, Laplacian interpolation works better than NN, as shown in these figures. Finally, EGM Laplacian interpolation using all nodes simultaneously versus non-simultaneously, and Cx Laplacian interpolation with the same time window for all nodes versus different time windows for sets of 120 nodes, are represented, respectively in figure 4.19D and 4.19E. The performance for both alternatives is very similar, especially for the EGM interpolation case shown in 4.19D. However, for SR model, using all nodes simultaneously has a better performance than using them in sets of 120 nodes. In conclusion, the best performance obtained for the temporal correlation coefficient in the reconstructed epicardial potentials from the SR model is achieved through EGM Laplacian interpolation using all nodes simultaneously. Finally, for this metric in particular, it can be seen that it is possible to reduce the initially provided spatial information down to (more or less) 500 nodes, while maintaining or surpassing Tikhonov's performance.

The interpolated and estimated epicardial potentials are also shown in figure 4.20, but this time the performance metric that is shown is the temporal relative difference measurement star. The same conclusions as the previous metric with respect to the best method of interpolation can be observed in this figure. Analogously to the previous case, interpolating of the electrogram gives better and more coherent results than interpolating on the covariance matrix, as shown in figure 4.20A. Once again, Laplacian's method is more precise than nearest neighbour, both for EGM and Cx approaches, as shown in figure 4.20B and 4.20C, respectively.

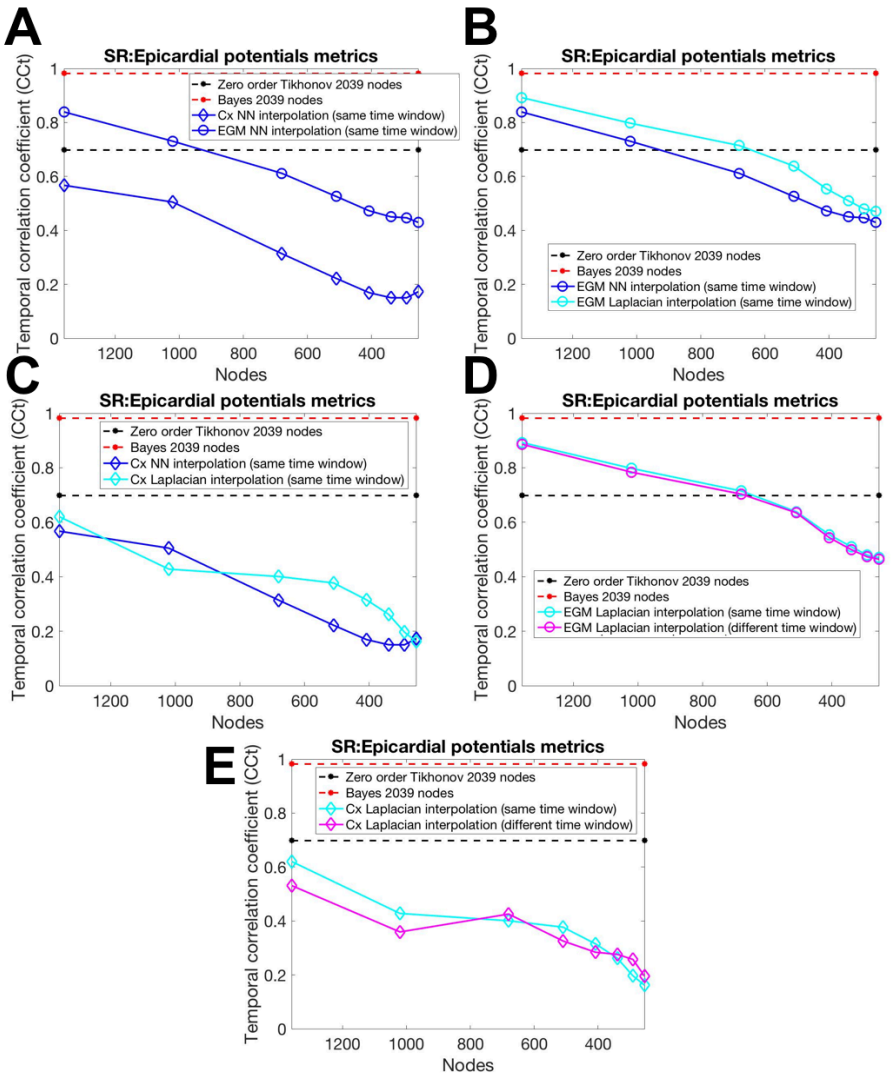

Figure 4.19: Temporal correlation coefficient in the reconstructed epicardial potentials from the model of sinus rhythm using different interpolation approaches, and comparison with zero order Tikhonov and Bayes regularizations without interpolating.

Temporal correlation coefficient in the reconstruction of epicardial potentials after applying different interpolation methods: (A) EGM vs. Cx NN interpolation using all nodes simultaneously, (B) EGM NN vs. Laplacian using the same time window for all nodes, (C) Cx NN vs. Laplacian using the same time window, (D) EGM Laplacian using the same time window vs. using different time windows for sets of 120 nodes, and (E) Cx Laplacian using the same time window vs. using different time windows for sets of 120 nodes.

Regarding the two alternatives in time windows used to calculate the covariance matrix, the same conclusions as those obtained for CCt results apply to RDMSt. Both alternatives have a very similar behaviour in terms of performance, but the one using the same time window for all the set of nodes in the model is slightly better, as shown in figures 4.20D and 4.20E. Hence, the conclusion for the SR's RDMSt between real and reconstructed epicardial potentials is the same as the CCt: the interpolation method which achieved the best performance is EGM Laplacian interpolation using all nodes simultaneously. Finally, for this metric in particular, it can be seen that it is possible to reduce the initially provided spatial information down to (more or less) 500 nodes, while maintaining or surpassing Tikhonov's performance.

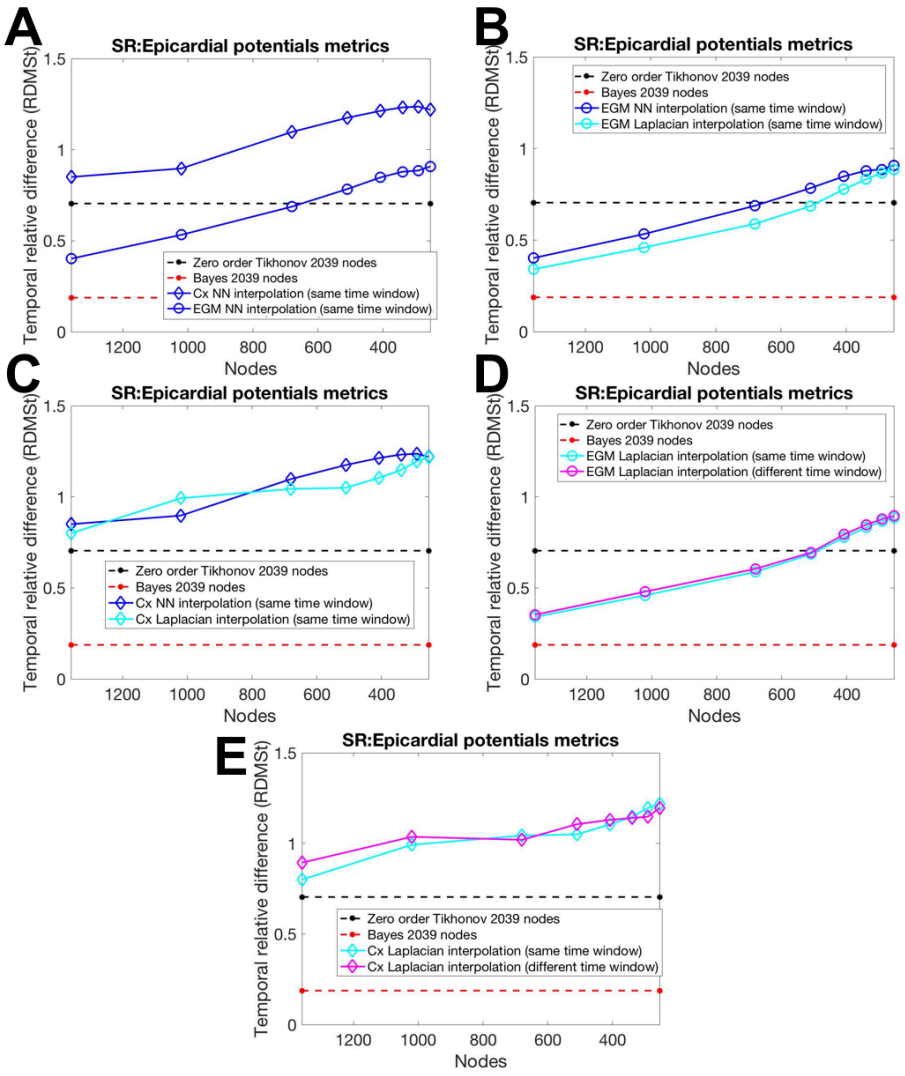

Figure 4.20: Temporal relative difference in the reconstructed epicardial potentials from the model of sinus rhythm using different interpolation approaches, and comparison with zero order Tikhonov and Bayes regularizations without interpolating.

Temporal relative difference in the reconstruction of epicardial potentials after applying different interpolation methods: (A) EGM vs. Cx NN interpolation using all nodes simultaneously, (B) EGM NN vs. Laplacian using the same time window for all nodes, (C) Cx NN vs. Laplacian using the same time window, (D) EGM Laplacian using the same time window vs. using different time windows for sets of 120 nodes, and (E) Cx Laplacian using the same time window vs. using different time windows for sets of 120 nodes.

The interpolated and reconstructed instantaneous phase from the Sinus Rhythm's model, are seen in figures 4.21 and 4.22. The temporal correlation coefficient is shown in figure 4.21, whereas the temporal relative difference between the real and estimated instantaneous phase can be seen in figure 4.22. Analogously to the epicardial potentials' performance metrics, this target parameter is reconstructed with more accuracy after interpolating the EGM and not the covariance matrix, as shown in figures 4.21A and 4.22A. Also, EGM and Cx Laplacian interpolation have a better performance than nearest neighbour, as illustrated in figures 4.21B and figure 4.21C. The same applies to the RDMSt, shown in figures 4.22B with EGM interpolation and 4.22C with Cx interpolation. For the reconstruction of instantaneous phase, there is an increase in the differences

between the results obtained when using the same time window or a different time window for different sets of nodes for calculating the covariance matrix. Still, the results are better when using all nodes simultaneously, as seen in figures 4.21D, 4.21E, 4.22D and 4.22E.

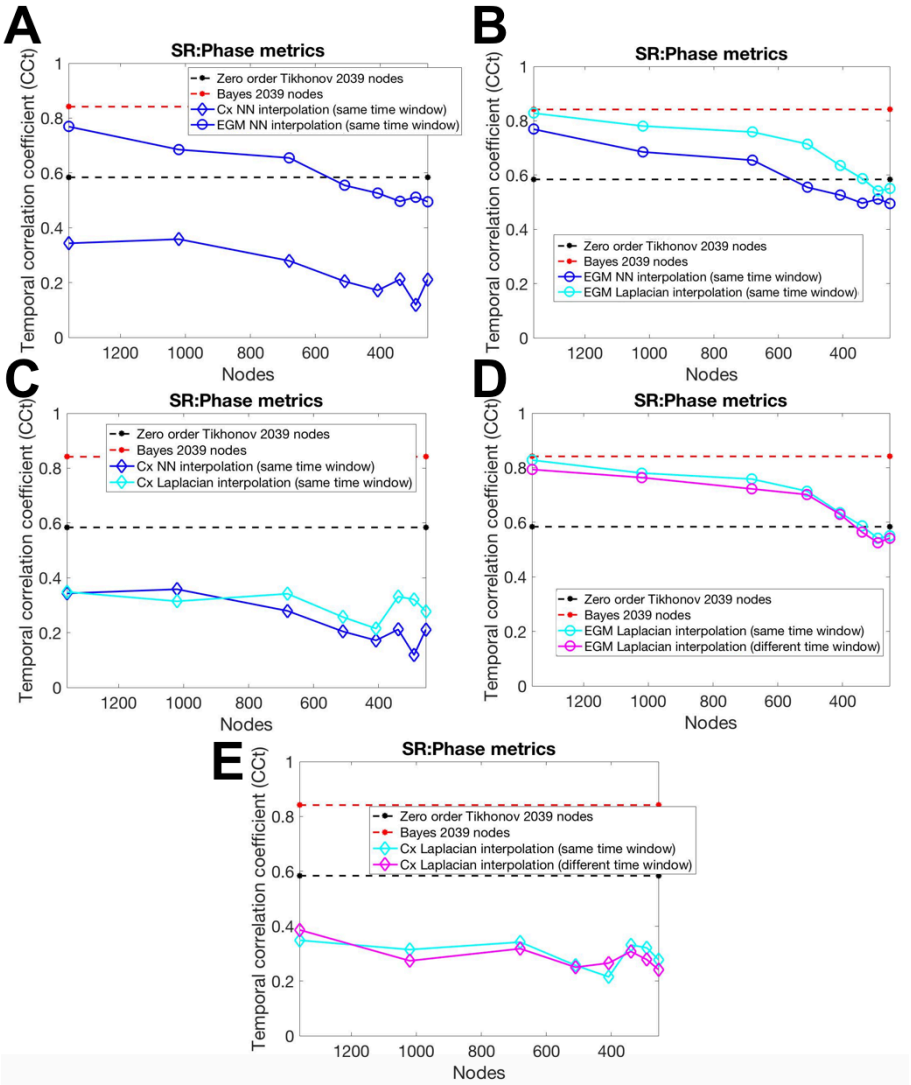

Figure 4.21: Temporal correlation coefficient in the reconstructed instantaneous phase from the model of sinus rhythm using different interpolation approaches, and comparison with zero order Tikhonov and Bayes regularization without interpolating.

Temporal correlation coefficient in the reconstruction of instantaneous phase after applying different interpolation methods: (A) EGM vs. Cx NN interpolation using all nodes simultaneously, (B) EGM NN vs. Laplacian using the same time window for all nodes, (C) Cx NN vs. Laplacian using the same time window, (D) EGM Laplacian using the same time window vs. using different time windows for sets of 120 nodes, and (E) Cx Laplacian using the same time window vs. using different time windows for sets of 120 nodes.

Hence, the performance metrics obtained for the SR instantaneous phase show that the best method of interpolation is the same as the one for the epicardial potentials: EGM Laplacian interpolation using the same time window for all nodes. These conclusions apply both to the instantaneous phase's CCt and RDMSt (Figures 4.21 and 4.22). Finally, it is possible to reduce the number of nodes to 340 for the instantaneous phase's CCt, as seen in 4.21D, and down to 300 nodes for the RDMSt, as shown in figure 4.22D, whilst maintaining Tikhonov's performance.

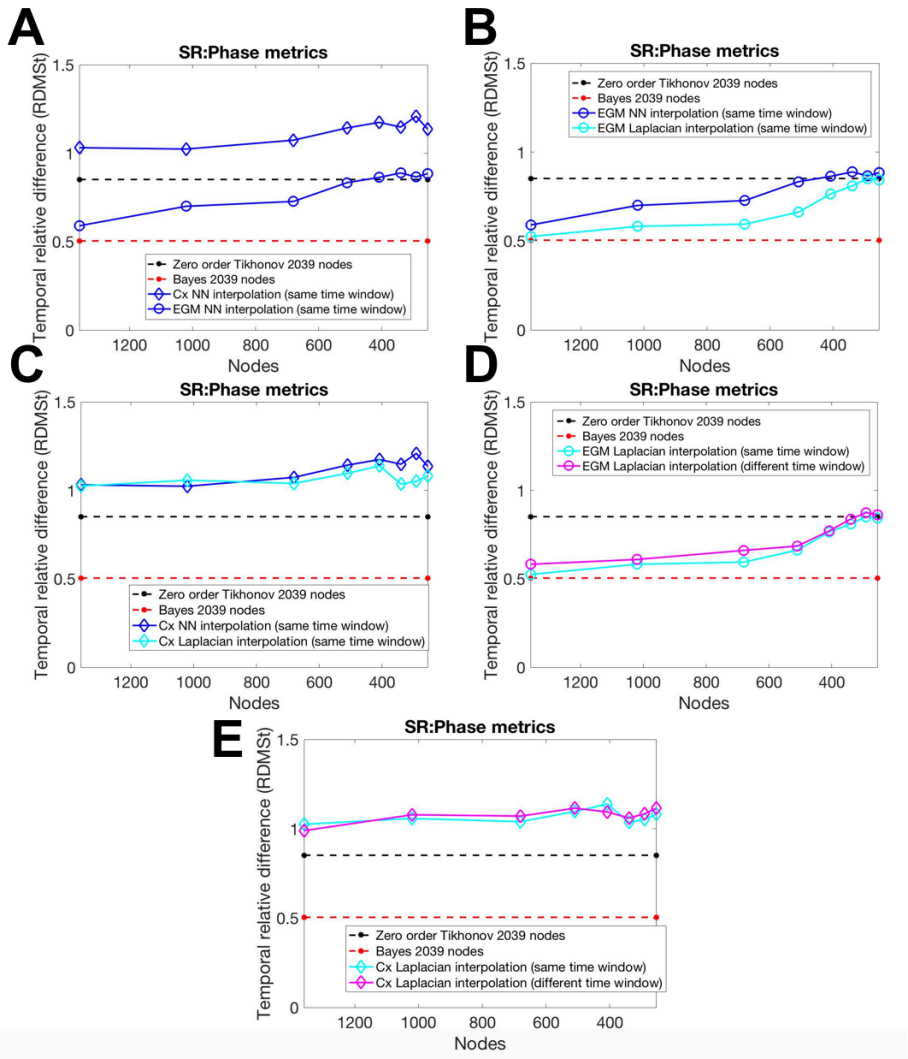

Figure 4.22: Temporal relative difference in the reconstructed instantaneous phase from the model of sinus rhythm using different interpolation approaches, and comparison with zero order Tikhonov and Bayes regularization without interpolating.

Temporal relative difference in the reconstruction of instantaneous phase after applying different interpolation methods: (A) EGM vs. Cx NN interpolation using all nodes simultaneously, (B) EGM NN vs. Laplacian using the same time window for all nodes, (C) Cx NN vs. Laplacian using the same time window, (D) EGM Laplacian using the same time window vs. using different time windows for sets of 120 nodes, and (E) Cx Laplacian using the same time window vs. using different time windows for sets of 120 nodes.

The second set of results corresponds to the performance metrics obtained for the simple atrial fibrillation model, and are represented in figures from 4.23 to 4.27. The performance metrics for the estimated epicardial potentials after interpolating the SAF model with reduced spatial information are illustrated in figure 4.23 and figure 4.24. The temporal correlation coefficient is shown in the former, whereas the temporal relative difference can be seen in the latter. Just like the previous model of epicardial activity, there is superior performance when interpolating the EGM instead of the covariance matrix, as shown in these two figures. This can be seen when comparing the epicardial potentials' CCt obtained with Cx NN interpolation versus EGM NN interpolation in figure 4.23A, both using all nodes simultaneously.As well as the RDMSt values obtained with these same approaches, seen in figure 4.24A.

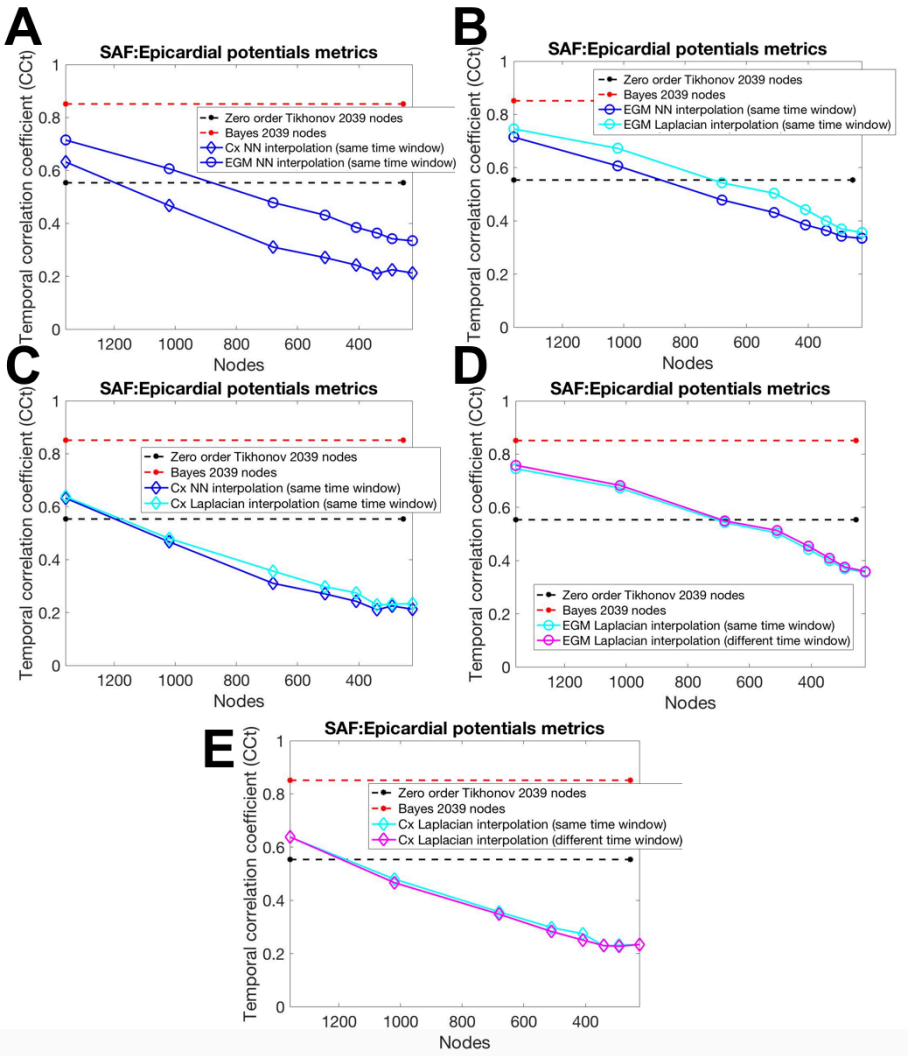

Figure 4.23: Temporal correlation coefficient in the reconstructed epicardial potentials from the model of simple atrial fibrillation using different interpolation approaches, and comparison with zero order Tikhonov and Bayes regularization without interpolating.

Temporal correlation coefficient in the reconstruction of epicardial potentials after applying different interpolation methods: (A) EGM vs. Cx NN interpolation using all nodes simultaneously, (B) EGM NN vs. Laplacian using the same time window for all nodes, (C) Cx NN vs. Laplacian using the same time window, (D) EGM Laplacian using the same time window vs. using different time windows for sets of 120 nodes, and (E) Cx Laplacian using the same time window vs. using different time windows for sets of 120 nodes.

Once again, the method with the best results is Laplacian interpolation for both performance metrics. This can be visualized in figures 4.23B and 4.23C.The epicardial potentials' CCt when performing EGM NN versus EGM Laplacian is shown in the former, and the obtained CCt with Cx NN versus Cx Laplacian is illustrated in the latter, all of them using all nodes simultaneously. The same conclusion is observed in the results for the RDMSt, which can be seen in figures 4.24B and 4.24C, in which the same methods that have just been described are represented.

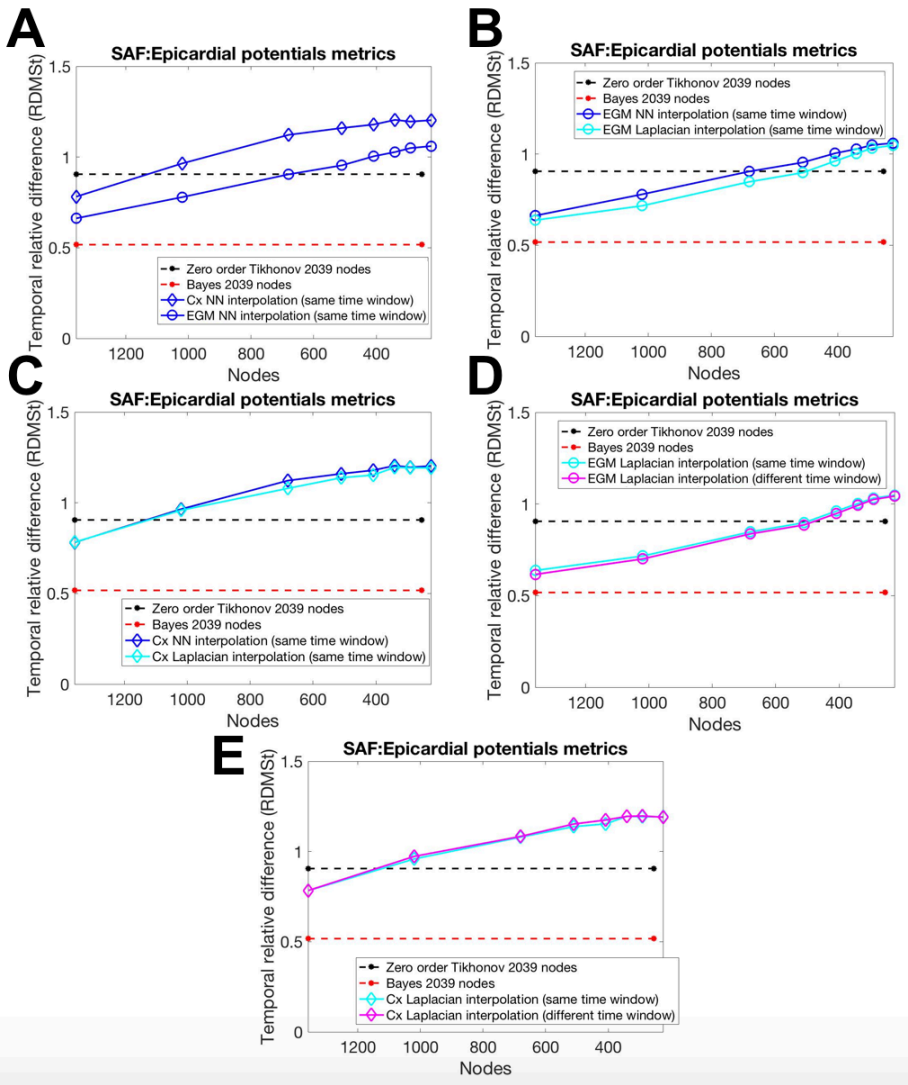

Figure 4.24: Temporal relative difference in the reconstructed epicardial potentials from the model of simple atrial fibrillation using different interpolation approaches, and comparison with zero order Tikhonov and Bayes regularization without interpolating.

Temporal relative difference in the reconstruction of epicardial potentials after applying different interpolation methods: (A) EGM vs. Cx NN interpolation using all nodes simultaneously, (B) EGM NN vs. Laplacian using the same time window for all nodes, (C) Cx NN vs. Laplacian using the same time window, (D) EGM Laplacian using the same time window vs. using different time windows for sets of 120 nodes, and (E) Cx Laplacian using the same time window vs. using different time windows for sets of 120 nodes.

However, this time a superior performance is achieved when using a different time window for every set of 120 nodes when calculating the covariance matrix on the EGM interpolation approach, as shown in the figures. This holds true for both measures, and can be seen in figures 4.23D and 4.24D. The opposite takes places when the interpolation is performed on the covariance matrix and not the electrogram. This can be observed in figures 4.23E and 4.24E, where a superior performance is obtained for both metrics when using all nodes simultaneously instead of sets of 120 nodes. Finally, the best performance for the reconstruction of SAF epicardial potentials is achieved through EGM Laplacian interpolation using different time windows for sets of 120 nodes. The number of nodes can be reduced down to 700 for the epicardial potentials' CCt, as seen in figure 4.23D, and it is possible

to go down to 480 nodes for the RDMSt metric and maintain the same accuracy as Tikhonov's approach, as shown in 4.24D.

The performance metrics for the reconstruction of instantaneous phase in the simple atrial fibrillation model are shown in figures 4.25 and 4.26. The temporal correlation coefficient is shown in the first one and the temporal relative difference in the second. Analogously to the epicardial potentials' case, the best results are obtained with EGM interpolation instead of Cx. This is illustrated in figure 4.25A. In this figure, the instantaneous phase's CCt when using EGM versus Cx Nearest Neighbour interpolation is represented, both methods using the same time window. The instantaneous phase's RDMSt analogous representation is shown in figure 4.26A.

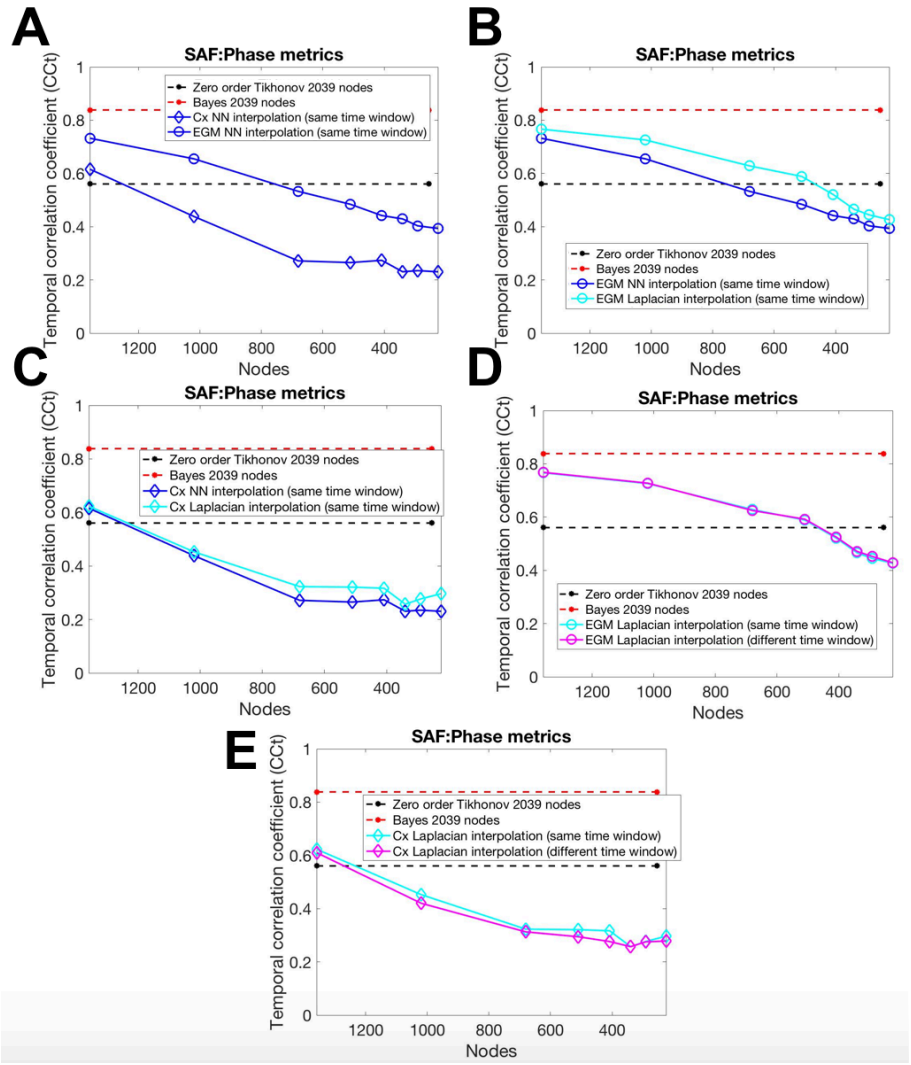

Figure 4.25: Temporal correlation coefficient in the reconstructed instantaneous phase from the model of simple atrial fibrillation using different interpolation approaches, and comparison with zero order Tikhonov and Bayes regularization without interpolating.

Temporal correlation coefficient in the reconstruction of instantaneous phase after applying different interpolation methods: (A) EGM vs. Cx NN interpolation using all nodes simultaneously, (B) EGM NN vs. Laplacian using the same time window for all nodes, (C) Cx NN vs. Laplacian using the same time window, (D) EGM Laplacian using the same time window vs. using different time windows for sets of 120 nodes, and (E) Cx Laplacian using the same time window vs. using different time windows for sets of 120 nodes.

Once again, Laplacian interpolation gives a better performance and allows a greater decrease in the number of initial spatial information while maintaining or surpassing Tikhonov's performance. This can be seen in figures 4.25B and 4.25C, which hold that no matter where the interpolation is performed, better CCt values for the instantaneous phase are obtained when the method is Laplacian and not Nearest Neighbour. The same holds for the values of the instantaneous phase's RDMSt, illustrated in figures 4.26B and 4.26C. Regarding the two alternatives between time windows for calculating the covariance matrix, this time the results for both alternatives are almost completely overlapped for the EGM case, both for the instantaneous phase's CCt and RDMSt. This can be seen in figure 4.25D and 4.26D. However, there is a slightly superior performance when implementing a different time window for sets of 120 nodes.

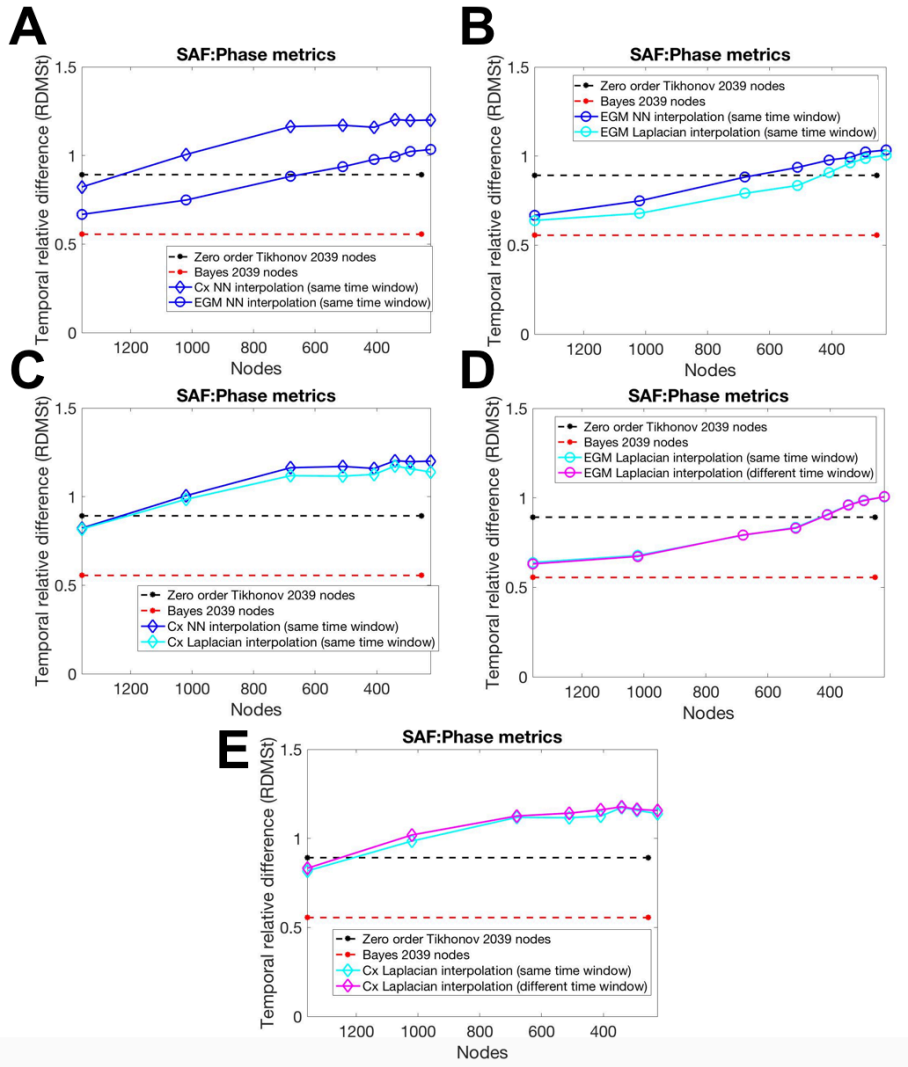

Figure 4.26: Temporal relative difference in the reconstructed instantaneous phase from the model of simple atrial fibrillation using different interpolation approaches, and comparison with zero order Tikhonov and Bayes regularization without interpolating.

Temporal relative difference in the reconstruction of instantaneous phase after applying different interpolation methods: (A) EGM vs. Cx NN interpolation using all nodes simultaneously, (B) EGM NN vs. Laplacian using the same time window for all nodes, (C) Cx NN vs. Laplacian using the same time window, (D) EGM Laplacian using the same time window vs. using different time windows for sets of 120 nodes, and (E) Cx Laplacian using the same time window vs. using different time windows for sets of 120 nodes.

However, that this does not hold true when the interpolation is performed over the covariance matrix instead of the EGM, as shown in figures 4.25E and 4.26E. In these figures, a superior performance is shown when using all nodes simultaneously for Cx interpolation. Overall, the best approach in the reconstruction of instantaneous phase for the SAF model is the same as the one for the epicardials' potentials: EGM Laplacian interpolation using a different time window to calculate Cx for sets of 120 nodes. For the correlation coefficient case, it is possible to reduce the number of intracavitary information down to 460 nodes, which is represented in figure 4.25D. Regarding the relative difference, the results for this metric show that the spatial information can be reduced to, more or less, 420 nodes, as shown in figure 4.26D.

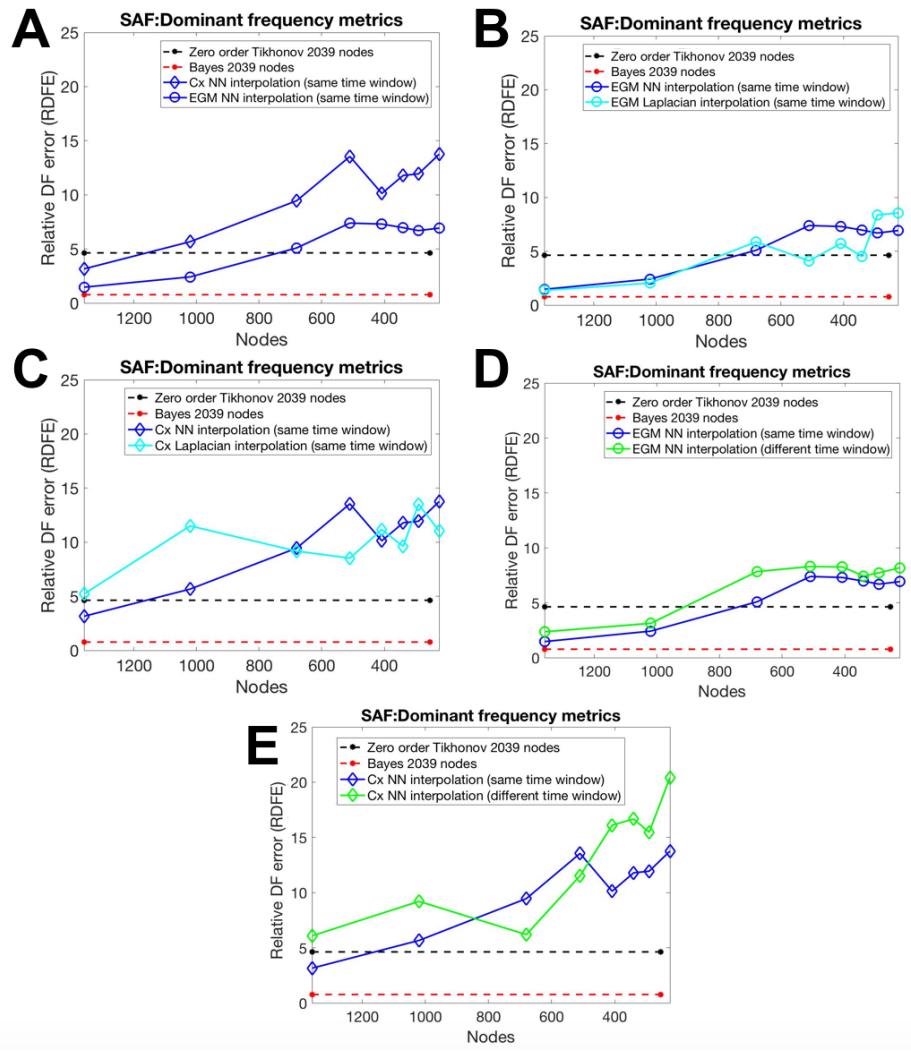

Figure 4.27: Relative error in the reconstructed dominant frequencies from the model of simple atrial fibrillation using different interpolation approaches, and comparison with zero order Tikhonov and Bayes regularization without interpolating.

Relative dominant frequency error in the reconstruction of dominant frequencies after applying different interpolation methods: (A) EGM vs. Cx NN interpolation using all nodes simultaneously, (B) EGM NN vs. Laplacian using the same time window for all nodes, (C) Cx NN vs. Laplacian using the same time window, (D) EGM NN using the same time window vs. using different time windows for sets of 120 nodes, and (E) Cx NN using the same time window vs. using different time windows for sets of 120 nodes.

Finally, the relative dominant frequency error between the real and estimated dominant frequencies for the SAF model is shown in figure 4.27. The results for this metric are unstable and oscillating. However, the method that seems to achieve the best performance is once again interpolation of the EGM, as illustrated in figure 4.27A. This time however, Nearest Neighbour interpolation instead of Laplacian is the one that performs the best, as illustrated in figures 4.27B and 4.27C. Also, contrary to the previous two parameters of this model, using the same time window for all nodes shows better results than using the non-simultaneous approach, which is shown in figures 4.27D and 4.27E. Hence, the best method for this performance metric in particular from the SAF model is EGM Nearest Neighbour interpolation using all nodes simultaneously. Through this method, it is possible to reduce the number of intracavitary information down to 710 nodes while maintaining Tikhonov's performance.

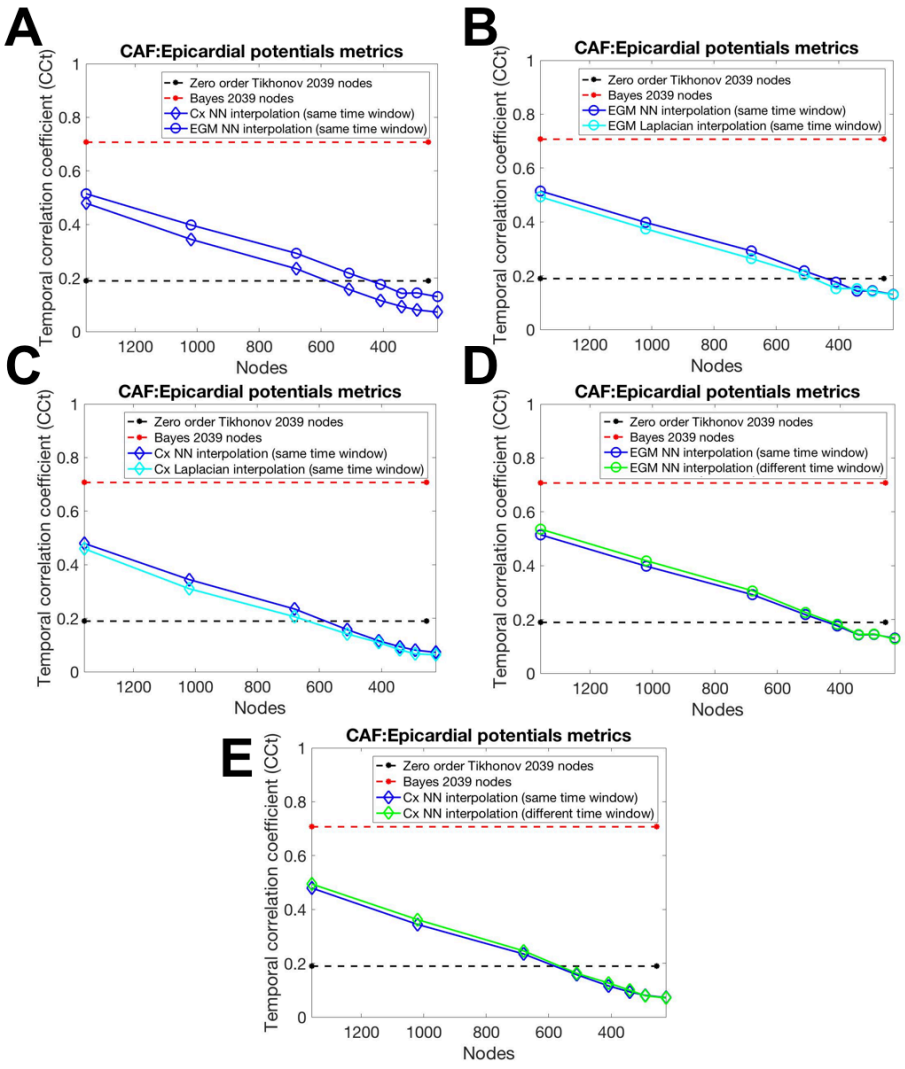

Figure 4.28: Temporal correlation coefficient in the reconstructed epicardial potentials from the model of complex atrial fibrillation using different interpolation approaches, and comparison with zero order Tikhonov and Bayes regularization without interpolating.

Temporal correlation coefficient in the reconstruction of epicardial potentials after applying different interpolation methods: (A) EGM vs. Cx NN interpolation using all nodes simultaneously, (B) EGM NN vs. Laplacian using the same time window for all nodes, (C) Cx NN vs. Laplacian using the same time window, (D) EGM NN using the same time window vs. using different time windows for sets of 120 nodes, and (E) Cx NN using the same time window vs. using different time windows for sets of 120 nodes.

The third and last set of results represent the performance metrics for the estimation of the complex atrial fibrillation model, and are illustrated in figures from 4.28 to 4.32. The performance metrics in the reconstruction of epicardial potentials are shown in the first two figures, 4.28 and 4.29. In these figures, the temporal correlation coefficient and relative difference can be seen. Once again, a superior performance is achieved by means of interpolating the EGM and not the covariance matrix. This can be seen in figures 4.28A and 4.29A. This time however, the results from Cx interpolation are not as separated from those obtained by EGM as the previous models. Also, it is important to notice that for this model, the best results are obtained for both metrics with Nearest Neighbour interpolation instead of Laplacian, as illustrated in figures 4.28B, 4.28C, 4.29B and 4.29C.

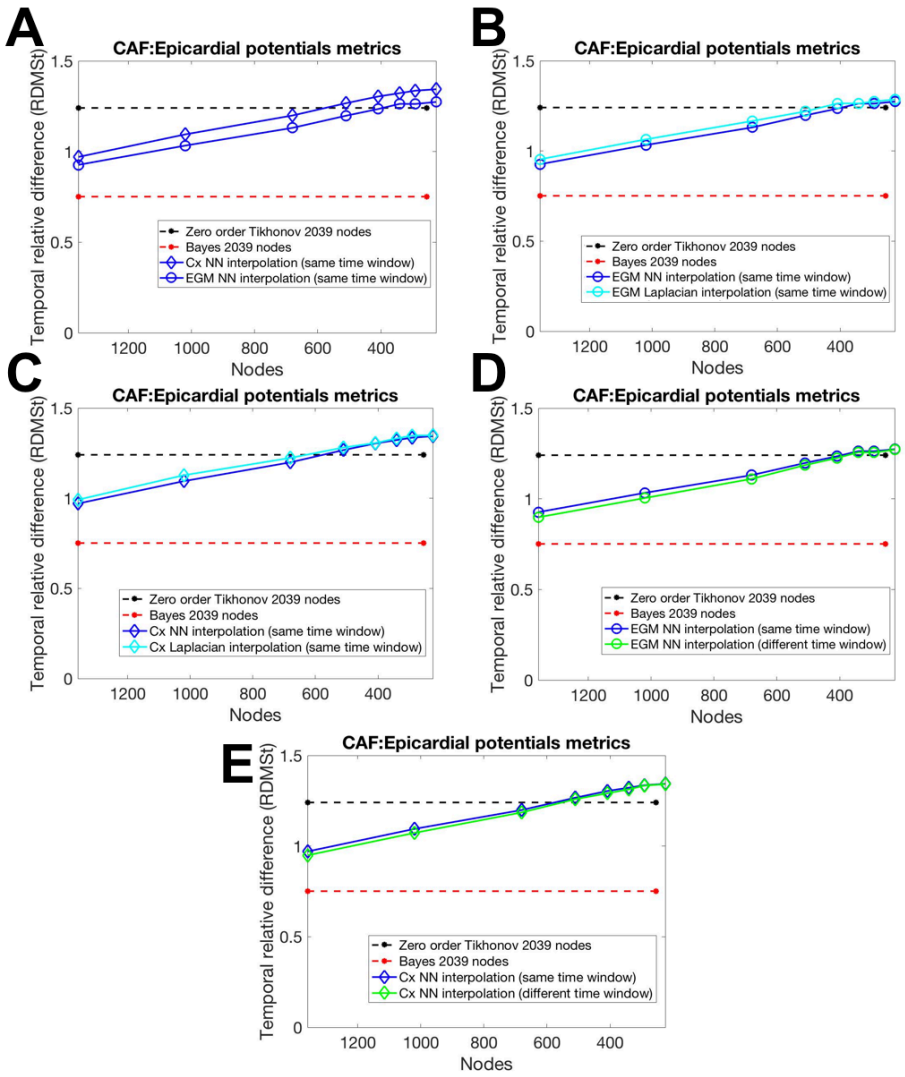

Figure 4.29: Temporal relative difference in the reconstructed epicardial potentials from the model of complex atrial fibrillation using different interpolation approaches, and comparison with zero order Tikhonov and Bayes regularization without interpolating.

Temporal relative difference in the reconstruction of epicardial potentials after applying different interpolation methods: (A) EGM vs. Cx NN interpolation using all nodes simultaneously, (B) EGM NN vs. Laplacian using the same time window for all nodes, (C) Cx NN vs. Laplacian using the same time window, (D) EGM NN using the same time window vs. using different time windows for sets of 120 nodes, and (E) Cx NN using the same time window vs. using different time windows for sets of 120 nodes.

Finally, both metrics show a better performance when using a non-simultaneous time window to calculate the covariance matrix. This can be seen in figures 4.28D, 4.28E, 4.29D and 4.29E. Hence, the best results in the reconstruction of epicardial potentials from CAF are obtained by means of EGM Nearest Neighbour interpolation using different time windows for sets of 120 nodes. With this approach it is possible to reduce the number of intracavitary signals to 410 for the CCt case, as shown in figure 4.28D, and 400 nodes for the RDMSt case, illustrated in figure 4.29D.

The performance metrics for the reconstructed instantaneous phase from the CAF model is represented in figures 4.30 and 4.31. The temporal correlation coefficient is shown in the former and the temporal relative difference measurement star can be seen in the latter. The same conclusions as the epicardial potentials' parameter can be seen in these figures. EGM interpolation is superior to Cx, as shown in figures 4.30A and 4.31A.

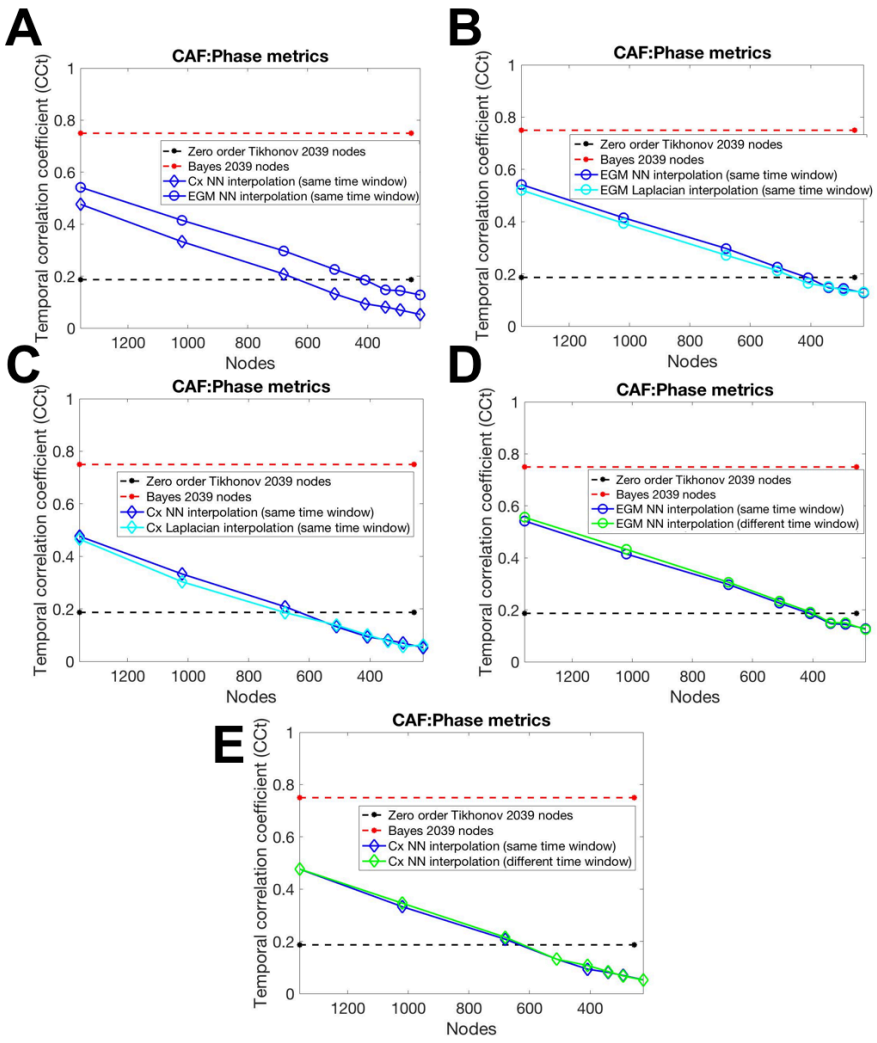

Figure 4.30: Temporal correlation coefficient in the reconstructed instantaneous phase from the model of complex atrial fibrillation using different interpolation approaches, and comparison with zero order Tikhonov and Bayes regularization without interpolating.

Temporal correlation coefficient in the reconstruction of instantaneous phase after applying different interpolation methods: (A) EGM vs. Cx NN interpolation using all nodes simultaneously, (B) EGM NN vs. Laplacian using the same time window for all nodes, (C) Cx NN vs. Laplacian using the same time window, (D) EGM NN using the same time window vs. using different time windows for sets of 120 nodes, and (E) Cx NN using the same time window vs. using different time windows for sets of 120 nodes.

Once again, interpolation method with the best results is Nearest Neighbour, whether performed over the EGM or the covariance matrix, as shown in figures 4.30B, 4.30C, 4.31B and 4.31C. Analogously to the previous target parameter, the computation of Cx with different time windows for sets of 120 nodes gives a better performance than a simultaneous window for all nodes, as shown in figures 4.30D, 4.30E, 4.31D and 4.31E. Therefore, the best approach for the interpolation of instantaneous phase from CAF is the same as epicardial potentials: EGM Nearest Neighbour using a different time window for sets of 120 nodes. Using this technique, the results in the reconstruction are better than Tikhonov's down to 400 nodes for the instantaneous phase's CCt, as seen in figure 4.30D; and it is possible to decrease the intracavitary information down to 380 nodes approximately for the instantaneous phase's RDMSt, shown in figure 4.31D.

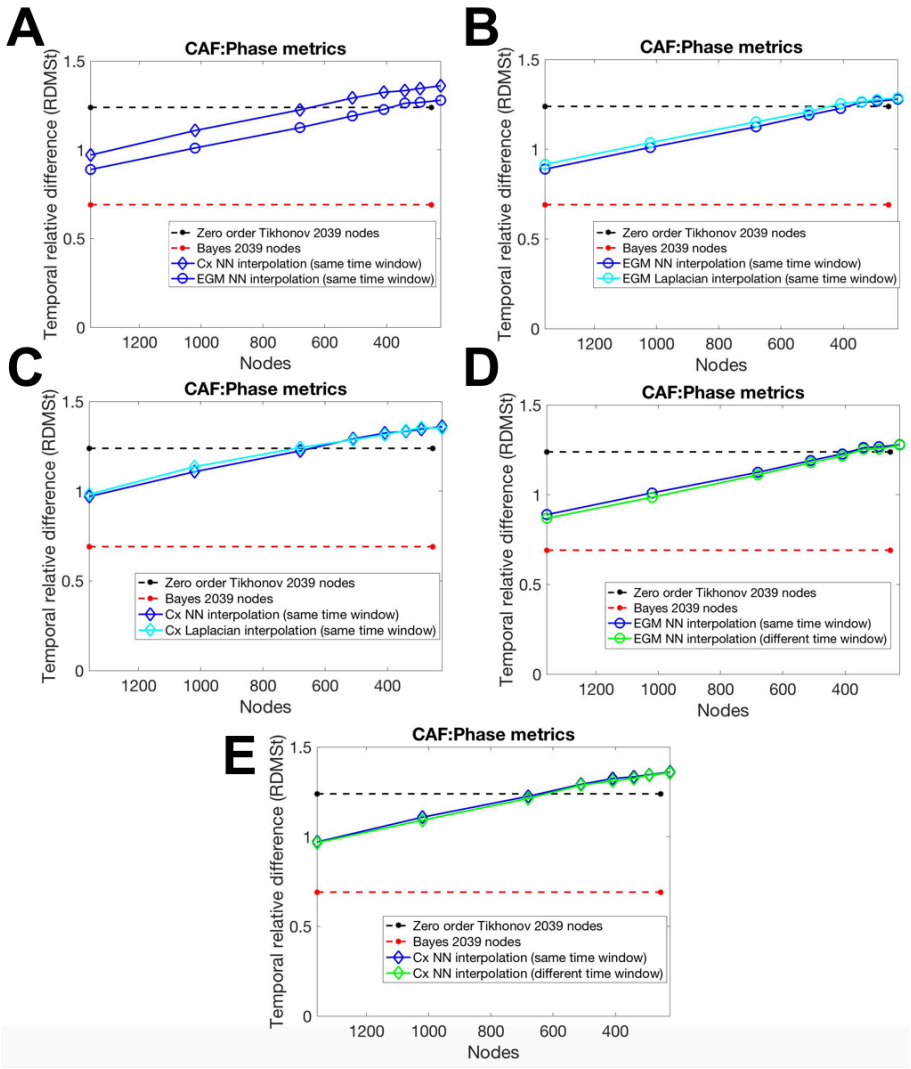

Figure 4.31: Temporal relative difference in the reconstructed instantaneous phase from the model of complex atrial fibrillation using different interpolation approaches, and comparison with zero order Tikhonov and Bayes regularization without interpolating.

Temporal relative difference in the reconstruction of instantaneous phase after applying different interpolation methods: (A) EGM vs. Cx NN interpolation using all nodes simultaneously, (B) EGM NN vs. Laplacian using the same time window for all nodes, (C) Cx NN vs. Laplacian using the same time window, (D) EGM NN using the same time window vs. using different time windows for sets of 120 nodes, and (E) Cx NN using the same time window vs. using different time windows for sets of 120 nodes.

Finally, the relative dominant frequency error between the real and reconstructed dominant frequencies for the CAF model is shown in figure 4.32. Just like the SAF model, the results obtained for the performance metric of this target parameter are unstable and oscillating. However, it can be clearly seen in figure 4.32A that the values obtained for the EGM interpolation is superior to Cx interpolation. Again, NN method performs better than Laplacian for the CAF model, as illustrated in figures 4.32B and 4.32C. Finally, using a non-simultaneous approach, better results are obtained compared to using all nodes simultaneously, as seen in figures 4.32D and 4.32E. Therefore, the best approach is EGM NN interpolation using different time windows for sets of 120 nodes. This method in particular performs better than Tikhonov's approach on the raw data, even with the smallest number or nodes tried, which was 255, as seen in figure 4.32D.

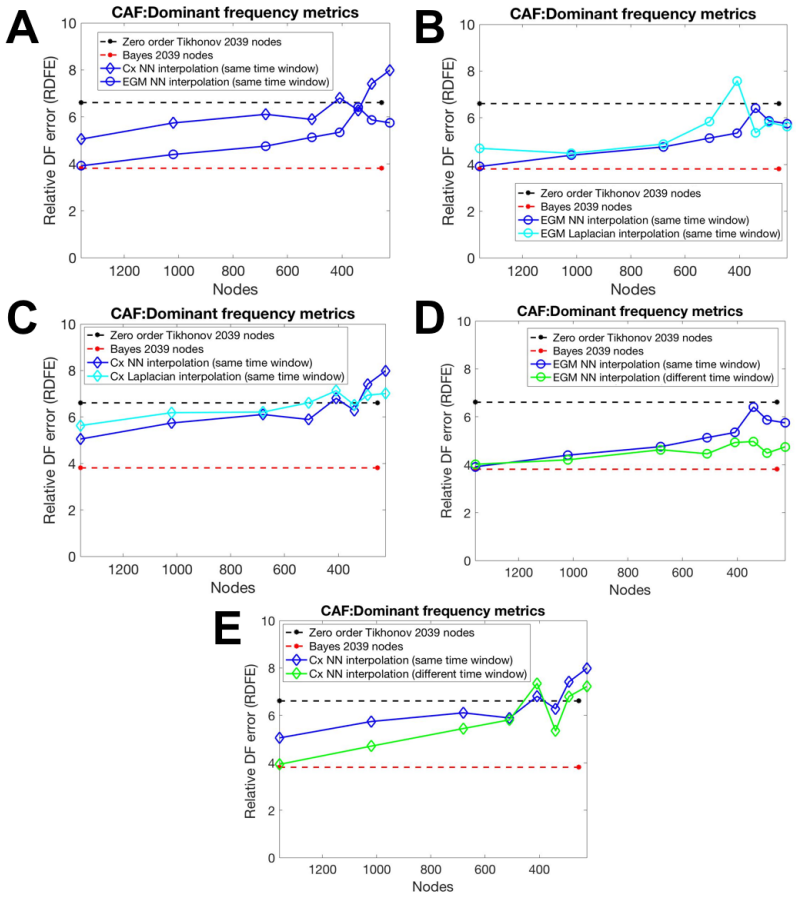

Figure 4.32: Relative dominant frequency error in the reconstructed dominant frequencies from the model of complex atrial fibrillation using different interpolation approaches, and comparison with zero order Tikhonov and Bayes regularization without interpolating.

Relative dominant frequency error in the reconstruction of dominant frequencies after applying different interpolation methods: (A) EGM vs. Cx NN interpolation using all nodes simultaneously, (B) EGM NN vs. Laplacian using the same time window for all nodes, (C) Cx NN vs. Laplacian using the same time window, (D) EGM NN using the same time window vs. using different time windows for sets of 120 nodes, and (E) Cx NN using the same time window vs. using different time windows for sets of 120 nodes

.

These interpolation results are summarized in tables 4.10, 4.11 and 4.12. The best interpolation method for each of the models available and target parameters is shown in these tables, as well as the minimum number of nodes needed in each one of them to outperform Tikhonov's regularization. The results of sinus rhythm's interpolation and reconstruction through Bayes regularization can be

seen in table 4.10. The best interpolation approach for estimating effectively all the target parameters was always EGM interpolation through Laplacian method, as shown in the table. Also, for this particular case, using the same window for all nodes when computing the covariance matrix was the alternative that worked best. The minimum number of nodes needed to achieve a performance equal to or superior than Tikhonov depended on the target parameter as well as the performance metric. In average, it can be concluded that for the model of sinus rhythm, it is possible to reduce the number of initial intracavitary signals down to 440 nodes.

Table 4.10: Summary of interpolation results for the model of sinus rhythm.

Model: Sinus rhythm

		Best interpolation approach	Minimum number of nodes to outperform Tikhonov
Epicardial potentials	**CCt**	EGM Laplacian	620
	RDMSt	EGM Laplacian	500
Instantaneous phase	**CCt**	EGM Laplacian	340
	RDMSt	EGM Laplacian	300

The results for the interpolation and reconstruction of the simple atrial fibrillation model are summarized in table 4.11. The best method of interpolation for the epicardial potentials and instantaneous phase was EGM interpolation using the Laplacian approach, just like the model of sinus rhythm. However, for this case in particular, changing the time window for the calculus of the covariance matrix every 120^{th} node gave the best results. The only target parameter which achieved a better performance through a different approach was the dominant frequency. As shown previously, the interpolation and reconstruction results for this parameter were oscillating and unstable, and the best performance was achieved through Nearest neighbour interpolation on the EGM. Just like the simple atrial fibrillation case, the minimum number of nodes needed to outperform Tikhonov varied depending on the target parameter as well as the performance metric. In average, a minimum of 560 nodes would be needed for the simple atrial fibrillation model to be able to reconstruct the epicardial activity better than Tikhonov's regularization on the raw data.

The results for the interpolation and reconstruction of the complex atrial fibrillation model using Bayes' regularization are summarized in table 4.12. For this model, the best interpolation approach was the same for all the target parameters. Once again, interpolation on the EGM showed the best results, however, this time the best method was Nearest Neighbour instead of Laplacian. Just like the case of simple atrial fibrillation, the alternative which used a varying time window in the computation of the covariance matrix for sets of 120 nodes worked best than the default approach. Despite the complexity of the activity represented by this model, it is the model that admits the least number of intracavitary signals while outperforming Tikhonov regularization, allowing to reduce the number of nodes to an average of 370 nodes. In fact, the target parameter which can be estimated with the least number of nodes is the dominant frequency, since the RDFE is lower than the one obtained through Tikhonov regularization for the smallest number of nodes that was tried, 255.

Table 4.11: Summary of interpolation results for the model of simple atrial fibrillation.

Model: Simple atrial fibrillation

		Best interpolation approach	Minimum number of nodes to outperform Tikhonov
Epicardial potentials	**CCt**	EGM Laplacian (non-simultaneous window)	700
	RDMSt	EGM Laplacian (non-simultaneous window)	480
Instantaneous phase	**CCt**	EGM Laplacian (non-simultaneous window)	460
	RDMSt	EGM Laplacian (non-simultaneous window)	420
Dominant frequency	**RDFE (%)**	EGM Nearest Neighbour	710

Table 4.12: Summary of interpolation results for the model of complex atrial fibrillation.

Model: Complex atrial fibrillation

		Best interpolation approach	Minimum number of nodes to outperform Tikhonov
Epicardial potentials	**CCt**	EGM Nearest Neighbour (non-simultaneous window)	410
	RDMSt	EGM Nearest Neighbour (non-simultaneous window)	400
Instantaneous phase	**CCt**	EGM Nearest Neighbour (non-simultaneous window)	400
	RDMSt	EGM Nearest Neighbour (non-simultaneous window)	380
Dominant frequency	**RDFE (%)**	EGM Nearest Neighbour (non-simultaneous window)	255

5. Conclusions

In this work, geometrical models of human atria and torso have been used together with mathematical models of epicardial activity and regularization methods, showing that it is possible to reduce the number of intracavitary signals available and reconstruct them effectively by solving the inverse problem of electrocardiography. It has been demonstrated that Bayes regularization is an accurate method for the reconstruction, allowing to detect atrial fibrillation events from mathematical models with reduced spatial information. Furthermore, it has been found that depending on the number of initial spatial information, the performance is the estimation can be better than the gold standard reconstruction method: zero order Tikhonov with instantaneous regularization parameter.

Regarding the interpolation approaches, it has been found that interpolation of the EGM is superior to interpolation of the covariance matrix which is used in Bayes' regularization. Also, it has been shown that the use of nearest neighbour or Laplacian interpolation methods depends on the type of epicardial activity from the mathematical model which is being estimated. For the SR and SAF models, Laplacian interpolation has a better performance than NN. However, the more complex epicardial activity from the CAF model is interpolated with better accuracy through NN method. Finally, it has been demonstrated that the use of non-simultaneous windows for sets of 120 nodes has a similar performance to using all nodes simultaneously.

It has been possible to effectively reduce the amount of spatial information from all models. However, the minimum number of intracavitary signals needed in all the models to outperform the gold standard was always higher than the maximum number of electrodes that are currently being used in catheters to record atrial activity. Nevertheless, the fact that the performance obtained in the non-simultaneous approach is similar to the simultaneous one, means that it is possible to use this technique effectively for reconstructing a reduced number of spatial signals. In this sense, using 120 electrode catheters and recording atrial activity a reduced number of times in different atrial positions for each different measurement, together with signals provided from torso recordings, the signals could be effectively interpolated and reconstructed. All in all, the activity from the whole atrial tissue could be predicted from a reduced number of spatial information, being able to estimate not only the intracardiac potentials, but also the instantaneous phase, dominant frequency regions as well as singularity points. The possibility of predicting these target parameters is essential in the characterization of arrhythmias such as atrial fibrillation, and could help in the detailed planning of the therapies that are currently being used for the condition, such as catheter ablation.

Among the many treatments for AF, catheter ablation has recently shown promising results [Atienza 2014]. However, the success of such therapy strongly depends on the identification of atrial regions responsible for the fibrillation event. To this respect, it has been found that these areas are characterized by the presence of high dominant frequency [Atienza 2009] as well as electrical re-entries, also known as rotors [Narayan 2012, Haïssaguerre 2014]. On the one hand, the parameter rough location of the highest DF site can be identified by means of BSPM [Guillem 2013], however the technique has limitations in detecting the precise localization of the fibrillatory source within the atrial tissue. On the other hand, it has been possible to detect rotors both invasively and non-invasively, through panoramic intracardiac mapping [Narayan 2013] and solving the inverse problem of electrocardiography [Haïssaguerre 2014], respectively.

The inverse problem of electrocardiography aims at estimating the epicardial activity provided torso measurements. However, the loss of information in the recorded surface potentials, together with the presence of noise or geometrical errors, reduces the accuracy of the reconstruction process. This has lead to the appearance of different regularization methods which aim to increase the performance of the estimation. Among the reported techniques, it has been shown that the use of a priori information in Bayes regularization outperforms all the other methods described so far [Figuera 2016]. The results obtained in this work demonstrate that this superior performance of Bayes' regularization is maintained when reducing the number of intracavitary signals from the different mathematical models of atrial fibrillation. The reconstruction has been effective not only for the estimation of epicardial potentials, but also for the instantaneous phase and dominant frequency maps. The identification of this last parameter by solving the inverse problem has been shown to be more accurate than the reconstruction of epicardial potentials for atrial fibrillation events [Pedrón-Torrecilla 2016]. Taking this into account, this work has shown that DF estimation can also be performed with reduced spatial information.

In conclusion, the most relevant parameters from atrial fibrillation mathematical models could be reconstructed solving the inverse problem of electrocardiography through Bayes regularization. Regarding the estimation process, the spatial information that was used from the models was less than one fifth of the original intracavitary signals, and still, the performance was superior to the gold standard regularization method using all the spatial information. Therefore, this work has shown that the activity from the whole atrial tissue can be reconstructed with a reduced number of signals using a priori information through Bayes regularization, being able to detect drivers of atrial fibrillation episodes.

6. Future works

This work has used different mathematical models of epicardial activity to create an algorithm which is able to reconstruct the models with a reduced number of intracavitary signals. At the same time, the performance in the interpolation and reconstruction process is equal to or better than Tikhonov's performance with the full spatial information. The number of nodes has been effectively reduced from 2039 down to 440, 560 and 370 for the SR, SAF and CAF models, respectively. Regarding the different approaches used, each model requires a different interpolation method to achieve the best performance.

Therefore, the future works related to this project would be, on the one hand, to be able to reduce the number of intracavitary signals to a number below 120 in order to achieve a clinical application. To this respect, the maximum number of electrodes which, so far, can be introduced into the human atria to measure the endocardial activity is 120. Hence, by achieving interpolation and reconstruction results superior than those provided by Tikhonov while reducing the spatial information below 120 signals, real endocardial measurements could be used instead of mathematical models of epicardial activity.

On the other hand, future works will have to find a unique interpolation approach able to achieve the best performance for all the models of epicardial activity. This could be achieved either by trying other interpolation or regularization methods to the ones proposed in this work.

7. References

[Abboud 1994] Abboud S, Eshel Y, Levy S, Rosenfeld M. Numerical calculation of the potential distribution due to dipole sources in a spherical model of the head. Comput Biomed Res 1994; 27:441-455.

[Aslandi 2011]Aslanidi OV, Colman MA, Stott J, Dobrzynski H, Boyett MR, Holden AV, Zhang H. 3D virtual human atria: A computational platform for studying clinical atrial fibrillation. ProgBiophysMolBiol 2011; 107:156-216.

[Atienza 2009] Atienza F, Almendral J, Jalife J, Zlochiver S, Ploutz-Snyder R, Torrecilla EG, Arenal A, Kalifa J, Fernandez-Aviles F, Berenfeld O. Real-time dominant frequency mapping and ablation of dominant frequency sites in atrial fibrillation with left-to-right frequency gradients predicts long-term maintenance of sinus rhythm. Heart Rhythm 2009;6:33 – 40

[Atienza 2011] Atienza F, Calvo D, Almendral J, Zlochiver S, Grzeda KR, Martinez-Alzamora N, Gonzalez-Torrecilla E, Arenal A, Fernandez-Aviles F, Berenfeld O. Mechanisms of fractionated electrograms formation in the posterior left atrium during paroxysmal atrial fibrillation in humans. J Am CollCardiol 2011;57:1081–1092.

[Atienza 2014] Atienza F, Almendral J, Ormaetxe JM, Moya A, Martínez-Alday JD, Hernández-Madrid A, Castellanos E, Arribas F, Arias MÁ, Tercedor L, Peinado R, Arcocha MF, Ortiz M, Martínez-Alzamora N, Arenal A, Fernández- Avilés F, Jalife J; RADAR-AF Investigators. Comparison of radiofrequency catheter ablation of drivers and circumferential pulmonary vein isolation in atrial fibrillation: a noninferiority randomized multicenter RADAR-AF trial. J Am CollCardiol 2014; 64:2455-2467.

[Berenfeld 2007] Berenfeld O. Quantifying activation frequency in atrial fibrillation to establish underlying mechanisms and ablation guidance. Heart Rhythm 2007;4:1225–1234.

[Cabo 1996] Cabo C, Pertsov AM, Davidenko JM, Baxter WT, Gray RA, Jalife J. Vortex shedding as a precursor of turbulent electrical activity in cardiac muscle. Biophys J 1996;70: 1105 – 1111.

[ColliFranzone1985] ColliFranzone P, Gnerri L, Tentonia S, Viganotti C, Baruffi S. A mathematical procedure for solving the inverse potential problem of electrocardiography. Analysis of the timespace accuracy from in vitro experimental data. Math Biosci 1985; 77:353-396.

[Cuculich 2010] Cuculich PS, Wang Y, Lindsay BD, Faddis MN, Schuessler RB, Damiano RJ Jr, Li L, Rudy Y. Noninvasive characterization of epicardial activation in humans with diverse atrial fibrillation patterns. Circulation 2010;122:1364–1372.

[Dobrev 2010] Dobrev D, Nattel S. New antiarrhythmic drugs for treatment of atrial fibrillation. Lancet 2010;375:1212–1223.

[Dössel 2012] Dössel O, Krueger MW, Weber FM, Wilhelms M, Seemann G. Computational modeling of the human atrial anatomy and electrophysiology. Med BiolEngComput 2012; 50:773-799.

[Einthoven 1906] Einthoven W. Le telecardiogramme. Arch InternatPhysiol 1906; 4:132-164.

[Figuera 2016] Figuera C, Suárez-Gutiérrez V, Hernández Romero I, Rodrigo M, Liberos A, Atienza F, Guillem MS, Barquero-Pérez O, Climet AM, Atienza FA. Regularization techniques for ECG imaging during atrial fibrillation: A computational study. Front Physiol 2016; 7:446-466.

[Fischer 2000]Fischer G, Tilg B, Modre R, Huiskamp GJ, Fetzer J, Rucker W, Wach P. A bidomain model based BEM-FEM coupling formulation for anisotropic cardiac tissue. Ann Biomed Eng 2000; 28:1229-1243.

[Ghosh and Rudy 2009] Ghosh S, Rudy Y. Application of l1-norm regularization to epicardial potential solution of the inverse electrocardiography problem. Ann Biomed Eng 2009; 37: 902–912.

[Greensite 2003] Greensite, F. The temporal prior in bioelectromagnetic source imaging problems. IEEE Trans Biomed Eng 2003; 50: 1152–1159.

[Guillem 2008] Guillem MS. Activation patterns in atrial fibrillation: contributions of body surface potential mapping. PhD thesis.

[Guillem 2009] Guillem MS, Climent AM, Castells F, Husser D, Millet J, Arya A, Piorkowski C, Bollmann A. Noninvasive mapping of human atrial fibrillation. J CardiovascElectrophysiol 2009;20:507 – 513.

[Guillem 2013] Guillem MS, Climent AM, Millet J, Arenal A, Fernandez-Aviles F, Jalife J, Atienza F, Berenfeld O. Noninvasive localization of maximal frequency sites of atrial fibrillation by body surface potential mapping. CircArrhythmElectrophysiol 2013;6:294–301.

[Guillem 2016] Guillem MS, Climent AM, Rodrigo M, Fernández-Avilés F, Atienza F, Berenfeld O. Presence and stability of rotors in atrial fibrillation: evidence and therapeutic implications. Cardiovasc Res 2016; 109:480-492.

[Haissaguerre 1998] Haissaguerre M, Jais P, Shah DC, Takahashi A, Hocini M, Quiniou G, Garrigue S, Le Mouroux A, Le Metayer P, Clementy J. Spontaneous initiation of atrial fibrillation by ectopic beats originating in the pulmonary veins. N Engl J Med 1998;339:659–666.

[Haissaguerre 2013] Haissaguerre M, Hocini M, Shah AJ, Derval N, Sacher F, Jais P, Dubois R. Noninvasive panoramic mapping of human atrial fibrillation mechanisms: a feasibility report. J CardiovascElectrophysiol 2013;24:711 – 717.

[Haissaguerre 2014] Haissaguerre M, Hocini M, Denis A, Shah AJ, Komatsu Y, Yamashita S, Daly M, Amraoui S, Zellerhoff S, Picat MQ, Quotb A, Jesel L, Lim H, Ploux S, Bordachar P, Attuel G, Meillet V, Ritter P, Derval N, Sacher F, Bernus O, Cochet H, Jais P, Dubois R. Driver domains in persistent atrial fibrillation. Circulation 2014;130:530 – 538.

[Hanna 2009] Hanna R, Jiang Y, Farina D, and Dössel O. Imaging of cardiac electrical sources using a novel spatio-temporal map-based regularization method, in World Congress on Medical Physics and Biomedical Engineering, September 7-12, 2009, Munich, Germany, eds O. Dössel and W. C. Schlegel (Munich: Springer), 813–816.

[Hansen 1992] Hansen PC, Sekii T, and Shibahashi H. The modified truncated SVD method for regularization in general form. SIAM J. Sci. Stat Comput 1992;13:1142–1150.

[Hansen 1993] Hansen PC, O'Leary DP: The use of the L-curve in the regularization of discrete ill-posed problems. SIAM J Sci Stat Comput 1993; 14:1487-1503.

[Hansen 2007] Hansen PC. Regularization tools version 4.0 for matlab 7.3. Numer. Algorithms 2007; 46:189–194.

[Horácek 1997] Horácek BM, Clements JC. The inverse problem of electrocardiography: a solution in terms of single- and double-layer sources of the epicardial surface. Math Biosci 1997; 144:119-154.

[Jacquement 2006]Jacquemet V, van Oosterom A, Vesin J, Kappenberger L. Analysis of electrocardiograms during atrial fibrillation - A biophysical model approach. IEEE Eng Med Biol Mag 2006; 25:79-88.

[Jais 1997] Jais P, Haissaguerre M, Shah DC, Chouairi S, Gencel L, Hocini M, Clementy J. A focal source of atrial fibrillation treated by discrete radiofrequency ablation. Circulation 1997; 95:572 – 576.

[Jalife 2002] Jalife J, Berenfeld O, Mansour M. Mother rotors and fibrillatory conduction: a mechanism of atrial fibrillation. Cardiovasc Res 2002;54:204–216.

[Krueger 2011] Krueger MW, Schmidt V, Tobon C, Weber FM, Lorenz C, Keller DUJ, Barschdorf H, Burdumy M, Neher P, Plank G, Rhode K, Seeman G, Sanchez-Quintana D, Saiz J, Razavi R, Dössel O. Modeling atrial fiber orientation in patient-specific geometries: A semi-automatic rule-based approach. Functional Imaging and Modeling of the Heart 2011; 6666:223-232.

[Lankveld 2014] Lankveld TA, Zeemering S, Crijns HJ, Schotten U. The ECG as a tool to determine atrial fibrillation complexity. Heart 2014; 100:1077-1084.

[Mandapati 2000] Mandapati R, Skanes A, Chen J, Berenfeld O, Jalife J. Stable microreentrant sources as a mechanism of atrial fibrillation in the isolated sheep heart. Circulation 2000;101: 194 – 199.

[Mansour 2001] Mansour M, Mandapati R, Berenfeld O, Chen J, Samie FH, Jalife J. Left-to-right gradient of atrial frequencies during acute atrial fibrillation in the isolated sheep heart. Circulation 2001;103:2631 – 2636.

[Messinger-Raport 1990] Messinger-Rapport BJ, Rudy Y. Noninvasive recovery of epicardial potentials in a realistic heart-torso geometry. Normal sinus rhythm. Circ Res 1990; 66:1023-1039.

[Milanic 2014] Milanic M, Jazbinšek V, MacLeod RS, Brooks DH, Hren R. Assessment of regularization techniques for electrocardiographic imaging. J Electrocardiol 2014;47: 20–28.

[Moe 1962] Moe GK. On the multiple wavelet hypothesis of atrial fibrillation. Arch IntPharmacodyn 1962;CXL:183 – 188

[Narayan 2012] Narayan SM, Krummen DE, Shivkumar K, Clopton P, Rappel WJ, Miller JM. Treatment of atrial fibrillation by the ablation of localized sources: CONFIRM (Conventional Ablation for Atrial Fibrillation with or Without Focal Impulse and Rotor Modulation) trial. J Am CollCardiol 2012;60:628–636.

[Narayan 2013] Narayan SM, Krummen DE, Clopton P, Shivkumar K, Miller JM. Direct or coin- cidental elimination of stable rotors or focal sources may explain successful atrial fibrillation ablation. J Am Coll Cardiol 2013;62:138–147.

[Onal and Serinagaoglu 2009] Onal M, Serinagaoglu Y. Spatio-temporal solutions in inverse electrocardiography. 4th European Conference of the International Federation for Medical and Biological Engineering (Heidelberg: Springer).2009;180–183.

[Parkash 2011] Parkash R, Tang AS, Sapp JL,Wells G. Approach to the catheter ablation technique of paroxysmal and persistent atrial fibrillation: a meta-analysis of the randomized controlled trials. J Cardiovasc Electrophysiol 2011;22:729–738.

[Pedrón-Torrecilla 2016] Pedrón-Torrecilla J, Rodrigo M, Climent AM, Liberos A, Pérez-David E, Bermejo J, et al. Noninvasive estimation of epicardial dominant high-frequency regions during atrial fibrillation. J Cardiovasc Electrophysiol 2016;27: 435–442.

[Rahimi 2016] Rahimi A, Sapp J, Xu J, Bajorski P, Horacek M, Wang L. Examining the impact of prior models in transmural electrophysiological imaging: a hierarchical multiple-model bayesian approach. IEEE Trans Med Imaging 2016; 35:229-243.

[Ramanathan 2003] Ramanathan C, Jia P, Ghanem R, Calvetti D, Rudy Y. Noninvasive electrocardiographic imaging (ECGI): application of the generalized minimal residual (GMRes) method. Ann Biomed Eng 2003; 31: 981–994.

[Rodrigo 2014] Rodrigo M, Guillem MS, Climent AM, Pedrón-Torrecilla J, Liberos A, Millet J, Fernández-Avilés F, Atienza F, Berenfeld O. Body surface localization of left and right atrial high-frequency rotors in atrial fibrillation patients: a clinical-computational study. Heart Rhythm 2014;11:1584–1591.

[Rodrigo 2016] Rodrigo M, Climent AM, Liberos A, Calvo D, Fernández-Avilés F, Berenfeld O, Atienza F, Guillem MS. Identification of dominant excitation patterns and sources of atrial fibrillation by causality analysis. Ann. Biomed. Eng. 2016;44: 2364–2376.

[Rodrigo 2016] Rodrigo M. Non-invasive identification of atrial fibrillation drivers. PhD thesis

[Rudy 2013] Rudy Y. Noninvasive electrocardiographic imaging of arrhythmogenic substrates in humans. Circ Res 2013;112: 863–874.

[Sanders 2005] Sanders P, Berenfeld O, Hocini M, Jais P, Vaidyanathan R, Hsu LF, Garrigue S, Takahashi Y, Rotter M, Sacher F, Scavee C, Ploutz-Snyder R, Jalife J, Haissaguerre M. Spectral analysis identifies sites of high-frequency activity maintaining atrial fibrillation in humans. Circulation 2005;112:789–797.

[Seger 2005] Seger M, Fischer G, Modre R, Messnarz B, Hanser F, Tilg B. Lead field computation for the electrocardiographic inverse problem: finite elements versus boundary elements. Comput Methods Programs Biomed 2005; 77:241-252.

[Serinagaoglu 2005] Serinagaoglu Y, Brooks DH, MacLeod RS. Bayesian solutions and performance analysis in bioelectric inverse problems. IEEE Trans Biomed Eng 2005; 52: 1009–1020.

[Serinagaoglu 2006] Serinagaoglu Y, Brooks DH, Macleod RS. Improved performance of bayesian solutions for inverse electrocardiography using multiple information sources. IEEE Trans Biomed Eng 2006; 53: 2024–2034.

[Tikhonov 1963] Tikhonov AN. On the solution of incorrectly posed problems and the method of regularization. Sov Math Dokl 1963; 4:1035-1038.

[Tobón 2013] Tobón C, Ruiz-Villa CA, Heidenreich E, Romero L, Hornero F, Saiz J. A three-dimensional human atrial model with fiber orientation:electrograms and arrhythmic activation patterns relationship. Plos One 2013; 8:e50883.

[Trayanova 2006] Trayanova N. Defibrillation of the heart: Insights into mechanisms from modelling studies. ExpPhysiol 2006; 91:323-337.

[Van Dam 2009] Van Dam PM, Oostendorp TF, Linnenbank AC, van Oosterom A. Non-invasive imaging of cardiac activation and recovery. Ann Biomed Eng 2009;37: 1739–1756.

[Walker 1987] Walker S, Kilpatrick D. Forward and inverse electrocardiographic calculations using resistor network models of the human torso. Circ Res 1987; 61:504-513.

[Wang 2010] Wang D, Kirby RM, Johnson CR. Resolution strategies for the finite- element-based solution of the ECG inverse problem. IEEE Trans Biomed Eng 2010; 57:220-237.

[Wilber 2010] Wilber DJ, Pappone C, Neuzil P, De Paola A, Marchlinski F, Natale A, Macle L, Daoud EG, Calkins H, Hall B, Reddy V, Augello G, Reynolds MR, Vinekar C, Liu CY, Berry SM, Berry DA, ThermoCool AFTI. Comparison of antiarrhythmic drug therapy and radiofrequency catheter ablation in patients with paroxysmal atrial fibrillation: a randomized controlled trial. JAMA 2010;303:333–340.

[Zlochiver 2008] Zlochiver S, Yamazaki M, Kalifa J, Berenfeld O. Rotor meandering contributes to irregularity in electrograms during atrial fibrillation. Heart Rhythm 2008;5:846–854.

UNIVERSITAT POLITÈCNICA DE VALÈNCIA

ESCUELA TÉCNICA SUPERIOR INGENIEROS INDUSTRIALES VALENCIA

BUDGET

Index of contents

Index of tables

1. Objective

This part of the work describes the costs of the master's project. To do develop the budget personnel, hardware and software costs have been considered, which are explained in detail. Finally, an overview of the budget is also included.

2. Detailed budget

2.1. Personnel costs

To develop the present work personnel costs were needed for the bibliographic review, development and implementation of the algorithms, and finally results evaluation. Particularly, the work has been developed by a biomedical engineer. To develop the budget appropriately, unit costs have been calculated as well as chargeable costs without the employer's contribution and finally chargeable costs with employer's contribution. Numerical data on unit costs and employer's contribution have been extracted from Comunidad Valenciana's official college of industrial engineers (COIICV). These detailed personnel costs are summarized in table 2.1 and sum up to **nineteen thousand two hundred and forty-three Euros** (19243€).

Table 2.1: Personnel costs needed for the development of the project.

Personnel costs

Profile	**Tasks**	**Working hours**	**Unit costs**	**Chargeable costs (without employer's contribution)**	**Employer's contribution (37.45%)**	***Total chargeable costs***
Biomedical engineer	Bibliographic review, development, implementation and evaluation	350 hours	40€ / hour	14000€	5243€	*19243€*
Subtotal (including employer's contribution)						***19243€***

2.2. Hardware costs

The hardware needed in the development of the project has been the worker's personal computer. The detailed hardware costs are summarized in table 2.2 and sum up to **two thousand two hundred Euros** (2200€).

Table 2.2: Hardware costs needed for the development of the project.

Hardware costs

Description	**Total equipment cost (without VAT)**	**Units**	**Amortisation period**	**Period of use**	**Chargeable costs (without VAT)**	**VAT (21%)**	***Total chargeable costs***
Intel® Core™ i5-2.9GHz, 8 GB RAM 2133MHz LPDDR3, Intel® Iris™ Graphics 550 1536MB	1818.20€	1	4 years	6 months	1818.20€	381.80€	*2200€*
Subtotal (including VAT)							***2200€***

2.3. Software costs

Several software licenses have been needed in the development, implementation and evaluation of the present work. The detailed software costs are summarized in table 2.3 and sum up to **two thousand one hundred and forty-nine Euros** (2149€).

Table 2.3: Software costs needed for the development of the project.

Software costs

Description	**Total license cost (without VAT)**	**Number of licenses**	**Duration of the license**	**Period of use**	**Chargeable costs (without VAT)**	**VAT (21%)**	***Total chargeable costs***
MATLAB R2016b	1652.90€	1	Indefinite	6 months	1652.90€	347.10€	*2000€*
Operating system macOS Sierra 10.12.2 (16C67)	0€	1	Indefinite	6 months	0€	0€	*0€*
Microsoft Office home and students version 2016	123.14€	1	Indefinite	6 months	123.14€	25.86€	*149€*
Subtotal (including VAT)							***2149€***

3. Budget overview

The personnel, hardware and software costs are summarized in table 3.1, as well as the total cost of the whole project, which sums up to **twenty-three thousand five hundred and ninety-two Euros** (23592€).

Table 3.1: Budget overview and total costs needed for the development of the project

Budget overview (including employer's contribution and VAT)

Personnel costs	19243€
Hardware costs	2200€
Software costs	2149€
Total costs	***23592€***